Sequential chemical extraction and radiocarbon analysis of soils in Central Germany

Master thesis

to obtain the academic degree: Master of Science (M.Sc.) in Geoecology

at the Faculty of Geoscience, Geoengineering and Mining of the

Technische Universität Bergakademie Freiberg, Germany

B.Sc. Sophie F. von Fromm

born on the 25th of February 1993 in Berlin, Germany

Supervisors:

Prof. Dr. Marion Tichomirowa (TU Bergakademie Freiberg)

Prof. Dr. Susan E. Trumbore (MPI for Biogeochemistry, Jena)

Dr. Valérie F. Schwab (MPI for Biogeochemistry, Jena)

Submitted: 24th of April 2019

Table of Contents

world of soil radiocarbon and for helping me to better understand it. They never became tired in answering my questions about several techniques and methods that are used in order to investigate radiocarbon in soil systems. Special thanks go to Jeffrey who also carefully proof-read and commented on the first manuscript version of my thesis.

My time at the MPI would have not be the same without **Dr. Steffi Rothardt** and all others who made my stay special during e.g. lunch and coffee breaks, and social events. Special thanks go to Steffi who not only helped me professionally with organizing my master project, but became a good friend.

Many thanks go to my parents, **Christel** and **Lutz**, and my siblings, **Max**, **Lena**, and **Paula**, for their unconditional love and support throughout my entire life.

Last but not least, I deeply thank **Jörg**, for his never-ending love, encouraging support and patience during the last years. I enjoy every moment with you and our endless (scientific) discussions.

Declaration

I hereby declare that this thesis was written entirely by myself, without any improper help from a third party, and without using any sources other than those cited. All ideas derived directly or indirectly from other sources are identified as such, including figures and tables. This thesis was neither submitted to any other authority to receive an academic degree, nor was it previously published.

Freiberg, 24th of April 2019   _____

                                                                    Sophie von Fromm

Abstract

Soils are the second largest carbon pool after the oceans. Therefore, they play a crucial role in the global climate system. Yet, terrestrial C turnover rates represent one of the largest uncertainties in global climate models. This is mainly caused by the complexity and heterogeneity of soil organic matter (SOM). C with long turnover rates (centuries to millennia) is currently assumed to make up a large portion of SOM. Several hypotheses have been presented to explain the existence of old soil organic carbon (SOC), such as chemical recalcitrance, physical isolation by interactions with minerals, recycling and the influence of environmental and ecosystem properties.

Here, links between SOM age and chemistry of were investigated at the molecular level by applying a sequential chemical extraction technique. The nature of the SOM in the extracts and the residues is based on its chemical structure and recalcitrance (e.g., types of lignin, sugars or fatty acids), and its mineral association. Those fractions (extracts and residues) were analyzed for their C-isotopic composition (^{13}C and ^{14}C) allowing further insights into the relations between SOM compounds and their age distribution.

The influence of soil parent material on the age and chemistry of SOM was investigated for two different depths (0–10 cm and 30–60 cm) from six different sites in central Germany. These sites had the same vegetation (European beech forest: *Fagus sylvatica L.*) and overall climate, but distinct bedrock types (limestone and sandstone).

At all sites, the age of the extracts increased with depth. Differences between the two layers for the $\Delta^{14}C$ values were larger at the limestone sites (TOP: -5.9 ‰, BOT: -236.0 ‰) compared to the sandstone sites (TOP: 2.4 ‰, BOT: -61.2 ‰). Those values clearly indicate an influence of parent material, with consistently older SOM found at the limestone sites compared with sandstone. The oldest C values were found in the microbially-derived fractions at the limestone sites. It is likely that this C comes from carbonates in the soils. Under climate change, organic C in the carbonates might get released due to enhanced weathering. If this is the case, this C would be available for microorganisms as an energy source and become part of the fast turnover SOC pool.
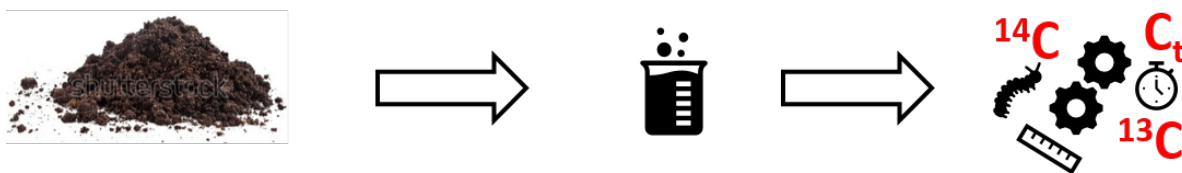
List of abbreviations

AHY	Acid hydrolysis		Mya	Million years ago
a.s.l.	Above sea level		NIST	National Institute of Standards and Technology
ASTM	American Society for Testing and Materials		NOX	New oxalic acid
BHY	Basic hydrolysis		OC	Organic carbon
CLRTAP	Convention on Long-range Transboundary Air Pollution		OX-I	Oxalic acid I standard
CuO	Copper oxidation		PTFE	Polytetrafluorethylen
CZE	Critical Zone Exploratory		PE	Polyethen
DCM	Dichlormethane		POS	Possen
EA	Elemental analyzer		ROMA	Routine Measurements & Analysis
GC-MS	Gas chromatography-mass spectrometry		Rpm	Rounds per minute
GHG	Greenhouse gas		RSD	Relative standard deviation
GLP	Good laboratory practice		SD	Standard deviation
GOT	Goettingen Forest		SE	Standard error
HAI	Hainich		SOC	Soil organic carbon
HOL	Holzland		SOL	Solling
HUM	Hummelshain		SOM	Soil organic matter
LLQ	Lower limit of quantification		ULQ	Upper limit of quantification
LMW	Low molecular weight		UNECE	United Nations Economic Commission for Europe
IAEA	International Atomic Energy Agency		TC	Total carbon
IC	Inorganic carbon		TCD	Thermal conductivity detector
ICP Forest	International Co-operative Program on Assessment and Monitoring of Air Pollution Effects on Forests		TLUG	Thüringer Landesanstalt für Umwelt und Geologie
			TLWJF	Thüringer Landesanstalt für Wald, Jagd und Fischerei
MAP	Mean annual precipitation		TN	Total nitrogen
MAT	Mean annual temperature		TSE	Total solvent extraction
MFM	Muffle-Furnace-Method		WGS	World Geodetic System
MICADAS	Mini Carbon Dating System		WRB	World Reference Base for Soil
MTBE	Methyl-tert-butylether			

List of tables

List of figures

1.   Introduction

Researchers have investigated drivers and processes of stabilizing organic matter in soils (SOM) over the past several decades. We still lack the understanding of SOM dynamics needed to adequately predict the response of SOM to abrupt environmental change. This work aims at investigating parent material and depth effects on radiocarbon ages at the molecular level in chemical fractions of Central Germany soils. Radiocarbon determination is a powerful tool to better understand SOM stabilization and destabilization processes.

1.1   The climate system and the global carbon cycle

In a globally changing world, especially in terms of anthropogenic climate change, a better understanding of processes that drive those changes is crucial. Yet, it is even more important to not only focus on those drivers, but to fully understand the underlying feedback processes and cycles in our climate system. This is especially true for the global C cycle.

The third IPCC assessment report (Baede et al. 2001) defined the climate system as an interactive system consisting of five major compounds: *atmosphere*, *hydrosphere*, *cryosphere*, *biosphere* and *pedosphere* (plus *lithosphere*). All of those components are influenced by various natural and anthropogenic external and internal factors, with the sun being the most important natural and external one.

The *atmosphere* is the most unstable and rapidly changing part of the Earth system. Its composition has significantly changed various times in Earth history (Baede et al. 2001). Today, the most important gases in terms of relative concentration are nitrogen (N_2), oxygen (O_2) and argon (Ar), the trace components carbon dioxide (CO_2), nitrous oxide (N_2O), methane (CH_4), ozone (O_3), and water vapor (H_2O). These latter, so-called greenhouse gases (GHGs), absorb infrared radiation emitted from the Earth surface and keep the energy in the troposphere. This causes a temperature increase by about 33 K to an average global surface temperature of 15 °C (Baede et al. 2001). This natural greenhouse effect is increasingly enhanced by anthropogenic GHG emissions into the atmosphere (Cubasch et al. 2013). Besides GHGs the troposphere also consists of aerosols and clouds, which interact with incoming and outgoing radiation. The atmosphere contains today about 829 Pg C (1 Pg = 10^{15} g), of which almost one third was emitted into the atmosphere by human activities within the last three decades (Ciais et al. 2013).

The *hydrosphere* includes all liquid fresh and saline water in rivers, lakes, aquifers, as well as oceans and seas. The oceans cover approximately 70 % of the Earth's surface, and store up to about 40,450 Pg C (Baede et al. 2001; Ciais et al. 2013). About 150 ± 30 Pg C were additionally added to the oceans by human activities during the Industrial Period (1750–2011; Ciais et al. 2013).

The *cryosphere* combines the ice sheets of Greenland and Antarctica, continental glaciers and snow fields, sea ice and permafrost soils. Due to the high reflectivity of ice (albedo), the cryosphere mainly influences the effect of solar radiation at the Earth's surface. Due to increasing global surface temperature, the large amount of melt water stored in the cryosphere contributes to rising sea levels (Ciais et al. 2013).

The marine and terrestrial *biosphere* mainly has an impact on the uptake and release of GHGs into the atmosphere (Baede et al. 2001). Plants (mainly terrestrial) store up to 453–653 Pg C through photosynthesis. That storing capacity will probably decrease by 30–45 Pg C with ongoing climate change (Ciais et al. 2013).

The *pedosphere* consists mostly of soils. They are the second largest C pool (~1,500–2,400 Pg C) after the oceans and therefore play a crucial role in the global climate system (Ciais et al. 2013). Biosphere and pedosphere are strongly interlinked. In particular, forest, including tropical, temperate and boreal forest, is the most important natural land-cover type which helps to protect and preserve soils. Globally, forest biomass stores up to 504 Pg C, equivalent to more than 80 % of the total C stored in plants. Temperate forests are, after tropical ones, the second largest C reservoir of terrestrial biomass and store up to 130 Pg C (Schlesinger and Bernhardt 2013). However, this is a small amount compared to the storage capacity of soils. Yet, most of the highly complex processes of the terrestrial C cycle are not fully understood and cause the highest uncertainties in most Earth System Models (Friedlingstein et al. 2014). That limits our ability to forecast how soils will react and behave under climate change – and underlines the importance of better understanding the processes of gaining and losing C in soils. To investigate the various processes within the soil C cycle, the different C-isotopes provide powerful tools.

Carbon isotopes. In general, isotopes are forms of the same element that differ in the number of neutrons in the atomic nucleus. Isotopes of the same element behave chemically similar. However, different isotopes differ in mass; therefore, their individual bonds are slightly different. The three most abundant C-isotopes are: ^{12}C, ^{13}C, and ^{14}C, with ^{12}C and ^{13}C being stable and ^{14}C radioactive. All C-isotopes have 6 protons and between 6 and 8 neutrons. The abundance decreases with increasing number, with 98.89 % of the C atoms on Earth being ^{12}C and only 1.11 % ^{13}C. The relative abundance of the two stable C-isotopes has not changed since their production by nucleosynthesis in stars. Yet, since C atoms are constantly transferred between different forms (organic and inorganic) and among and within the six major Earth spheres (atmosphere, hydrosphere, cryosphere, biosphere, pedosphere, and lithosphere), the relative abundance of ^{12}C and ^{13}C can change in any specific reservoir. This process is called isotope fractionation and can be used to better understand and identify processes that occur in the different reservoirs. This also applies for soils (Fry 2006; Trumbore et al. 2016).

Since ^{14}C is radioactive, its characteristics and application are different from the stable isotopes ^{12}C and ^{13}C. ^{14}C is naturally formed in the stratosphere when cosmic rays interact with the Earth's atmospheric N_2. Between production in the stratosphere and decay, ^{14}C is oxidized to $^{14}CO_2$ and mixed in the atmosphere before entering the terrestrial or hydrological C cycle. For soils, the main input pathways are through plant photosynthesis and decomposition of biota. In the past, the range of production and decay of ^{14}C resulted in an abundance of about 10^{-10} % in the pre-industrial atmosphere (Trumbore et al. 2016). Yet, the ^{14}C concentration in the atmosphere decreases constantly since the industrial period. This depletion is caused by the input of 'old' C from fossil-fuel burning into the atmosphere. C from fossil fuels is so old that it has no significant ^{14}C signature anymore. This unnatural dilution process, the so-called Suess effect (Suess 1955; Figure 1), results in general depletion of ^{14}C in the atmosphere. Nuclear weapon testing created a new ^{14}C source in the atmosphere in the early 1960s. This accidental global labeling experiment can be used as a precise tracer. Since anthropogenic ^{14}C behaves identically to the natural one, it enters the different reservoirs and can be used to analyze different C pathways and turnover times. Such age determinations can help identify and conclude different dynamics of soils and of C cycling within those soils. Due to the pulse of so-called 'bomb' ^{14}C, timescales of years to decades can be investigated. The natural ^{14}C abundance allows investigating much longer timescales of centuries to millennia (Schuur et al. 2016b).
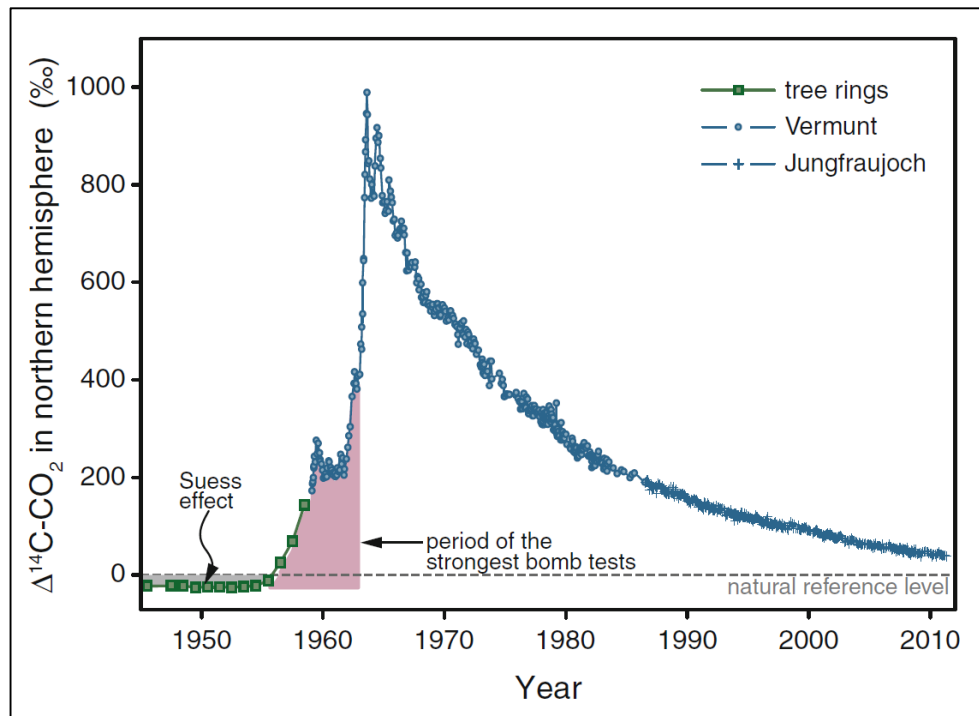
Figure 1: Development of northern hemispheric atmosphere $\Delta^{14}CO_2$ over the last 60 years due to the production of ^{14}C by atmospheric nuclear weapon testing. Data before 1959 were obtained from tree ring measurements; data after 1959 from atmospheric measurements (Trumbore et al. 2016).

1.2   Soil organic matter (SOM)

Soils can be described as natural bodies of various ages that develop through different soil-forming processes. Those processes rely on the type of parent material and relief under a specific climate, and thus specific vegetation and litter with characteristics biotic communities (Blume et al. 2016). Due to the high variability of those factors, terrestrial reservoirs are the most heterogeneous components of the Earth's system. Compared to atmosphere and oceans, C transfer between different terrestrial components is relatively slow (Schuur et al. 2016a). This fact makes it difficult to predict how soils will react under climate change – they could store more or less C (Friedlingstein et al. 2014). To predict such response, the composition of soils needs to be better understood.

The chemical composition of SOM is heterogeneous because of its different sources (e.g. plant and animal residues) and the various degradation stages of those compounds. SOM includes all of the dead plant and animal residues and their organic transformation products found in soils. Living organisms and roots do not belong to SOM (Blume et al. 2016). SOM in general can be described as an open system, where new C is constantly added via photosynthesis and the death of plant material and organisms, while older C is continuously removed and recycled by microbial decomposition (Schuur et al. 2016a). Some of the soil organic carbon (SOC) is exposed to stabilization processes, which protect it to some extent against microbial decay. Different turnover rates for SOC are the result. Under constant environmental and vegetation conditions, an equilibrium is reached in the soil between supply and degradation, resulting in characteristic SOM (Blume et al. 2016). This implies that a major pool of SOC is sensitive to climate or local environmental change (Schmidt et al. 2011). The feedbacks between SOM and climate are not fully understood and global C models predict contradictory scenarios for e.g. increasing CO_2 in the atmosphere (Friedlingstein et al. 2014; Schmidt et al. 2011). Those opposing scenarios are mainly caused by uncertainties in the response of the terrestrial C cycle to climate change (Friedlingstein et al. 2014).

One large uncertainty in those models is the existence of SOC with different ages and turnover rates that have distinct sensitivity to decomposition (Trumbore 2009). C with long turnover rates (centuries to millennia) is currently assumed to make up a large portion of SOM (Schmidt et al. 2011). However, it still remains unclear how and under which condition this old or protected C is formed in soils and how it will respond to environmental change (Lehmann and Kleber 2015). To analyze the existence of such C in soils that developed from different parent material is the main focus of this work.

In the past, the molecular structure of SOM was assumed to control long-term decomposition rates in mineral soil (Figure 2: ① and ②). Such chemical recalcitrance was explained with the creation of new stable compounds during decomposition processes in soils – so-called humic substances. Therefore, the molecular structure of soil biota and organic materials determines timescales of persistence (Kögel-Knabner 2000; Schmidt et al. 2011). However, several studies have shown that organic compounds that were assumed to have long turnover rates (e.g. lignin or plant lipids) have similar rates compared to bulk SOM (Marschner et al. 2008; Schmidt et al. 2011). Those studies suggest that the molecular structure of plant inputs and organic matter is less important for determining protected or old (centuries to millennia) SOC. New approaches suggest that long C turnover rates mainly depend on the biotic and abiotic (e.g. temperature sensitivity) environment and is more of an ecosystem property (Kleber et al. 2011; Schmidt et al. 2011). This would mean that environmental effects on microbial composition and characteristic determine whether SOM will be decomposed or retained in the soil.

Besides, additional properties that result in protected C can be physical occlusion (e.g. aggregates), organo-mineral interaction (e.g. clay minerals) and changing of environmental conditions (e.g. freezing/thawing processes; Figure 2: ③−⑧). Additionally, it is likely that deeply-buried C, which is usually characterized by very long turnover times (Schmidt et al. 2011), is vulnerable to decomposition and responds to land-use changes on a larger time scale than expected (Jobbágy and Jackson 2000). An additional hypothesis suggests that the persistence of SOC might be caused by its constant recycling through resynthesis of new molecules (Gleixner et al. 2002; Rethemeyer et al. 2004). However, most approaches did not consider the influence of different geochemical soil composition resulting from bedrock material on composition and stabilization of SOM (Doetterl et al. 2018), especially in subsoils (Angst et al. 2018).

In the past, total clay content has been used to model SOM stability, predicting a negative correlation between clay content and SOM stabilization in soils. Recent studies suggest that this assumption might not apply across diverse soil systems which developed under different climate conditions and from different bedrock materials. Current understanding suggests other physiochemical parameters (e.g. pH-value, mineral composition) to be better predictors of SOM content and stabilization (Rasmussen et al. 2018). Yet, all of those drivers and processes are still highly uncertain and difficult to quantify. This is why most of the models do not take them into account. Until currently, related parameter quantification poses a significant challenge (Schmidt et al. 2011).

SOM differentiation. Contradictory results and assumptions of SOM stabilization processes are currently under discussion (Finke et al. 2019; Rasmussen et al. 2018). Since all organic molecules are unstable with respect to their decomposition to inorganic forms, it remains unclear why organic molecules are present and not immediately decomposed in soils (Gleixner 2013). As a consequence, various methods have been introduced to analyze SOM composition and cycling (von Lützow et al. 2007). All related studies and experiments agree that

SOM is a complex polymer that can only be studied after it has been separated from the in-organic soil fraction. This results in the necessity to break it down into smaller units. Such approaches are known and have been tested for several decades (e.g. Forsyth 1947; Goh and Reid 1975; Sinha 1972; Trumbore et al. 1989). However, all of the methods developed and applied so far have their shortcomings. So far, no 'perfectly' appropriate method could be developed.
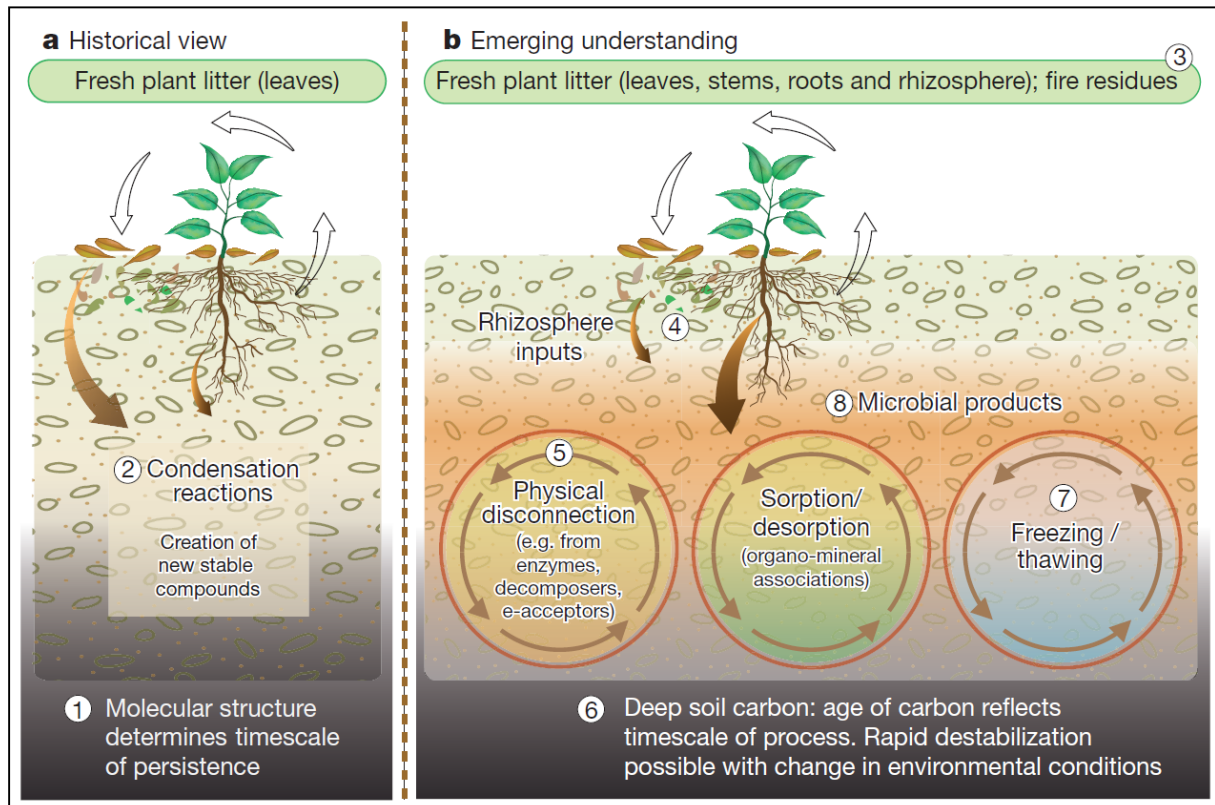
Figure 2: Historical (a) and emerging view (b) of soil organic carbon cycling (Schmidt et al. 2011)

The two major approaches to separate SOM into different mechanistically-relevant fractions are i) physical separation, e.g. by density or size and ii) chemical fractionation to obtain dif-ferent organic compounds (Trumbore and Zheng 1996; von Lützow et al. 2007). Physical fractionation methods are designed to separate soil organic matter into pools of different turnover times. They differentiate between free particulate organic materials and organic ma-terials associated with soil minerals (Kögel-Knabner 2000). This approach assumes that the association of soil particles and their spatial distribution play an important role in SOM dy-namics, because the accessibility of organic material is crucial for decomposition processes. Physical fractionation involves various methods to separate soil particles: dry and wet siev-ing, dispersion by ultrasonication in water, density and particle size separation, sedimenta-tion, and aggregate fractionation. The short-coming of those approaches is that the generat-ed SOM pools are usually still too heterogeneous to gain meaningful conclusions about SOM turnover rates (von Lützow et al. 2007).

In contrast, chemical fractionation methods are based on the breakdown of macromolecular soil structures on the molecular level (Kögel-Knabner 2000). They can be based on the ex-traction of SOM in aqueous solutions with and without electrolytes, in organic solvents, on the hydrolysability of SOM with water or acids, or on the resistance of SOM to oxidation. Other chemical extraction methods are based on destroying different mineral phases. Such methods provide pure organic fractions that should be free of mineral components, which is

advantageous for analyzing SOM (von Lützow et al. 2007). Although there is no single fractionation method that can be applied to all soils and delivers a complete separation of SOM with different turnover times, combinations of physical and chemical separation, and sequential extraction methods are options (Poeplau et al. 2018; Trumbore and Zheng 1996). The advantage of compound-specific analysis of soils (e.g. through sequential chemical extraction) is that it helps to better understand which compounds tend to be more part of the fast or of the slow C turnover pool. This knowledge can then be used to identify ecosystem properties (e.g. parent material) that may influence the distribution of different-aged C among those compounds (von Lützow et al. 2007).

This brief literature overview shows that few methods are unequivocally useful to characterize SOM dynamics. Despite numerous approaches to improve and combine fractionation methods, a major remaining problem is that most of these methods do not result in the extraction of homogenous or functional soil organic matter pools. To better understand stabilization processes in soils, the entire soil profile and its pedogenesis needs to be taken into account. Furthermore, compound-specific stable isotope and radiocarbon analysis may help to improve the understanding of SOM dynamics and allow the differentiation of functional pools within heterogeneous fractions (von Lützow et al. 2007). Although different C sources may have similar chemical composition, their C-isotope signature may be different due to dissimilar biochemical synthesis and degradation (Glaser 2005). In consequence, it is important to understand that ^{14}C age determinations of SOC do not measure the stability of individual fractions. The measured ^{14}C concentration of SOM presents the time since the C-atoms in the molecule were separated from equilibrium with the atmospheric C pool. Therefore, low $\Delta^{14}C$ values (old/protected C) do not necessarily imply chemical recalcitrance. They might just point at repeated recycling of C-atoms through more labile molecules (Gleixner 2013) or at the input/uptake of old C from different sources (Seifert et al. 2011).

1.3   Aims and objectives

This work presents a new sequential chemical extraction method, which has been adapted from an existing approach (Otto and Simpson 2007). It aims at separating heterogeneous SOM into relatively homogenous compounds in order to analyze internal SOM dynamics. Understanding those dynamics is crucial to better understand which components are involved in the stabilization of SOC and under which condition this protected C may be decomposed and released from the soil into the atmosphere. The nature of the SOM in extracts and residues is based on its chemical structure and recalcitrance (e.g., types of lignin, sugars or fatty acids), and its mineral association (e.g. iron). Soil extraction with organic solvents, followed by alkaline hydrolysis, likely isolates free- and ester-bound lipids of SOM. Acidic hydrolysis is an approved method to extract carbohydrates, amino acids, and peptides. Oxidation of SOM with CuO yields mainly phenolic and aliphatic monomers, which are indicators for lignin, suberin, and cutin (Kögel-Knabner 2000; Otto and Simpson 2007). Those compound-specific fractions were analyzed for their stable C-isotopes and radiocarbon (extracts and soil residues), allowing further insight into the relations between SOM molecular structure, mineral association and age.

Since SOM is not only influenced by the input of plant residues, but also by the mineralogy of and the microbial community in the surrounding soil (Figure 2), this work shows the result of applying the above-mentioned method in soils that developed from different bedrock material. Parent material is the mineral substrate for soil development and has various influences on SOM composition and stocks. Bedrock affects soil chemistry and fertility and therefore plant productivity and texture. The latter determines soil moisture retention and thus produc-

tivity and decomposition, as well as clay content and mineralogy, which alter SOM stabilization (Torn et al. 2009). The influence of soil parent material on SOM age and chemistry was investigated for two different depths (0–10 cm and 30–60 cm) from six sites in central Germany. These sites had similar vegetation (European beech forest: *Fagus sylvatica L.*) and overall climate and surface age, but distinct bedrock types: the sedimentary rocks limestone and sandstone.

Sedimentary rocks cover about 75 % of the Earth's surface and are therefore very significant for soils and their turnover rates (Blume et al. 2016). Those rock types are products of weathering, transport and deposition processes from pre-existing rocks or organic materials. Sandstones show more than 50 % of their particle size fraction as (mostly) quartz sand (0.063–2 mm). They can be found in all geological periods and derive from rock weathering, transport and subsequent sedimentation. Limestones contain more than 75 % carbonates. They are grain-size transitions to claystones (dominant particle fraction < 2 µm) and sandstones. Most carbonate rocks were formed biogenically in the ocean, so that they often have high fossil content (Blume et al. 2016). It has been shown in several studies that microorganisms are capable of taking up this ancient C from soils and sediments (Kuzyakov et al. 2009; Rethemeyer et al. 2004; Seifert et al. 2011).

The six different sites are characterized in chapter 2, followed by the materials and method (Chapter 3). That chapter briefly explains the sampling procedure, gives a detailed overview about the applied sequential chemical extraction method and characterizes the analytical methods used to analyze the extracts and residues from the extraction method. The analytical methods are divided into physical (pH-value) and chemical (C and N content, stable C-isotopes and radiocarbon analysis) characterization. Based on this differentiation, the results of this work are presented in chapter 4 and discussed in detail. Conclusions (Chapter 5) and an outlook (Chapter 6) close this work, completed by the references and an annex.

Overall, this work attempts to contribute to better understand internal SOM turnover processes. The usage of a sequential chemical extraction method allows the differentiation of functional fractions obtained from the soil which shall then give an idea which compounds may protect SOC from decomposition. Those mechanisms can be influenced by various soil and ecosystem properties (e.g. parent material and climate). Three major research questions have been developed from literature review and open research questions in order to investigate internal SOM dynamics and stabilization processes. Those questions will be answered in the second last chapter (5) Conclusions. The research questions (Q) are:

Q1: How do the two different bedrock materials influence $\Delta^{14}C$ and $\delta^{13}C$ values in the bulk soil samples?

Q2: How much do the $\Delta^{14}C$ and $\delta^{13}C$ values differ in the individual chemical fractions, soil depths and bedrock materials?

Q3: Do age distribution and differences in $\Delta^{14}C$ among chemical fractions change with depth?

2.   Study Areas

The study was carried out at six different beech-forest sites in Thuringia and Lower Saxony, Central Germany (Figure 3), since beech is a representative tree species in this region. European beech (*Fagus sylvatica L.*) is the most competitive tree species in Central Europe. It would be the most abundant one under natural conditions. However, centuries of land cultivation have changed tree-species composition and land-cover types dramatically (Ellenberg 1988). Nowadays, only few near-natural beech-forest sites can be found in Central Europe. For this study, beech-forest sites with a mean age older than 80 years were selected.
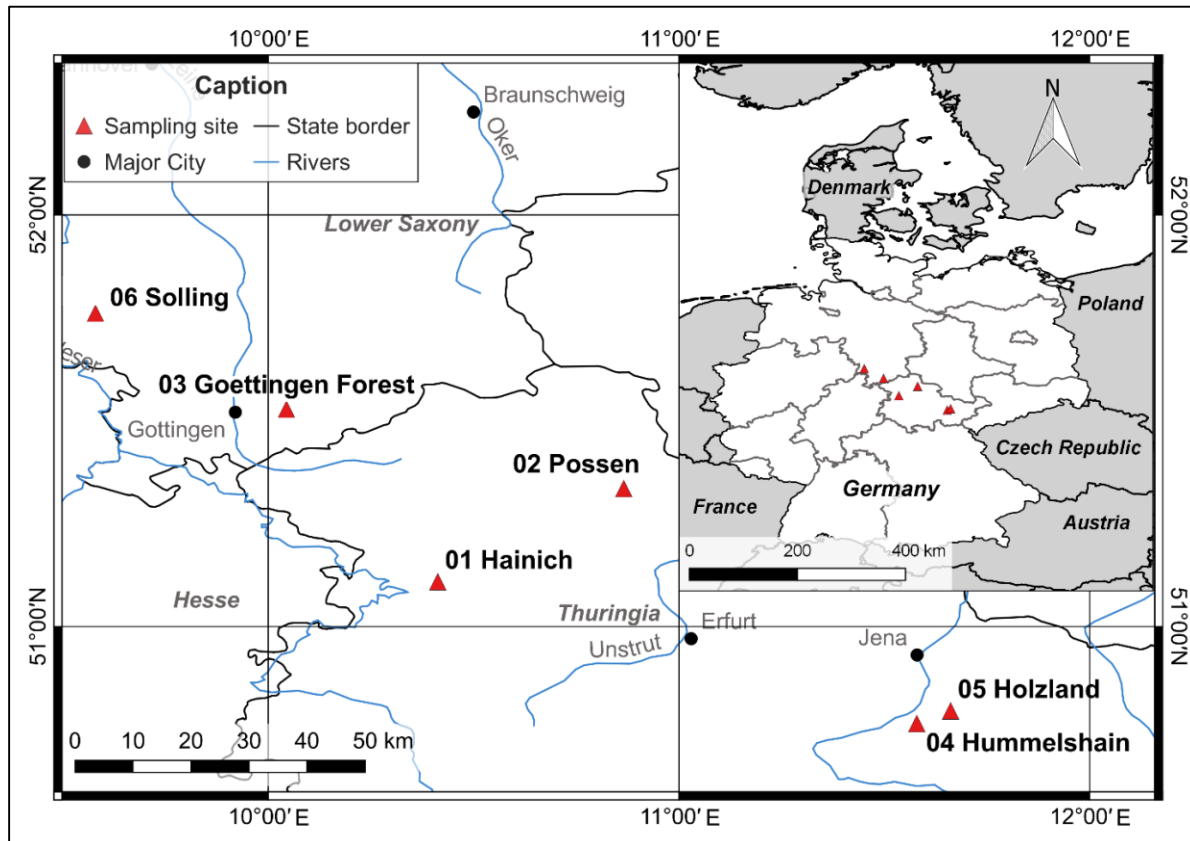
Figure 3: The six study sites in Thuringia and Lower Saxony, Germany (QGIS 2.18.14 Las Palmas)

Half of the sites are located on limestone, the other half on sandstone bedrock material. Both rock types developed in the *Triassic* geological period, spanning 47 million years from the late *Permian* period 250 million years ago (Mya) to the beginning of the *Jurassic* period 203 Mya. The investigated sandstone sites developed in the era of the *Buntsandstein* (250–240 Mya), whereas the limestone sites are from the era of the *Muschelkalk* (240–230 Mya). Soils formed above those two geological formations (*Buntsandstein* and *Muschelkalk*) common in Central Germany (Asch et al. 2003) share distinct properties, such as inorganic and organic C content, clay content, and mineral composition (Blume et al. 2016). Besides the described differences, all study sites have relatively young soils (~10'000 years) that have been influenced by periglacial processes like cryoturbation, solifluction, and erosion (Ash et al. 2003).

This chapter will characterize the locations in detail. The two different bedrock material locations will be referred to as limestone and sandstone sites and the individual sites will be labelled with subscript 'L' or 'S', respectively.

2.1   Limestone bedrock material

This section provides an overview about the site characteristics of Hainich and Possen (Thuringia), and Goettingen Forest (Lower Saxony). All three sites are dominated by wild garlic-rich beech forest (*Hordelymo-Fagetum*), developed over limestone parent material. Those forest communities are unusually rich in spring-flowering geophytes, in particular wild garlic (*Allium ursinum*). They require very high soil fertility and are drought sensitive (Ellenberg 1988).

Hainich (HAI$_L$). The investigated site is situated on a northeastern slope of the Hainich low mountain range in north-western Thuringia, Germany (Figure 3), at an elevation of about 365 m a.s.l. (Table 1). The site is part of the Hainich Critical Zone Exploratory (CZE), an observational transect with different land-use management systems to investigate soil, vegetation, and groundwater properties (Küsel et al. 2016). The beech-forest has remained unmanaged since 1997, when the neighboring Hainich National Park was established. The tree community, with heterogeneous age structure mainly consists of European beech (*Fagus sylvatica L.*). Other tree species in the plot are maple (*Acer platanoides, Acer pseudoplatanus), ash* (*Fraxinus excelsior*), hornbeam (*Carpinus betulus*), linden (*Tilia platyphyllos*), and elm (*Ulmus glabra;* Metzger et al. 2017). The forest floor is covered by wild garlic (*Allium ursinum*), wind-flower (*Anemone nemorosa*), and dog's mercury (Mercurialis perennis) in spring and summer (Knohl et al. 2003). Therefore, the natural vegetation at this site would be a wild garlic-rich beech forest (*Hordelymo-Fagetum;* Ellenberg (1988). Biological activity and bioturbation in soils at the site are high and have initiated a mull type litter layer (Schrumpf et al. 2014), with a thickness of 2–3 cm. Soils at the HAI$_L$ location can mainly be described as Cambisols and Luvisols according to the World Reference Base System (Metzger et al. 2017; Schrumpf et al. 2014; WRB 2015). The soils are clay-rich, with a clay content (< 2 µm) of 20.5 % at 7.5 cm depth and of 28.0 % at 27.5 cm (Huss 2017).

Middle Triassic limestone (Upper Muschelkalk) layers form the bedrock material, overlain by shallow Pleistocene loess loam (Küsel et al. 2016; Metzger et al. 2017). Mean annual temperature is about 8.0 °C and annual precipitation ranges from 850–900 mm at the site (Küsel et al. 2016; TLUG 2011c). The plot is within a hunting ground that uses a wild boar wallow to feed animals.

Possen (POS$_L$). This site is part of the Intensive Forest Monitoring Program (Level II) of the International Co-operative Program on Assessment and Monitoring of Air Pollution Effects on Forests (ICP Forests) under the United Nations Economic Commission for Europe (UNECE) Convention on Long-range Transboundary Air Pollution (CLRTAP; Thünen Institute of Forest Ecosystems 2018). It is located in north-western Thuringia, Germany, 40 km to the northwest of Erfurt (Figure 3) at an elevation of about 420 m a.s.l. on a plateau (Table 1). The location is protected by a fence to keep animals out.

The POS$_L$ tree community is similar to the one at Hainich, consisting mainly of European beech (*Fagus sylvatica L.*) with a dense ground cover of geophytes. This would lead to a wild garlic-rich beech forest (*Hordelymo-Fagetum*) under natural conditions (Ellenberg 1988). The tree stand was established in 1937, indicating a mean tree age of 81 years in the plot (TLWJF 2009). Soils at the site are deeper than at the other sites and can be described as Luvisols (TLWJF 2009; WRB 2015). In contrast, the mull-type litter layer only has a thickness of 2–3 cm, indicating high bioturbation and bioactivity. The clay content of the mineral soils is similar to the HAI$_L$ site and ranges between 16.8 % at 0–5 cm depth and 26.4 % between 30–65 cm depth (Thüringen Forst 2007).

POS$_L$ lies within in the 'Trochitenkalk' formation, limestone from the upper Muschelkalk (TLUG 2018b), and has a characteristic loess layer (TLWJF 2009). Mean annual temperature is about 7.5 °C (TLUG 2011d). Annual average precipitation is about 700 mm at POS$_L$ (TLUG 2011a).

Table 1: Site characteristics of the three beech-forest locations on limestone (HAI$_L$, POS$_L$, GOT$_L$) bedrock in Thuringia and Lower Saxony, Germany

	01_Hainich	02_Possen	03_Goettingen Forest
Coordinates (WGS84)	N 51°06'30.3"; E 010°24'46.5"	N 51°20'05.9"; E 010°51'57.1"	N 51°31'40.3"; E 010°02'40.1"
Elevation [m] a.s.l.	365	420	420
Slope [%]	5	0	0
Exposition	NE	Plateau	Plateau
Tree age [a] (2018)	Heterogeneous[1]	81[8]	151[14]
Natural Vegetation	Wild garlic-rich Beech (*Hordelymo-Fagetum*)[2]	Wild garlic-rich Beech (*Hordelymo-Fagetum*)[2]	Wild garlic-rich Beech (*Hordely-Fagetum*)[2]
Humus type	Mull[3]	Mull[8]	Mull[14]
Soil Type WRB	Luvisol, Cambisol[1,3]	Luvisol[9]	Leptosol, Cambisol[14]
Clay content [%]	24.3[4]	21.4[10]	42.5[15]
Bedrock	Triassic limestone[5]	Triassic limestone[11]	Triassic limestone[14]
MAP [mm]	850[6]	700[12]	710[14]
MAT [°C]	8.0[7]	7.5[13]	7.4[14]

a.s.l.: above sea level; WRB: World Reference Base; MAP: Mean annual precipitation; MAT: Mean annual temperature

[1] Metzger et al. (2017)
[2] Ellenberg (1988)
[3] Schrumpf et al. (2014)
[4] Huss (2017)
[5] Küsel et al. (2016)
[6] TLUG (2011c)
[7] TLUG (2011f)
[8] TLWJF (2009)
[9] TLUG (2018a)
[10] Thüringen Forest (2007)
[11] TLUG (2018b)
[12] TLUG (2011a)
[13] TLUG (2011d)
[14] Meesenburg and Brumme (2009); tree age recalculated
[15] Meesenburg et al. (2009)

Goettingen Forest (GOT$_L$) is located 7 km to the east of Goettingen in Lower Saxony, Germany (Figure 3) on a plateau at about 420 m a.s.l. (Table 1). The site is surrounded by a fence to keep wild animals out. The almost pure European beech (*Fagus sylvatica L.*) stand is accompanied by ash (*Fraxinus excelsior*), maple (*Acer platanoides, Acer pseudoplatanus*), oak (*Quercus petraea, Quercus robur*), and elm (*Ulmus glabra*) trees with an average tree age of 151 years. The tree community is quite similar to the one at HAI$_L$ and POS$_L$, except for the oaks. The dense herb layer is dominated by wild garlic (*Allium ursinum*), wind-flower (*Anemone nemorosa* and *Anemone ranunculoides*) in spring; and wild ginger (*Asarum europaeum*) and dog's mercury (*Mercurialis perennis*) in summer (Meesenburg et al. 2011). Natural vegetation at this site would be a wild garlic-rich beech forest (*Hordelymo-Fagetum;* Ellenberg (1988). Soil conditions at the site are relatively humid, high in nutrient content; the soil texture of the upper soil layer is loose (Meesenburg and Brumme 2009). This is typical for wild garlic-rich forest and indicates high soil biological activity (Ellenberg 1988). The thin mull type litter layer (2–3 cm) at GOT$_L$ supports this hypothesis. In general, soils are shallow (20–50 cm) and can be characterized as Leptosols and Cambisols according to the WRB System (Meesenburg and Brumme 2009; WRB 2015). GOT$_L$ has the highest clay content of 38.5 % between 0–10 cm and of 46.5 % between 10–30 cm (Meesenburg et al. 2009).

The location is mainly underlain by rocks from the Middle Triassic and the soils developed from layers of Upper Muschelkalk. The bedrock material has a calcite content of about 95 % (Meesenburg et al. 2009). Average precipitation is about 710 mm at GOT$_L$ with an annual temperature of 7.4 °C (Meesenburg and Brumme 2009). Similar to POS$_L$, GOT$_L$ is part of the ICP Forest Level II long-term monitoring program (Thünen Institute of Forest Ecosystems 2018).

2.2   Sandstone bedrock material

The following section describes the three additional study sites Hummelshain, Holzland (Thuringia), and Solling (Lower Saxony) in detail. All three locations share their development over Triassic *Buntsandstein* formations. The dominant forest type is woodrush-beech forest (*Luzulo-Fagetum*) at all three sites. Those forest communities are usually species-poor and thrive on silicate rocks that are poor in bases, e.g. sandstone. In Central Germany, this type of beech forest would be the dominant natural vegetation. In the past, these stands have often been replaced by conifers (Ellenberg 1988).

Hummelshain (HUM$_S$). The north-east facing site lies 18 km to the south of Jena in southern Thuringia (Figure 3) at an elevation of about 280 m a.s.l. (Table 2). In contrast to all other sites, HUM$_S$ is located at a slope of circa 10–15 %. Like HAI$_L$, HUM$_S$ will become part of the Critical Zone Exploratory (CZE; pers. comm. Robert Lehmann, University of Jena). Mean annual precipitation is about 700 mm (TLUG 2011b) and mean annual temperature about 8.5 °C (TLUG 2011e).

The tree community is beech-conifer mixed forest, with European beech (*Fagus sylvatica L.*) being the dominant species. Spruce (*Picea abies*) and Pine tree (*Pinus sylvestris*) are accompanying species. Shrub and underground cover were not visible during sampling in early June. Younger trees are dominated by *Fagus sylvatica L.* This species would be dominating within a natural vegetation of woodrush-beech forest (*Luzulo-Fagetum*; Ellenberg 1988; Thüringen Forst 2011). Those communities are common on acidic soils that developed from silicate rocks poor in bases. A typical humus type for forests with almost no herb layer and nutrient poor soils is moder. This kind of humus usually develops under deciduous and coniferous forests, monocultures or cool climate conditions (Blume et al. 2016). The moder cover is richer in plant nutrients under such conditions and less acid than the mineral soil beneath. Therefore, plants that grow under such conditions usually have a more shallow root system and are more vulnerable to drought (Ellenberg 1988). Such litter moder type was also found at HUM$_S$. The underlying soil can be mainly described a Cambisol and Podzol (Thüringen Forst 2011; TLUG 2018a). HUM$_S$ is located within the natural region Saale-Sandstein-Plate and lies on the 'Volpriehausen'-Formation, consisting of middle *Buntsandstein* sediments, lower Triassic (TLUG 2018b). The tree stand is 134 years (2018) old on average.

Holzland (HOL$_S$). This site lies only 7 km to the north-east of HUM$_S$ (Figure 3) at an elevation of about 350 m a.s.l., facing north (Table 2). The Friedrich-Schiller University of Jena runs a research station at the site, which was established as so-called 'Grünes Auge' ('*Green eye*') in the 1930s and 1940s. This explains planting of deciduous trees (e.g. *Fagus* sylvatica *L.*) on a clear-cut area within a conifer forest to increase forest diversity. Within this process, the organic soil was piled to dams and the area in between was ploughed. Young, circa 0.5 m high European beech (*Fagus sylvatica L.*) trees were planted within the ploughed area with a distance of roughly 30 cm. The wavy morphology is still visible and shows disturbance of the plot. The total area of this site is only 250 m² (Großherr 2011). Even though the beech forest site was planted, natural vegetation would be woodrush-beech forest (*Luzulo-Fagetum*) on acid soil as described in Ellenberg (1988). This is supported by the development of Podzols at this site, which are usually found over sandstone bedrock material (Blume et al. 2016; TLUG 2018a). The moder type humus layer was thicker, compared to the limestone bedrock material sites; typical for Podzols as well (Blume et al. 2016). Typical for sandstone sites, the clay content is much lower with 3.5 % in 0–20 cm and 7.1 % in 20–35 cm depth as compared to the limestone sites (Thüringen Forst 2007). HOL$_S$ is underlain

by the 'Rothensteiner'-Formation (*Buntsandstein* sediments, lower Triassic; TLUG 2018a). Mean annual temperature is about 8.0 °C and mean annual precipitation is circa 700 mm (TLUG 2011f).

Table 2: Site characteristics of the three beech-forest locations on sandstone (HUM_S, HOL_S, SOL_S) bedrock in Thuringia and Lower Saxony, Germany

	04_Hummelshain	05_Holzland	06_Solling
Coordinates (WGS84)	N 50°45'50.0"; E 011°34'45.5"	N 50°47'40.3"; E 011°39'42.2"	N 51°45'40.3"; E 009°34'45.7"
Elevation [m] a.s.l.	280	350	504
Slope [%]	10–15	1	0
Exposition	NE	N	Plateau
Tree age [a] (2018)	134[1]	80–90[7]	171[9]
Natural Vegetation	Woodrush-Beech (*Luzulo-Fagetum*)[2]	Woodrush-Beech (*Luzulo-Fagetum*)[2]	Woodrush-Beech (*Luzulo-Fagetum*)[2]
Humus Type	Moder	Moder[8]	Moder[9]
Soil Type WRB	Cambisol, Podzol[1,3]	Podzol[3]	Cambisol[9]
Clay content [%]	NA	5.3[8]	17.0[10]
Bedrock	Triassic Bundsandstein[4]	Triassic Bundsandstein[4]	Triassic Bundsandstein[9]
MAP [mm]	700[5]	700[5]	1'190[9]
MAT [°C]	8.5[6]	8.0[6]	6.9[9]

a.s.l.: above sea level; WRB: World Reference Base; MAP: Mean annual precipitation; MAT: Mean annual temperature; NA: not available

[1] Thüringen Forst (2011); tree age recalculated
[2] Ellenberg (1988)
[3] TLUG (2018a)
[4] TLUG (2018b)
[5] TLUG (2011b)
[6] TLUG (2011e)
[7] Großherr (2011); tree age recalculated
[8] Thüringen Forst (2007)
[9] Meesenburg and Brumme (2009)
[10] Meesenburg et al. (2009)

Solling (SOL_S). The site is located on a plateau at an elevation of about 500 m a.s.l. (Table 2) 30 km to the north-west of Goettingen in Lower Saxony, Germany (Figure 3). Similar to POS_L and GOT_L, SOL_S is part of the ICP Forest Level II long-term monitoring program (Thünen Institute of Forest Ecosystems 2018). The plot is surrounded by a fence to keep wild animals out. The pure beech (*Fagus sylvatica L.*) stand is about 171 (2018) years old, representing the oldest forest within the study. The soil is covered by a spare herb layer, dominated by wood sorrel (*Oxalis acetosella*) and woodrush (*Luzula luzuloides*; Meesenburg and Brumme 2009). This plant community is typical for woodrush-beech forest (*Luzulo-Fagetum*), the natural vegetation in this region. Those communities usually develop on soils with low pH-values and base content (Ellenberg 1988). Those characteristics were particularly described for the SOL_S site by Meesenburg and Brumme (2009). In this work they also described the underlying geological unit as Triassic *Buntsandstein*. The common soil type is a Cambisol, covered by a moder type humus (Meesenburg and Brumme 2009). Cambisols indicate near-natural woodrush-beech forest. Under natural conditions, the small amount of bases produced by the sandstones suffices to prevent the development of real raw humus. This precludes soil podzolization which usually accompanies raw humus. Leaching of top soils in those stands only happens, when natural vegetation has been removed in the past (Ellenberg 1988). The average clay content is 17.0 % in both depth intervals, 0–10 cm and 10–40 cm (Meesenburg et al. 2009). Due to location and relative high elevation, the site is characterized by the lowest mean annual temperature of 6.9 °C and the highest annual precipitation of 1'190 mm (Meesenburg and Brumme 2009) of the study sites.

The above characterization of the six study sites shows that the two distinctive bedrock materials result in different site characteristics. Yet, the individual sites also show dissimilar properties independently of their bedrock materials. Four sites (HAI$_L$, POS$_L$, GOT$_L$, and SOL$_S$) are influenced by loess deposition. This suppresses the influence of the original bedrock material to some extent. The limestone sites show higher average clay contents (21–42 %) compared to the sandstone sites (5–17 %). The litter layer at the latter is moder compared to mull at the limestone sites. A mull type litter layer indicates that more nutrients are available and that the microbial activity is higher compared to moder. The natural vegetation at all sites would probably be beech forest, yet with different characteristics due to different bedrock materials. At the limestone sites, wild garlic-rich beech forests would dominate, which are unusually rich in spring-flowering geophytes and require high soil fertility, whereas the woodrush-beech forests at the limestone sites are less species-rich. This differences in species richness could have been observed for the individual study sites. MAP is quite similar for all sites, except for SOL$_S$. This results in higher variability at the sandstone sites (MAP: 700 to 1'190 mm) compared to the limestone sites (MAP: 700 to 850 mm); the same is true for the MAT (limestone sites: 7.4–8.0 °C; sandstone sites: 6.9–8.5 °C), probably related to the higher elevation (504 m a.s.l.). At the limestone sites, the elevation ranges from 365 to 420 m a.s.l, whereas the other two sandstone sites (HUM$_S$ and HOL$_S$) have an elevation of 280 and 350 m a.s.l., respectively. Cambisols are the dominant soil types among all six sites. Other soil types are Luvisol (POS$_L$) and Podzol (HUM$_S$). The latter one is the only site of the sandstone sites with a distinct slope of 10–15 % and no domination by beech-forest but by a beech-conifer mixed forest. At the limestone sites only HAI$_L$ is located on a slope of 5 %. The tree age is heterogeneous distributed between all sites, ranging from 80 years (POS$_L$ and HOL$_S$) to almost 200 years (SOL$_S$).

3.   Materials and Methods

This chapter delivers a detailed description of the sampling campaign and the techniques applied during laboratory work. It is divided into the sections 3.1 *Sampling*, 3.2. *Sequential chemical degradation* and 3.3. *Physical and chemical characterizations;* with the latter briefly explaining determinations done on the samples, including pH-value, C and N, as well as C-isotopic (^{13}C and ^{14}C) measurements. Section 3.2. about the sequential chemical degradation describes the related method development, the main focus of this chapter.

The laboratories at the Max-Planck-Institute for Biogeochemistry in Jena, Germany, apply good laboratory practice (GLP). Lab gloves were worn to avoid sample contamination at all times, during field sampling and in the labs. Glass equipment was pre-combusted by heating for 5 h at 500 °C (Thermo Scientific Heraeus WU 6100, Germany), and covered with pre-combusted aluminum foil until usage. Non-glass equipment, e.g. plastic spoons and tips, was not used in order to prevent samples from contamination through C-containing devices. This would have led to subsequent errors in radiocarbon analysis.

3.1.   Sampling

Two different depths (TOP and BOT) were sampled at each location (n = 6) with a pre-cleaned manual soil auger (Eijkelkamp, Netherlands). To reduce the direct influence of tree species on the physical and chemical soil composition, samples were always taken at a distance of at least 1 m to the next tree. After removing the litter layer carefully with laboratory gloves, TOP samples were taken from 0–10 cm depth. That hole was overdrilled thereafter to 30 cm. That material was discarded to prevent cross-contamination between the two samples. BOT samples were taken at the interface between soil and parent material, varying at the different sites from 30 to 60 cm. The interface was defined at the depth, where larger bedrock material (> 2 mm) became visible (Table 3). Three samples of 200–300 g were taken at each location and each depth (n = 36) to grant representativity. Those replicates were combined to one composite sample per location and depth (n = 12) in the lab. Samples were put into pre-combusted aluminum boxes in the field, covered with pre-combusted aluminum foil and stored in a cooling box during transport to the lab in Jena, Germany. After finishing the drilling, holes were closed with left-over soil and litter material to leave the site as undisturbed as possible.

Table 3: Sampling depths at the different locations

	01_Hainich	02_Possen	03_Goettingen Forest
TOP [cm]	0–10	0–10	0–10
BOT [cm]	30–40	50–60	30–40
	04_Hummelshain	05_Holzland	06_Solling
TOP [cm]	0–10	0–10	0–10
BOT [cm]	30–40	30–40	40–50

Following field work, samples were dried in their aluminum boxes at 50 °C for at least 72 h in a drying oven (Thermo Scientific Heraeus UT6760, Germany). When material could not be dried on the day of sampling, it was stored at -20 °C in aluminum boxes to avoid chemical or biological decomposition. After drying, larger root, plant and stone material was removed, before sieving through a 2 mm sieve. Larger soil aggregates were destroyed with porcelain mortar and pestle. Each sieved sample was again checked for non-soil material which, if found, was removed by hand. The sieve was cleaned for 15 min in an ultrasonic bath (Bandelin electronic Sonorex Super 10P DK 1028P, Germany) between different samples and

rinsed with dichloromethane (DCM). The porcelain mortar and other equipment used for siev-ing were washed with DCM as well and air-dried before preparing the next sample. Dried and sieved samples were stored at room temperature in glass flasks prior extraction. All meas-urements of the sieved samples were performed between June 2018 and February 2019.

3.2.   Sequential chemical extraction

Four sequential chemical degradation steps were performed to extract different SOM units, such as lipids, carbohydrates, amino acids, peptides, and phenolic monomers. Figure 4 shows a simplified scheme of the applied method. The detailed lab protocols can be found in the digital appendix.
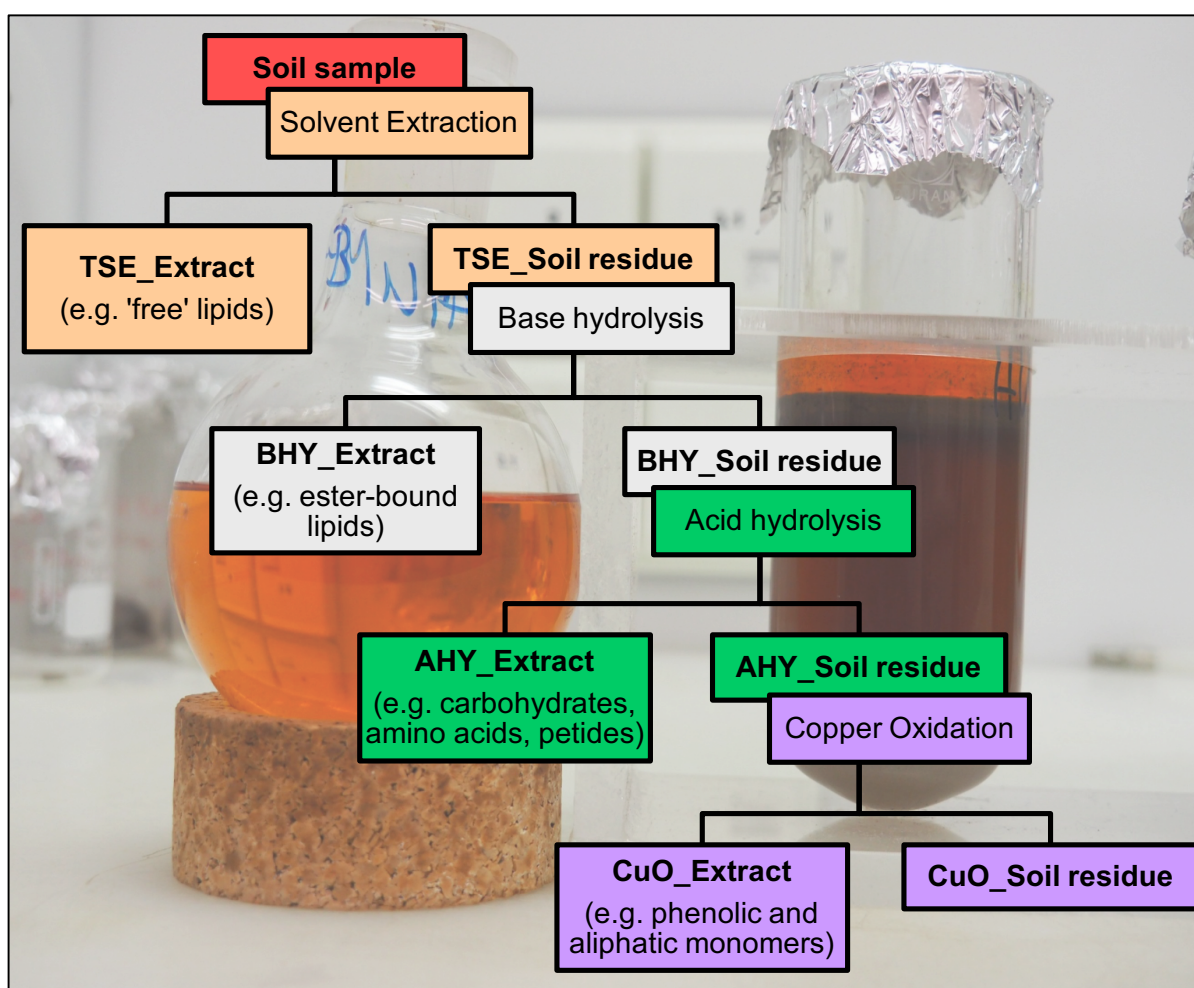
Figure 4: Simplified scheme of the sequential chemical extraction; TSE: Total solvent extraction, BHY: Base hydrolysis, AHY: Acid hydrolysis, CuO: Copper oxidation

The sequential extraction method, adapted from Otto and Simpson (2007), was initially test-ed with a random soil sample from Hainich National Park with two duplicates. This was done to ensure that the method works and to calculate the relative error between the two dupli-cates. Results of this test showed that the adapted method worked satisfactorily: the total error did not exceed 1 % RSD for the tested sample (Appendix A1). For practical reasons, minor amendments to the method were done prior to starting the extractions with the soil samples (e.g. centrifugation instead of filtration). The following section describes the chosen method in detail; test run results will not be discussed further in this work.

Total solvent extraction (TSE). From each dried soil sample (< 2 mm), 300 g were weighed (Mettler Toledo PB3002, Switzerland) into a beaker. The sample was sonicated (Bandelin electronic Sonorex Super RK103H, Germany) for 20 min at 25 °C with 300 mL of dichloromethane (DCM) as organic solvent. The usage of an organic solvent is a common technique to separate 'free' lipids from soil (Kögel-Knabner 2000). The liquid phase on top of the soil sample after the ultrasonic bath was collected with a filter system through glass microfiber filters (Whatman GF/F, England) under vacuum at 500 mbar. After removing the solvent phase, another 200 mL of DCM were added to the soil, sonicated for a second time, and collected with the same filter system. After the second filtration, the filter system was washed with DCM to remove any remaining soil residues. The collected liquid phase was then concentrated by rotary evaporation (BÜCHI Rotavapor R-114, Switzerland) at 40 °C and 500 mbar. The extract was thereafter dried under N_2 gas flow and transferred into pre-labeled and pre-weighted glass vials. The weight of this extract was determined to calculate the total yield of extractable ('free') lipids and stored in the glass vial at -20 °C until further analysis. The remaining soil residue from the first extraction step (TSE) was air-dried under the fume hood for several days and weighed as well, before performing the next (BHY) degradation step.

Base hydrolysis (BHY) was performed with the dry soil residue from the TSE extraction. The sample was re-wetted with 300 mL of 0.5 M potassium hydroxide (KOH) solution and put overnight under a total reflux system (Figure 5). Such system is used to heat up a liquid phase, and to collect and return its condensed vapors back to the system (Aditha et al. 2016). The system is placed on top of a round-bottom flask, which carries the reactant (soil) and the solvent (KOH). The reflux system is water-cooled to ensure that rising vapor condenses at the reflux system and flows back into the round-bottom flask at the bottom. Heating of the solution is necessary to increase the speed of the reaction time between reactant and solvent (Self 2005). For heating, a sand bath (PZ26-4, Präzitherm, Germany) was used at a temperature of 400 °C to gently boil the mixture within the round bottom flask.

After refluxing, 100 mL of 5 % sodium chloride (NaCl) was added to the mixture and transferred into a 1 L glass bottle. The pH-value was adjusted between 1 and 3 with 4 M HCl. 200 mL of methyl-tert-butylether (MTBE) were added to separate the solution into a watery and an organic phase. Ideally, the organic phase contains the ester-bound lipids, which have been extracted from the soil during refluxing. Phase separation usually took more than one day and was speeded up by stirring the solution from time to time. The upper organic phase (MTBE) was transferred into a fresh round-bottom flask. Separation of the two phases by adding MTBE to the soil mixture was repeated twice to increase efficiency of the BHY extraction. The organic phases of those repeated separation steps were combined and reduced with a rotary evaporator at 40 °C and 600 mbar. The soil mixture in the 1 L glass flask was separated from the remaining water phase by centrifugation at 3500 rpm for 15 min (Thermo Scientific Heraeus Megafuge 3.0R, Germany). The liquid phase was filtered through glass microfiber filters (Whatman GF/F, England) to remove any remaining soil in this phase. After centrifugation, leftovers of the organic solvent (MTBE) appeared on top of the solution, which were added to the combined extracts as well. The reduced and concentrated extract, containing the BHY products, was dried under constant N_2 flow in a pre-labeled glass vial. The soil residue was first put under the fume hood for several days to let the remaining solvent evaporate and put in the drying oven at 50 °C for another couple of days to completely dry the soil for the next (AHY) extraction step.

The base hydrolysis is an approved technique to extract ester-bound lipids from SOM that mainly stems from plant origin, yet an additional microbial-derived contribution is not unlikely (Naafs and van Bergen 2002). Ester-bound lipids are considered (bio)chemically labile compounds, yet they are commonly found in soils. Their abundance often increases with humification (Nierop et al. 2003). To calculate the total amount of ester-bound lipids in the soil, dried extract and soil residue were weighed.
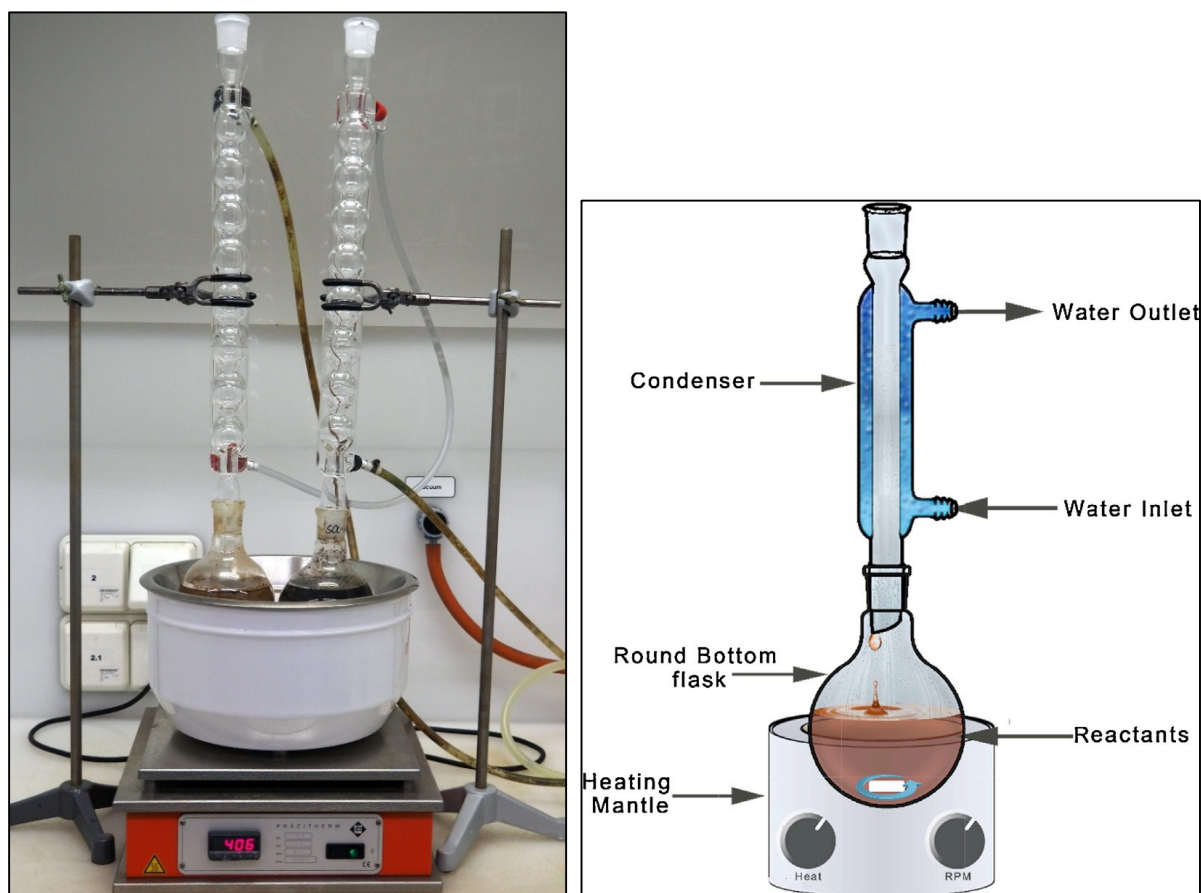
Figure 5: Left: Total reflux system with soil samples in round-bottom flasks; Right: Schematic picture of a total reflux system (from Aditha et al. 2016)

Acid hydrolysis (AHY) was done by hydrolyzing the dried soil residue after the BHY extraction under a reflux system (Figure 5) with 200 mL of 12 M HCl overnight. The solution was heated in a sand bath at 155 °C. After cooling, samples were centrifuged at 3500 rpm for 10 min at 24 °C to separate the liquid phase from the solid one. The liquid phase was decanted into a filter system and filtered through glass microfiber filters (Whatman GF/F, England) under vacuum. The remaining soil was transferred into pre-weighed petri-dishes and put under the fume-hood. This was done to ensure that most of the HCl evaporates under the fume-hood and not in a drying oven. After at least 48 hours, the petri-dish with the soil was completely dried in the oven at 50 °C, before performing the next (CuO) extraction step (see section below). To speed up the drying process, some of the soil samples were pre-dried with a rotary evaporator before putting them in the drying oven.

Water in the filtrate from the hydrolyzing step was evaporated with a rotary evaporator at 72 mbar and 50 °C until complete dryness. The dried extract was re-suspended with Milli-Q water (ultrapure water of Type 1, ASTM International D1193-91). After neutralizing the suspension with 1 M KOH to a pH-value between 6 and 7, the extract was centrifuged again at 3500 rpm for 10 min at 24 °C. This step helps removing any precipitate that may have

formed during the neutralization step (Otto and Simpson 2007). The liquid phase was then again evaporated until dryness with a rotary evaporator at 72 mbar at 50 °C. The dry extract was dissolved with methanol and centrifuged at 3500 rpm for 10 min at 24 °C to remove any salts, which were produced during the neutralization step (Otto and Simpson 2007). The liquid phase, containing the AHY products, was reduced with a rotary evaporator and dried under N_2 flow in a glass vial. The glass vial was stored at -20 °C to prevent any reaction and to keep it dry until further analysis. AHY products in the remaining extract are usually identified as carbohydrates, amino acids and peptides (Kögel-Knabner 2000; Martens and Loeffelmann 2003). To break down polymeric amino acid compounds such as peptides or proteins, a strong acid such as 12 M HCl is needed (Martens and Loeffelmann 2003). To quantify the total amount of the AHY products, the dried extract and the soil residue were weighed.

Copper oxidation (CuO) is the last step of the sequential chemical extraction. A PTFE (Teflon)-lined "bomb" reactor (Figure 6) is needed to perform this step. The reactor was self-built equipment from the former company Hermann Josef Groteklas Maschinen- und Stahlbau, Jülich, Germany. 200 g of the dried soil residue after AHY extraction was loaded in nine Teflon-lined bombs. Each bomb was first cleaned with acetone, then washed with isopropanol to minimize sample contamination risks during use (Ingalls et al. 2010). 10 g of pre-combusted copper oxide (CuO), 1 g of Ammonium–iron–II–sulfate–hexahydrate [$Fe(NH_4)_2(SO_4)_2 6H_2O$], and 25 mL of 2 M NaOH were added to each bomb. Before heating the Teflon-lined reactor for 2.5 h at 170 °C, the bombs were purged with N_2.
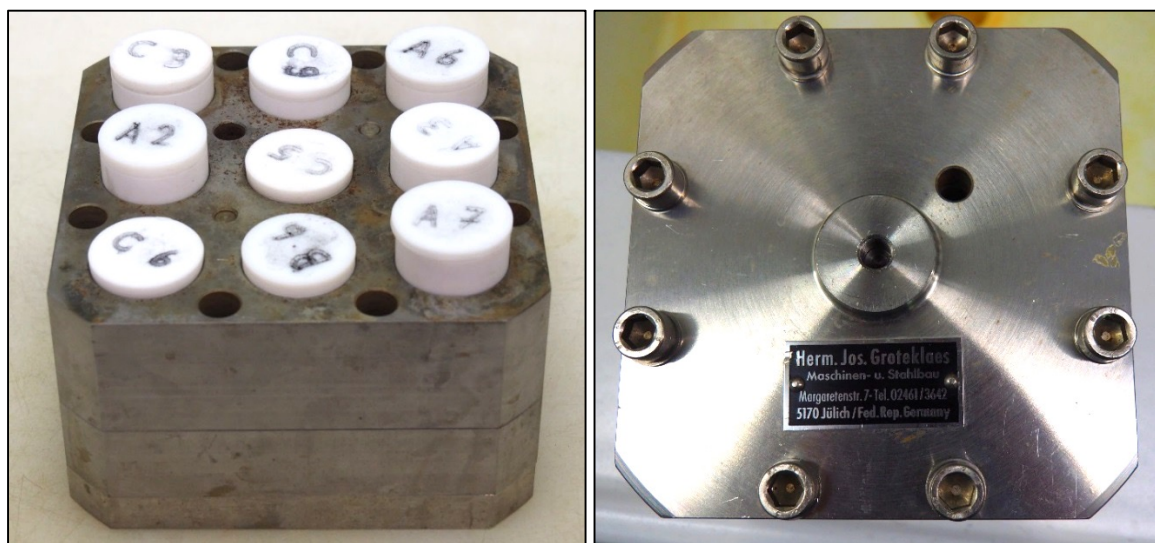
Figure 6: Teflon-lined "bomb" reactor. Left: Assembled with samples; Right: Closed

The CuO oxidation results in the extraction of phenolic and aliphatic monomers that indicate lignin, cutin, and suberin in soils (Hedges and Ertel 1982). Lignin is difficult to analyze chemically, because of its complex structure. Therefore, lignin needs to be depolymerized to be detectable with common chemical analytical instruments. CuO oxidation does not completely depolymerize lignin, but the method segregates aryl ether bonds and releases phenolic monomers. Consequently, this method is only a qualitative one. Yet, release and detection of monomers from the outer part of the lignin during the oxidation with CuO can be used as an indicator for lignin in the soil (Otto and Simpson 2006).

After heating, the bombs were cooled under running water; and the liquid phase was decanted into centrifuge tubes. The soil remaining in the bombs was transferred into a beaker to let

it dry in the oven at 50 °C for several days. The tubes were washed with Milli-Q water and the suspension was added to the centrifuge tubes. Samples in the tubes were centrifuged for 10 min at 3000 rpm (Thermo Scientific Heraeus Megafuge 1.0, Germany), acidified to a pH-value of 1 by using 6 M HCl, and kept for one hour in the dark at room temperature. This step is necessary to avoid polymerization of cinnamic acids (Otto and Simpson 2007). After another centrifugation for 20 min at 3000 rpm, the supernatant was transferred into a separation funnel. Circa 50 mL diethyl ether were added, and the solution then shaken gently to mix the watery phase (CuO extract) with the organic phase (diethyl ether) and to let it separate again. The lower, aqueous phase was discarded and the upper organic phase with the CuO products was collected in a round-bottom flask. After liquid-liquid extraction, the amount of the collected phase was reduced using a rotary evaporator. To remove any remaining water in the organic phase, the solution was filtered using a Na_2SO_4 column. The water-free ether phase, containing the CuO products, was completely dried under N_2 flow in a glass vial and weighed, just as the dried soil residue.

In conclusion, the described method results in four different fractions that can be differentiated by their chemical composition (Table 4), using, e.g. gas chromatography coupled with mass spectrometry (GC-MS). Due to time constraints, no GC-MS analyses were done in this work. As a consequence, the chemical composition of the individual fractions will be based on results from Otto and Simpson (2007).

Less than 20 % of the total extracted compounds were detectable by GC-MS in their work. The majority of the extraction products are likely high in molecular weight and/or too polar to be detectable by the selected GC column. Therefore, it should be noted that the detected components may be selective to the low molecular weight (LMW) and apolar or medium polarity compounds. Nevertheless, the authors showed that the method can be used to extract biomarkers from SOM to study biogeochemical cycles in soils (Otto and Simpson 2007). However, extraction methods can only be used to qualify certain compounds and not to quantify them, since the method is operationally-defined and empirical.

Table 4: Chemical components and their abundance in the four different fractions of the sequential chemical extraction method based on results from Otto and Simpson (2007)

Chemical components	Fractions			
	TSE	BHY	AHY	CuO
Aliphatic lipids	xxx	xxx	–	x
Steroids, terpenoids	xx	x	–	–
Benzyls, phenols	–	xx	–	xx
Carbohydrates	–	–	x	–
LMW hydroxy acids, polyalcohols	–	–	xxx	x
Amino acids	–	–	xx	–
Amino sugars and amides	–	–	x	–

LMW: low molecular weight; TSE: Total solvent extraction; BHY: Base hydrolysis; AHY: Acid hydrolysis; CuO: Copper Oxidation; x–xxx: relative abundance; –: no or very low abundance

The total solvent extraction (TSE) fraction contains various aliphatic lipids, steroids, and terpenoids. Those compounds indicate that a major input of lipids derived from higher plants and only minor amounts of microbial lipids. Yet, Otto and Simpson (2007) could only identify 30 % of the total compounds by GC-MS in the TSE fraction. Since this fraction mainly contains lipids that were extractable with an organic solvent, this fraction will be called 'free-lipids' from now on. The base hydrolysis (BHY) fraction also contains a series of aliphatic lipids. Additionally, benzyls, phenols, and small amounts of steroids and terpenoids were identified (Otto and Simpson 2007). The aliphatic lipids identified in this fraction are mainly de-

rived from vascular plants and contain only minor amounts of microbial organic matter, similar to the TSE fraction. Most of the compounds (96 %) in the BHY fraction were detectable with GC-MS. For practical reason, the samples derived from this fraction will be named 'ester-bound lipids'. The third fraction (AHY: acid hydrolysis) contains mostly LMW hydroxy acids and polyalcohols, amino acids, amino sugars, amides and carbohydrates. Amino sugars are specific for certain groups of microorganisms and are suggested as suitable biomarkers to estimate bacterial vs. fungal OM in soils (Otto and Simpson 2007; Zhang and Amelung 1996). However, only 5 % of the total AHY fraction could be identified by GC-MS (Otto and Simpson 2007). This fraction will be summarized as 'sugars'. Copper oxidation (CuO), the last fraction of the sequential extraction, consist mainly of phenols and benzyls. Minor abundance of aliphatic lipids and LMW acids were also detected. The CuO method is an established approach to analyze phenols derived from lignin. The detected benzyls are not derived from lignin but from proteins. In this fraction, Otto and Simpson (2007) were able to detect 19 % of the total CuO fraction. The samples of this extraction step will be called 'lignin'. For more detailed information about the composition of the individual fractions, the reader may be referred to Otto and Simpson (2007).

3.3. Physical and chemical characterization

Small sub-samples (20 g) of the soils were powdered with a mixer mill (Retsch MM 400, Germany) for 5 min at a frequency of 30 sec^{-1} for chemical (C and N content, C-isotope) characterization. This was done to ensure that the samples are homogenous and that no artifacts will be measured or analyzed.

Soil acidity/alkalinity was determined for all untreated bulk soil samples (n = 12). Small sub-samples (10 g) of the sieved (< 2 mm) soil material were transferred into 250 mL PE-bottles and 25 mL of deionized water was added. Samples were shaken overhead (Heidolph Reax 20, Germany) for 1 h and let rest for another 1 h afterwards. The pH-value was measured at room temperature with a single rod electrode (WTW SenTix 61, Germany) attached to a pH-Meter (WTW pH 538, Germany). Before the measurement, the pH-Meter was calibrated with two buffer solutions of pH = 4.006 and 6.865 (WTW Buffer Puffer, Germany).

For quality control, duplicates (n = 3) were measured simultaneously (Table 5). The precision of those samples was equal to, or better than 0.02. For further analysis, the mean value of each duplicate was used.

Table 5: Quality control of pH determination

Sample	Site	Depth	Bedrock	Duplicate	pH-value
HAI_A	Hainich	TOP	Limestone	1	5.83
HAI_A	Hainich	TOP	Limestone	2	5.82
GOT_B	Goettingen	TOP	Limestone	1	7.19
GOT_B	Goettingen	TOP	Limestone	2	7.17
HOL_B	Holzland	BOT	Sandstone	1	4.34
HOL_B	Holzland	BOT	Sandstone	2	4.36

Elemental carbon and nitrogen (CN) were determined by the *Routine Measurements & Analysis* (RoMA) lab, a scientific service group at the Max-Planck-Institute for Biogeochemistry, by using a Vario MAX CN instrument (Elementar Analysensysteme GmbH, Germany). 250 mg of fine soil from each sample (n = 60) was weighed (Mettler Toledo AT261 Delta-Range, Switzerland) into reusable ceramic cups. 400–500 mg of tungsten trioxide (WO_3) was added as a catalyst. Additionally, two reference samples, Soil 1 (IVA Analysetechnik, Germany) and Soil 1.1 (HEKAtech Analysetechnik, Germany), were prepared and measured

simultaneously. Both are certified reference materials with a mean total carbon (TC) content of 3.50 ± 0.07 wt-% and 3.43 ± 0.06 wt-% respectively. The N content is 0.22 ± 0.01 wt-% for Soil 1 and 0.23 ± 0.01 wt-% for Soil 1.1. The values of the two reference materials are relatively close to each other, because Soil 1 will be replaced by Soil 1.1 in the future. The standard Soil 1 has an OC content of 2.28 ± 0.20 wt-%, resulting in an inorganic carbon content of 1.22 ± 0.27 wt-%. For the other standard no certificated values are available for the organic and inorganic C content. The lower limit of quantification (LLQ) was 0.03 wt-% for C and 0.01 wt-% for N, whereas the upper limit of quantification (ULQ) was 0.15 wt-% for C and 0.04 wt-% for N.

Samples were transferred into the combustion tube filled with WO_3 and heated to a temperature of 1100 °C to be measured. After introduction of a sample, the carrier gas helium was temporarily mixed with pure oxygen; flash combustion takes place. Quantitative oxidation is achieved by passing the gases over the catalyst. A second combustion tube, filled with a blend of copper oxide and platinum, was heated to 900 °C. Once sample combustion had been accomplished, the gas mixture moved into a reduction tube filled with tungsten trioxide and was heated to 830 °C. Excess oxygen was eliminated, and nitrogen oxide (NO_2) reduced to nitrogen (N_2). A small packing of silver wool adsorbed any halogens. The gases (N_2 and CO_2) were separated by absorbing CO_2 on heatable columns. Therefore, N_2 passed through these columns first, and was measured by thermal conductivity detector (TCD). After integration of the N_2 signal, CO_2 was released from the adsorption column, passed to the TCD, and measured. For the two measured elements (CN) two different peaks were recorded. The concentration of each element was determined using the area under the peak and the sample weight (Elementar Analysensysteme n.d.).

To measure the inorganic C content of the samples, 250 mg of each sample was combusted at 450 °C for 16 h in a muffle furnace (Heraeus Instruments M110, Germany). This method is the so-called Muffle-Furnace-Method (MFM) resulting in the combustion of any organic C in the sample. After combustion, 400–500 mg of WO_3 were added to the remaining soil and measured with the same Vario MAX CN instrument and method as described before.

To calculate the organic C (OC) content of the sample, the following equation (1) was used. Where TC is the total amount of C in the sample, and IC the inorganic C content.

$$OC = TC - IC \quad (1)$$

For quality control, a daily factor for the Vario Max CN is determined by regular re-analysis of pure organic reagents. The factor is re-calculated after measuring about 20 samples to correct for possible drift. As mentioned before, to test accuracy and reliability of the results, reference materials are analyzed on a regular basis. The TC content of the two standards was always in the range of the reported error. The IC content of the Soil 1 standard was always at the lower range of the reported IC value, yet still within the error. Additionally, every five samples (n = 12), a replicate was measured for total and inorganic C. The precision of the measured duplicates was equal to, or better than 0.01 wt-% for C and N, except for the samples HUM-A_TSE and POS-B where the precision for C was 0.03 wt-% and 0.05 wt-% respectively (Appendix A2). For further analysis, the mean value of each duplicate was used.

The C content of the extracts (n = 48) was quantified with an elemental analyzer which is coupled to an isotope-ratio mass spectrometer. The method will be described in the following section.

Carbon stable isotopic composition (^{13}C) of the samples (n = 108) were determined using a DeltaPlus isotope ratio mass spectrometer (Thermo Fisher, Germany) coupled via a ConFlow III open-split to an elemental analyzer (Thermo Fisher Scientific Carlo Erba 1100 CE analyzer, Italy). Analysis was performed by the *Stable Isotopes Laboratory (IsoLab)*, a scientific service group at the Max-Planck-Institute for Biogeochemistry, Jena.

Samples, reference material aliquots, and blanks are weighed into small tin capsules. The elemental analyzer is needed to combust the sample into gases such as CO_2, N_2O, SO_2, and H_2O. For isotope ratio determination the product gases have to be purified or separated from each other before being introduced into the mass spectrometer (Werner et al. 1999). For separation, a coupling interface is used. The ConFlow III includes two open splits, one for the coupling, the other one for reference gas introduction. The coupling split can be varied over a wide range from zero to 64-fold dilution of the effluent stream without causing detectable isotopic fractionation. The ConFlow III directs one of the gases to the ion source of the isotope mass spectrometer, while the other gas flows to a waste vacuum line, and the other way around. The ion currents are measured separately from each other and compared a number of times. The measured relative difference in ion current ratios is then calculated relative to an internationally agreed isotope ratio scale (Werner and Brand 2001). The δ^{13}C values are given on the δ^{13}C IAEA-603 – LSVEC scale by analyzing the samples against a calibrated in-house-standard (Acetanilide: -30.06 ± 0.05 ‰). A quality control standard (Caffeine: -40.46 ± 0.11 ‰) was interspersed between samples. Additionally, duplicates of the soil extracts (n = 12) and residues (n = 15) were measured. The precision of the standards and duplicates was equal to, or better than 0.4 ‰. This is not true for the duplicates of the soil residue sample POS-A_BHY which had a precision of 0.7 ‰ (Appendix A3). For further analysis, the mean value of each duplicate was used.

Soil samples (n = 5) with an IC content above the upper limit of quantification (Table 6 and 7; Chapter 4) needed to be decalcified before measuring the δ^{13}C value. For each sample, duplicates were treated with 160 µL of sulfurous acid (H_2SO_3) and dried at 50 °C. The measurement itself was done the same way as described above.

δ^{13}C values are calculated using equation (2), where 13Rsample is the ^{13}C/^{12}C ratio of the sample, and 13Rstandard denotes the ^{13}C/^{12}C ratio of the standard. Values are expressed in per mil (‰) by multiplying the δ value with the factor 1000 (Brand and Coplen 2012; Coplen 2011).

$$\delta^{13}C = \left(\frac{13\text{Rsample} - 13\text{Rstandard}}{13\text{Rstandard}} - 1 \right) * 1000 \qquad (2)$$

Isotope ratio measurements are often disturbed by interfering ion currents from other species hitting the same Faraday cup detectors. When using CO_2 gas, δ^{13}C cannot be measured independent of the oxygen isotope ratio. Therefore, and because of the abundance of different C-isotope ratios, CO_2 contains a number of species with different masses. Those masses occur at the mass-to-charge-ratios m/z = 44, 45, and 46 for CO_2. All combinations of stable isotopes are present after combusting the sample to CO_2. However, some of the abundances are smaller and can be neglected when determining δ^{13}C, others need to be taken into account and corrected (Werner and Brand 2001). Such corrections have been done to all of the samples by the IsoLab service group.

Carbon radioactive isotopic composition (^{14}C). Accelerator mass spectrometry (AMS) is a technique to determine isotope ratios by combining mass spectrometry with an accelerator. Such a combination is needed, since the ratio of radioactive isotopes (e.g. ^{14}C) is below the

detection limit of conventional mass spectrometry (Steinhof 2016). [14]C measurements of all soil samples (n = 60) and extracts (n = 48) were done at the [14]C Laboratory in Jena, Germany. The ^{14}C-Analytik service group uses a 200 kV accelerator (MICADAS: Mini carbon dating system) with simultaneous injection of all three C-isotopes (^{12}C, ^{13}C, ^{14}C; Steinhof et al. 2017).

Samples (n = 44) that contained no significant IC were directly combusted in the elemental analyzer (NC2500, Carlo Erba, Italy). The combustion is done in a pre-baked sealed quartz tube which is filled with pre-baked copper oxide (CuO) and silver (Ag) wire. CuO is added to provide oxygen for the oxidation, and Ag is needed to remove sulfur and chlorine that might be in the sample and would interfere with C oxidation. The quartz tube with the sample and chemicals is evacuated and flame-sealed with a small torch. Afterwards, the sample is transferred into a muffle furnace and combusted at 900 °C (Trumbore et al. 2016). Samples (n = 23) that contained IC require chemical pretreatment (decalcification) before combustion to avoid contamination of old carbonates with SOM. 500 µL of H_2O are added to wet the sample, followed by 500 µL of 8 M HCl. The samples were shaken for 1 h, before controlling the pH-value to be ≤ 2. Before transferring samples into the elemental analyzer (EA), they need to be dried again (Steinhof et al. 2017).

The dry extracts from the sequestration were solubilized with the last solvent respective before transferring the samples with a Hamilton syringe into pre-combusted silver capsules. The solution was dried again in a drying oven before combustion with the EA. Sample weight depends on the C content of each sample or extract. To precisely measure ^{14}C, a sample should at least contain 0.5 mg C/g (Steinhof et al. 2017).

After production of CO_2 from a sample in the EA, 5–10 % of the gas is measured with an isotope ratio mass spectrometer (Delta Plus, ThermoQuest, Germany) to obtain the ^{13}C value of the sample. The rest of the produced CO_2 are separated from other gases (e.g. N_2, O_2, and H_2O) by using a chemical trap, before graphitization and analysis for [14]C. Graphitization is performed with hydrogen (H_2) as reducing reagent and iron as catalyst (Steinhof et al. 2017). After sample injection, it is split into atoms in the ion source by adding or removing electrons. For ^{14}C, the ionization results in negative ions to suppress ^{14}N, which has the same mass as ^{14}C, yet cannot form negative ions. The negative C ions are further accelerated away from the ion source. After acceleration, the ions are filtered by a high-energy beam-line and counted by the detector (Steinhof 2016).

The modern ^{14}C isotopic ratio (^{14}C/^{12}C) is defined as 95 % of the NIST (National Institute of Standards and Technology) Oxalic Acid I (OX-I) standard, measured in 1950. Both measurements are corrected for isotopic fractionation. Similar to the stable isotope ^{13}C, ^{14}C concentrations in the environment are affected by mass-dependent-fractionations. To gain meaningful radiocarbon results, this effect needs to be removed. [14]C fractionation is roughly twice as big as that of ^{13}C, since the mass difference between 12 and 14 is twice than between 12 and 13. Correction is done by normalizing the ^{13}C value to -25 ‰ (Steinhof 2013; Stuiver and Polach 1977; Trumbore et al. 2016).

As all radioactive materials, the OX-I standard undergoes radioactive decay over time. Therefore, the ^{14}C/^{12}C ratio will change depending on the year of the measurement. To detect the absolute amount of ^{14}C in a sample, radioactive decay of the OX-I standard from 1950 needs to be corrected for the year of measurement, using the half-life of 5730 years (mean lifetime = 8267 years). In the literature, the absolute amount of radiocarbon is expressed as $\Delta^{14}C$ in ‰ (Trumbore et al. 2016). Expressed this way, $\Delta^{14}C$ values larger than zero indicate the presence of bomb-produced radiocarbon, and those below zero indicate on

average that the sample has been isolated from exchange with atmospheric $^{14}CO_2$ for at least the last hundreds of years (Gaudinski et al. 2000). It is calculated by using equation 3 (Trumbore et al. 2016) and used to report $\Delta^{14}C$ values in this work.

$$\Delta^{14}C = \left[\frac{\left[\frac{^{14}C}{^{12}C}\right]_{sample,-25}}{0.95\left[\frac{^{14}C}{^{12}C}\right]_{OXI,-19} exp\left(^{(y-1950)}/_{8267}\right)} - 1 \right] \times 1000 \qquad (3)$$

The corrected $\Delta^{14}C$ values for all samples were provided by the ^{14}C-Analytik service group in Jena. Samples made from the C1, C5, C6, and C7 IAEA (International Atomic Energy Agency) reference material were used as standards, as well as from the OX-I and NOX (New Oxalic Acid) materials from NIST. NOX was used as a reference standard based on the well-measured ratio NOX to OX-I (Steinhof 2013). For detailed information about the IAEA standards, see Le Clercq et al. (1998).

The uncertainties of each sample are based on statistical uncertainty of the number of ^{14}C counts and the scattering of the single measurements of the respective sample plus a contribution from the calibration (Steinhof 2013). For the soil samples (n = 53) and the extracts (n = 48) the error did not exceed 4.9 ‰ (median: 1.9 ‰) and 2.0 ‰ (median: 1.8 ‰) respectively (Appendix A4), which is in the range of the analytical error of this method (Steinhof 2016).

Soil samples (n = 7) that had C contents below 0.5 % require a different sample preparation to gain meaningful results. Instead of graphitizing the samples, CO_2 is used as ion source. Yet, the disadvantage of this method is a lower ion current and a higher background as compared to the conventional method (Steinhof 2016). To reduce the error for each sample, individual samples were measured in duplicate or triplicate. The values ($\Delta^{14}C$) and the errors of each sample and each measurement were averaged using equation 4 (Roos et al. 1982).

$$\bar{x} \pm \delta\bar{x} = \left(\sum_i w_i x_i \Big/ \sum_i w_i \right) \pm \left(\sum w_i \right)^{-1/2}$$

$$w_i = (1/(\delta w_i)^2) \qquad (4)$$

With $\bar{x}$ and $\delta\bar{x}$ being the value and its error, respectively. The letter i indicates the number of n experiments. After calculating the weighted averaged for each of the seven samples the error ranged between 2.8 and 4.9 ‰ and is within the acceptable range and comparable with the graphitization method (Appendix A4).

4.   Results and Discussion

This chapter presents and discusses the results of the untreated bulk soil samples (4.1) and of the individual fractions of the sequential chemical extraction (4.2). A detailed table with all chemical and physical results for each single sample can be found in the appendix (A5 and A6). All statistical analyses and graphs were performed with the program *R* (3.4.3) using the package *tidyverse*, including *ggplot2*.

4.1   Bulk soil samples

Results of the bulk soil samples from the three limestone (HAI_L, POS_L, GOT_L) and the three sandstone sites (HUM_S, HOL_S, SOL_S) are presented and discussed. Samples from all sites represent the TOP (0–10 cm) and BOT (30–60 cm) layers.

Soil acidity/alkalinity can be used as an indicator for species composition and the function of plants and soil organisms (Blume et al. 2016), as well as for SOM stabilization (Nierop et al. 2003; Rasmussen et al. 2018). However, the relationship between pH and SOM stabilization is only indirect and very complex. The SOM stabilization mechanisms vary with increasing soil pH from predominantly organomineral complexation, to calcium complexation and cation bridging (Rasmussen et al. 2018).

The three limestone sites show significantly higher pH-values (median: 6.6) than the sandstone sites (median: 4.2; Table 6). TOP sample pH-values (median: 4.1) from all sites are significantly lower than those from BOT samples (median: 5.9). The pH-value range at the sandstone sites (4.0–4.6) is small compared to the limestone sites (4.2–7.5), especially at the TOP layers. This indicates that the limestone sites show higher variance than the sandstone sites. At the limestone sites, differences between TOP (median: 5.8) and BOT (median: 7.2) are larger than those at the sandstone sites (TOP: 4.0, BOT: 4.4). Yet, the pH-values of all six sites are within the preferred and common range of plants, microorganisms and soil animals in temperate regions (Blume et al. 2016).

Table 6: Physical (pH) and chemical (CN, $\delta^{13}C$ $\Delta^{14}C$) characteristics of TOP (0–10 cm) and BOT (30–60 cm) bulk soil samples for limestone (HAI_L, POS_L, GOT_L) and sandstone (HUM_S, HOL_S, SOL_S) sites

	Limestone						Sandstone					
	HAI_L		POS_L		GOT_L		HUM_S		HOL_S		SOL_S	
	TOP	BOT	TOP	BOT	TOP	BOT	TOP	BOT	TOP	BOT	TOP	BOT
pH	5.8	7.1	4.2	7.5	6.2	7.2	4.0	4.3	4.0	4.4	4.0	4.6
IC [wt-%]	LLQ	0.05	LLQ	1.39	0.08	0.63	LLQ	LLQ	LLQ	LLQ	0.04	LLQ
SOC [wt-%]	3.02	1.65	2.02	0.47	6.02	2.94	2.54	0.71	2.34	0.64	4.42	1.61
TN [wt-%]	0.26	0.15	0.12	0.05	0.53	0.27	0.13	0.04	0.10	0.03	0.26	0.11
C/N	12	12	17	9	11	11	20	18	23	21	17	15
$\delta^{13}C$ [‰]	-26.90	-25.90	-27.42	-25.66	-25.98	-25.75	-27.80	-27.7	-27.53	-27.11	-27.19	-27.44
$\Delta^{14}C$ [‰]	13.5	-44.8	2.8	-495.8	-89.9	-177.3	18.4	-19.9	47.5	-37.9	-11.9	-231.0

IC: Inorganic carbon; SOC: Soil organic carbon; TN: Total nitrogen; LLQ: below lower limit of quantification

All three **limestone sites** show slightly acidic to acidic pH-values in the TOP layer. HAI_L and GOT_L have less acidic soil conditions with pH-values of 5.8 and 6.2, respectively. The POS_L soil shows a much lower pH-value (4.2), resembling soils from the sandstone sites. That low pH value can be explained by a distinct carbonate-free loess cover. This applies to all limestone sites with pH-values below 7 (Section 2.1). Yet, POS_L has the thickest loess layer (up to 60 cm) of all three sites, resulting in the lowest pH-value (pers. comm. Rüdiger Süß, Thüringen Forst Gotha). The loess layer does not influence the lower layers (BOT) much, which show neutral to slightly alkaline soil conditions. All three limestone sites become slightly alkaline in the BOT layer due to the carbonate containing bedrock material (Figure 7), with POS_L having the highest pH-value (7.5) and HAI_L the lowest (7.1). Such pH-values (TOP and BOT) are an indicator that those sites will be dominated by bacteria, which prefer a pH range of 5–7. In contrast, fungi-dominated soils usually show a pH value below 5 (Blume et al. 2016). The measured pH-values at the three sites correspond well with Meesenburg et al. (2009), Schrumpf et al. 2013 and Thüringen Forst (2016).
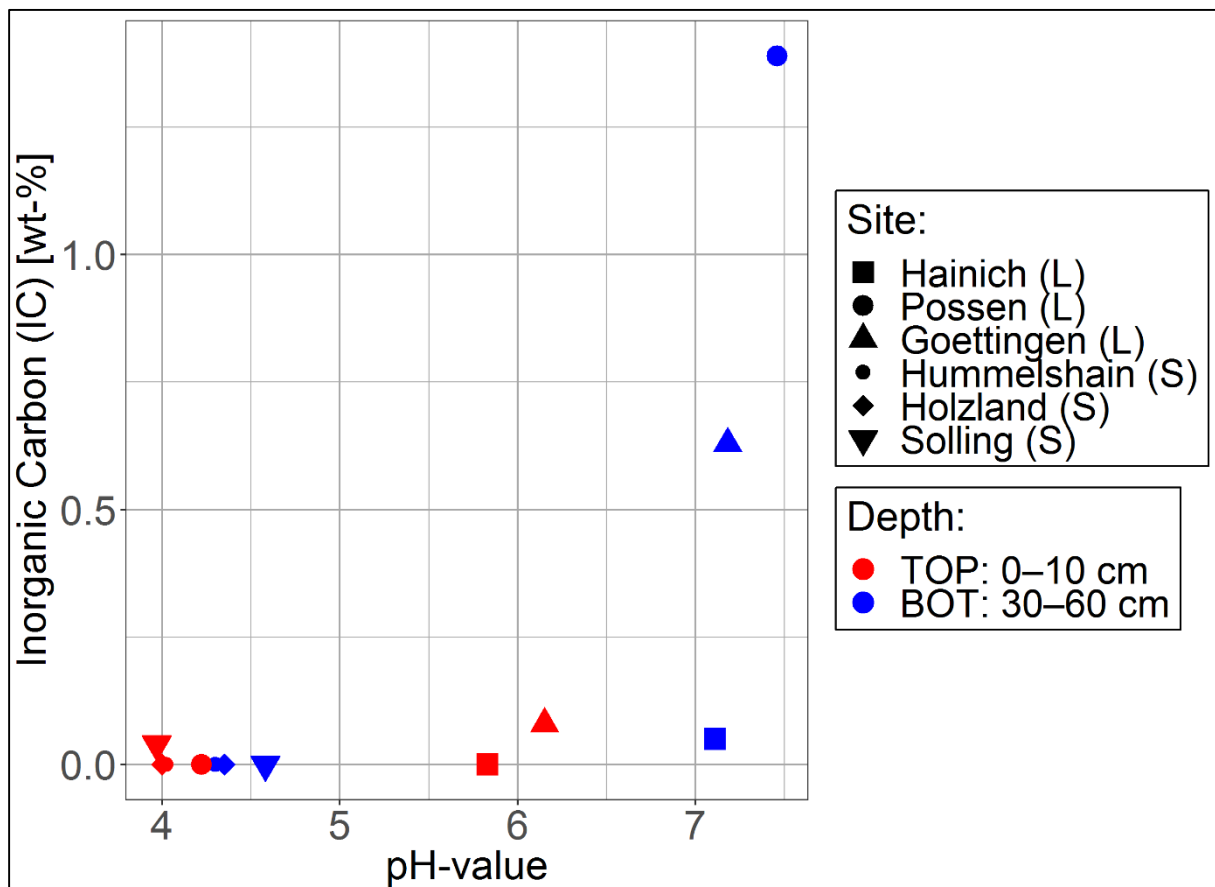

Figure 7: pH_{H2O} and IC [wt-%] of TOP (0–10 cm) and BOT (30–60 cm) bulk soils samples for the limestone (HAI_L, POS_L, GOT_L) and the sandstone (HUM_S, HOL_S, SOL_S) sites. Samples below LLQ were set to 0 for IC.

All **sandstone sites** show acidic soil conditions at both depths. In the TOP layer (0–10 cm), all three sites have pH-values of 4.0. In the BOT layer (30–60 cm), HUM_S has the lowest pH-value (4.3) and SOL_S the highest (4.6). It can be assumed that the soils at those three sites developed under similar conditions. pH-values below 5 suggest the dominance of fungi that prefer acidic soil conditions in contrast to bacteria (Blume et al. 2016). The measured pH-values at SOL_S and HOL_S correspond well with Meesenburg et al. (2009) and Thüringen Forst (2016). No references were found for HUM_S because no soil observation studies have

been conducted at that site yet. Higher pH-values in BOT samples compared to TOP samples likely results from interactions with alkaline weathering products that consume protons (Blume et al. 2016; Figure 7).

Elemental carbon and nitrogen quantification showed that two samples from the BOT layer (POS_L and GOT_L; Table 6) contained significant amounts of inorganic carbon (IC). Significant is defined here as values above the upper limit of quantification (ULQ = 0.15 wt-%): POS_L 1.39 wt-%, GOT_L 0.63 wt-% IC. The total carbon (TC) of those two samples is 1.86 wt-% and 3.57 wt-%, respectively. By extracting IC from TC, this results in an organic carbon (OC) content of 0.47 wt-% for POS_L and of 2.94 wt-% for GOT_L. For the other samples (n = 10) TC equals OC (Table 6). The C_{org}/N ratio is calculated from the OC content and will be expressed as C/N from now. Since only the BOT layer of the limestone sites contain significant IC, the observations made by the pH-value determination (only alkaline soils in the BOT layer) are confirmed (Figure 7). Yet, HAI_L does not contain any significant IC. This phenomenon might be caused by unintentionally sampling the loess layer only. The soil profiles at HAI_L are relatively shallow, with a median depth of only 37 cm (Metzger et al. 2017). Sampling depth was deepest at POS_L (up to 60 cm), which might explain the relative high IC content of 1.39 wt-% compared to the other carbonate containing samples.

Soil organic carbon (SOC) has, in interaction with N, an important influence on all soil functions and on the global C cycle (Blume et al. 2016). Median SOC values of the limestone sites are higher at both layers (TOP: 3.02 wt-%, BOT: 1.65 wt-%) than those of the sandstone sites (TOP: 2.54 wt-%, BOT: 0.71 wt-%; Table 6). Since SOM is the main source of **N** in soils, the behavior of N resembles the one of SOC at all sites. Limestone sites have higher N content (TOP: 0.26 wt-% and BOT: 0.15 wt-%) than sandstone sites (TOP: 0.13 wt-%, BOT: 0.04 wt-%). The distribution of the sites with the lowest and highest N is the same as for SOC for all sites (Table 6).

SOC values vary less between the sandstone sites; similar to their pH-value behavior. Yet, differences between the TOP and BOT layers (Δ = 1.83 wt-%) are larger compared to the limestone sites (Δ = 1.37 wt-%), which is contradictory to the pH-values. It is likely that the root system at the sandstone sites is shallower compared to the limestone sites (Section 2.2), resulting in less C input from roots into deeper soil layers. However, SOL_S shows SOC concentrations that are comparable with the one from the limestone sites. SOL_S receives relatively high mean annual precipitation (MAP: 1'190 mm). The elevated precipitation may increase bioactivity, resulting in a higher decomposed SOC content, and trigger the transport of dissolved organic matter into deeper layers. Several studies have been investigating the effect of climate on the SOC content of soils. Yet, the results are inconclusive (Blume et al. 2016), and direction and magnitude of C response to climate change remains unclear (Doetterl et al. 2015). The authors of this study suggest that soil C storage is more dominated by an interaction between climate and soil geochemistry on the larger scale. They found a positive relation between MAP and SOC.

On average, the higher SOC content over limestone corresponds with its higher clay content of 17–47 % as compared to that of the sandstone sites (clay content: 5–17 %; Figure 8). Under similar climatic conditions and with the same C supply, soils developing from limestone (clay-rich) usually have a finer texture than soils from sandstone (sandy or silty soils), resulting in a higher content of OC and N (Welte 1969; Wlotzka 1972). The higher C content at the limestone sites and the positive relationship between clay content and C at these sites can be explained by i) Higher sorption capacity of clay minerals, aluminum and iron oxides to sorb organic substances and thus inhibit microbial decomposition, ii) Higher content of ag-

gregates, where C compounds are protected from decomposition by microorganisms, and iii) More frequent occurrence of anoxic conditions (Blume et al. 2016). However, the clay content at all sites increased or remained the same with depth, whereas the SOC content decreased (Figure 8). This supports the hypothesis, which has been pointed out by several other studies (Rasmussen et al. 2018; Schmidt et al. 2011) that the clay content alone cannot predict SOC content and that depth is a better predictor for SOC independent of bedrock material.
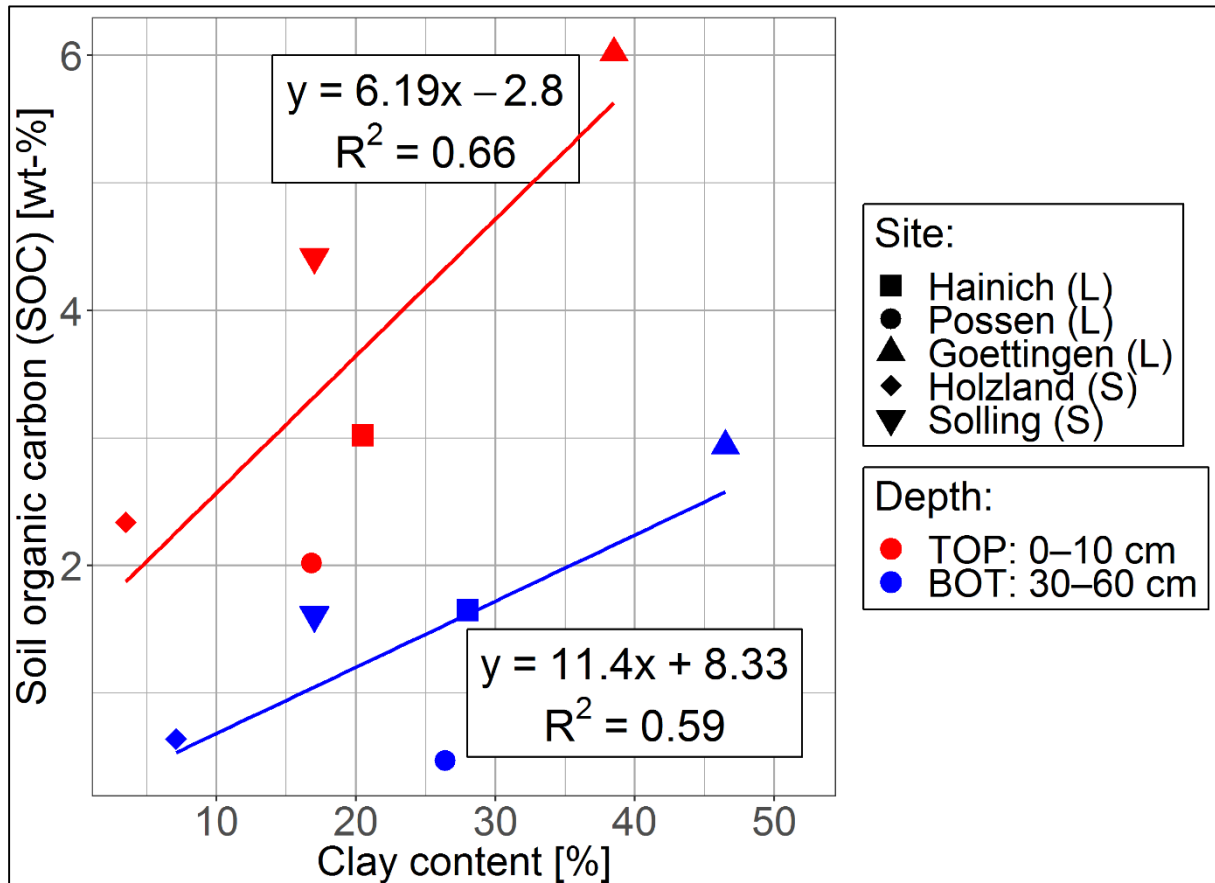
Figure 8: Soil organic carbon (SOC) [wt-%] and clay content [%] of TOP (0–10 cm) and BOT (30–60 cm) bulk soil samples for limestone (HAI$_L$, POS$_L$, GOT$_L$) and sandstone (HOL$_S$, SOL$_S$) sites. Clay data from Huss (2017), Meesenburg et al. (2009), and Thüringen Forst (2007); No data available for HUM$_S$.

The lower SOC content at the sandstone sites results in significant higher C/N (median: 19) compared to the limestone sites (median: 11; Table 6). Lower C/N ratios (7–15) are typical for soils with higher clay content and for a mull-type litter layer (Blume et al. 2016). Both characteristics apply to the limestone sites (Section 2.1). C/N ratios of 10–12 generally indicate that SOM is intensively processed (Rumpel and Kögel-Knabner 2011). The larger C/N ratios of the sandstone sites is common for moder type litter with typical C/N ratios of about 20 (Blume et al. 2016). Apparently, the limestone SOM seem to be more processed than that of sandstone and more N is available per unit C. Both types (limestone and sandstone) show slightly decreasing C/N ratios with depth (limestone: TOP: 12, BOT: 11; sandstone: TOP: 20, BOT: 18). This indicates that the BOT layers are more processed than the TOP layers. It is also likely that the SOM at lower depths contains more organic material from microorganisms than from plants. Microorganisms usually have a C/N ratio between 5 and 12, whereas for higher plant materials this ratio is between 15 and 300 (Gleixner 2013).

The variation of the C/N ratios is quite narrow at the **limestone sites**, except for POS$_L$. There, the highest C/N value (17) occurs in the TOP layer and the lowest (9) in the BOT layer, whereas the ratios of HAI$_L$ and GOT$_L$ range between 11 and 12. The large difference between TOP and BOT layers at POS$_L$ corresponds with the high increase of the pH-value (Δ = 3.3; Figure 9) and relative high increase of the clay content (Δ = 10 %; Figure 8) between the two layers. The low pH-value in the TOP layer may reduce the microbial activity, resulting in less processed organic material. In contrast, GOT$_L$ shows no difference between the TOP and BOT layers, resulting in an overall C/N ratio of 11. Reported C, N, and/or C/N ratios, correspond well with Huss (2017), Meesenburg et al. (2009), Schrumpf et al. (2013) and Thüringen Forst (2016).
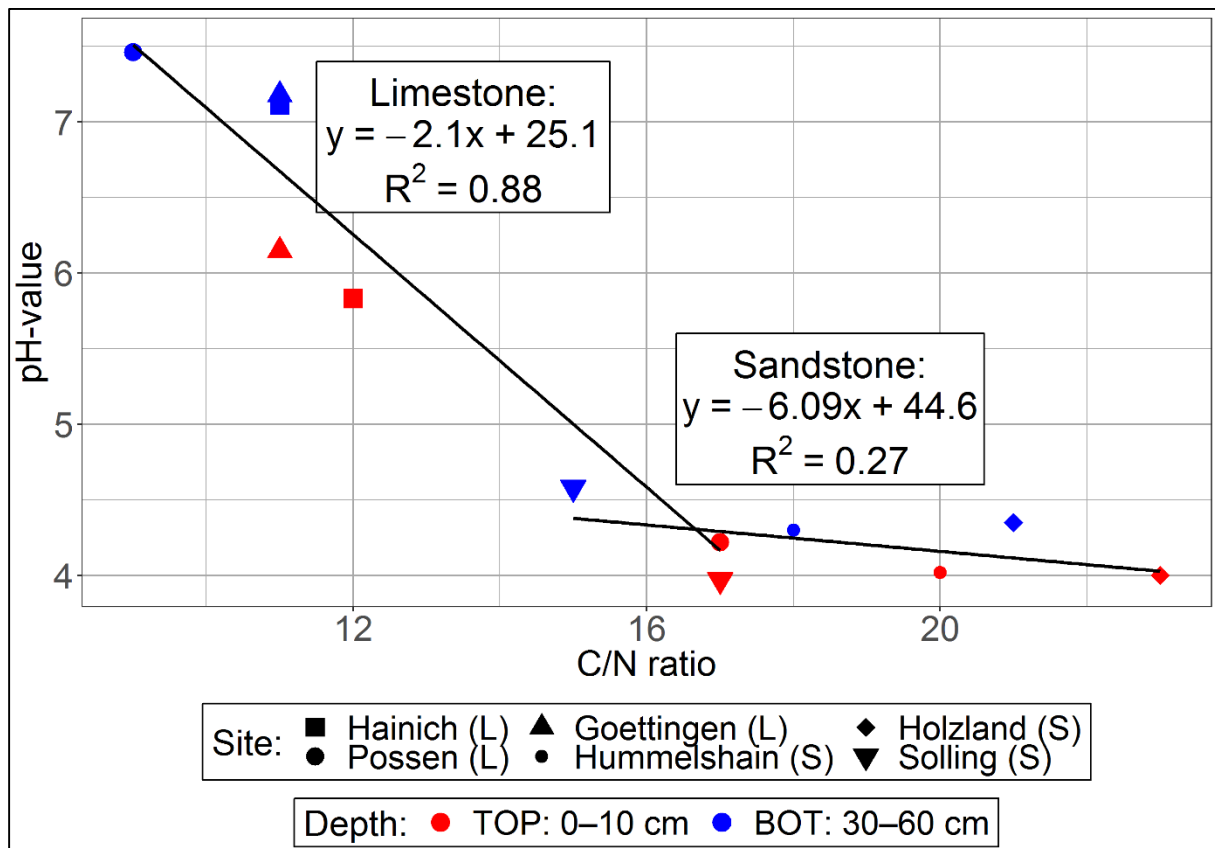
Figure 9: Carbon to nitrogen (C/N) ratio and pH-value of TOP (0–10 cm) and BOT (30–60 cm) bulk soil samples for limestone (HAI$_L$, POS$_L$, GOT$_L$) and sandstone (HUM$_S$, HOL$_S$, SOL$_S$) sites

At the **sandstone sites**, HOL$_S$ has the highest C/N ratio at both depths (TOP: 23, BOT: 21) and SOL$_S$ the lowest (TOP: 17, BOT: 15); Table 6. This might be caused by the higher precipitation at SOL$_S$, resulting in higher microbial activity. The ratio decreases by two with depth at all three sites, supporting the hypothesis of similar behavior between the sandstone sites. A general decrease of C/N ratios with depth is quite common (Rumpel and Kögel-Knabner 2011). Due to the lower variability of the pH-values between the sandstone sites, the correlation between pH-values and C/N ratios is less (R^2 = 0.27) compared to the limestone sites (R^2 = 0.88). However, a positive trend is still visible (Figure 9). The values of C, N and the C/N ratio at the sandstone sites HOL$_S$ and SOL$_S$ agree well with those found in Meesenburg et al. (2009) and Thüringen Forst (2016).

The stable isotopic carbon (^{13}C) composition shows distinct differences between limestone (HAI$_L$, POS$_L$, GOT$_L$) and sandstone sites (HUM$_S$, HOL$_S$, SOL$_S$; Table 6). The median δ^{13}C value of all limestone sites is by 1.54 ‰ larger than that of the sandstone sites (-27.46 ‰). Soils enriched in ^{13}C (higher δ^{13}C values) are usually more processed (Balesdent et al. 1993), correlating with the C/N ratio observations (Figure 10). Similar to the pH-values (Figure 7) and the C and N contents (Table 6), the variation of the entire soil profile at the limestone sites is much larger (-27.80 ‰ to -25.66 ‰) than that at the sandstone sites, which show a variation below 1 ‰.

The **limestone sites** range between -27.42 ‰ and -25.98 ‰ in the TOP layer (0–10 cm), with POS$_L$ showing the smallest value and GOT$_L$ the highest. BOT (30–60 cm) samples are more enriched in ^{13}C, with δ^{13}C values ranging between -25.90 ‰ and -25.75 ‰. BOT sample variations are smaller than that of the TOP samples, with HAI$_L$ having the lowest value and POS$_L$ the highest one. Similar δ^{13}C values for HAI$_L$ were given by Schrumpf et al. (2013). Therefore, POS$_L$ shows the largest difference between TOP and BOT, analogous to pH values (Figure 7) and C/N ratios (Figure 10). A general larger enrichment of ^{13}C with depth is common for sites without vegetation change (Balesdent et al. 1993). The higher nutrient availability (e.g., N, Table 6) in deeper soil layers may enhance root growth and foster microbial abundance, resulting in ^{13}C enrichment (Angst et al. 2018). This agrees with the strong correlation between the δ^{13}C values and C/N ratios ($R^2 = 0.81$) for those sites (Figure 10).
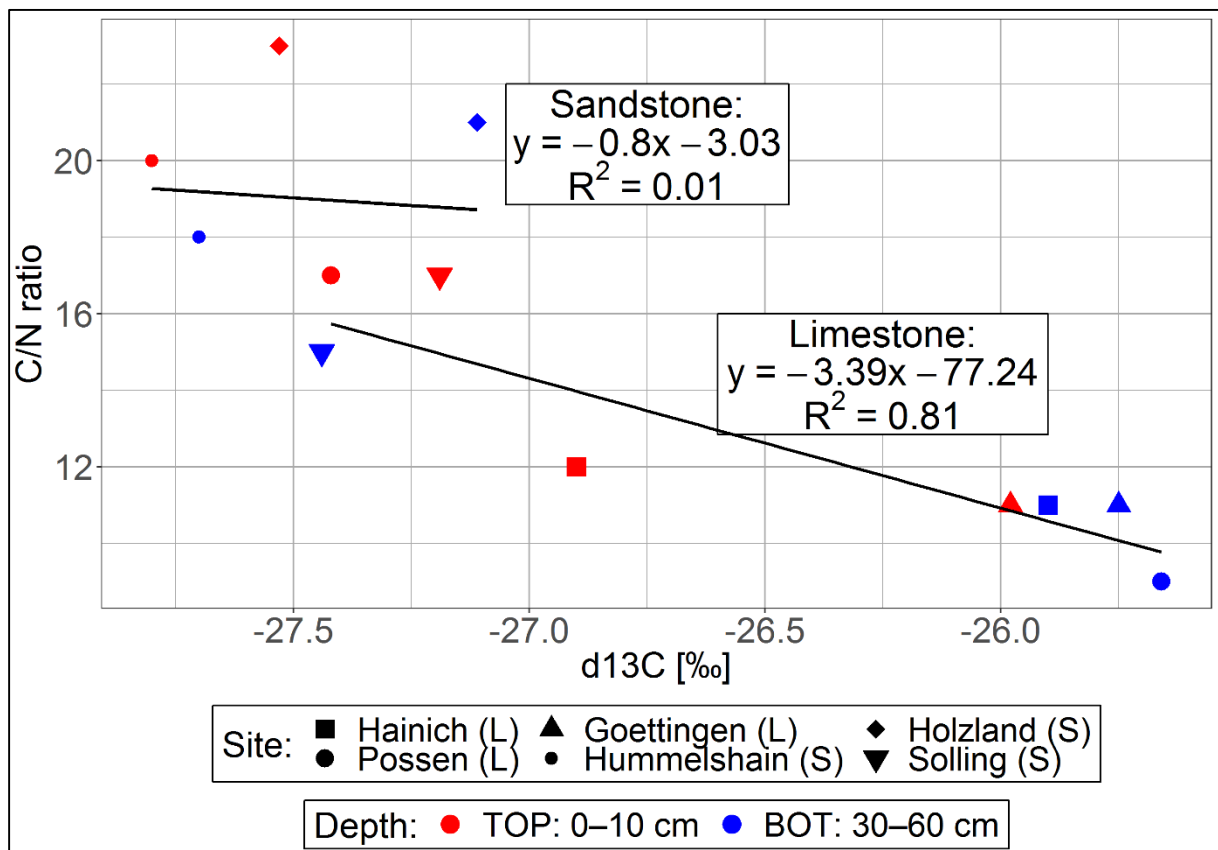
Figure 10: δ^{13}C [‰] and C/N ratio of TOP (0–10 cm) and BOT (30–60 cm) bulk soil samples for limestone (HAI$_L$, POS$_L$, GOT$_L$) and sandstone (HUM$_S$, HOL$_S$, SOL$_S$) sites

At the **sandstone sites** there is no clear difference between TOP (median: -27.53 ‰) and BOT (median: -27.44 ‰) samples (Table 6). The median value differs by less than 0.1 ‰ at both depths, which is smaller than the analytical error. Rumpel and Kögel-Knabner (2011) discussed two explanations for no change in δ^{13}C values with depth: i) Stabilization of ^{13}C

enriched components, such as polysaccharides and amino acids or/and ii) Decomposition of ^{13}C depleted compounds, such as lipids and lignin. No change of the $\delta^{13}C$ values with depth might also result from parent material characteristics, such as lower amounts of clay and nutrients at sandstone sites as compared to limestone sites. Such traits of bedrock material might at least partly control organic matter input and soil organic matter stabilization in the subsoils, and control the contribution of microbial-derived compounds (Angst et al. 2018). This assumption is supported by the low correlation between $\delta^{13}C$ values and C/N ratios ($R^2 = 0.01$) at the sandstone sites (Figure 10).

Radioactive isotopic carbon (^{14}C) results show significant differences between the limestone (HAI$_L$, POS$_L$, GOT$_L$) and the sandstone sites (HUM$_S$, HOL$_S$, SOL$_S$; Table 6). All six sites yield negative median values (limestone: -67.4 ‰, sandstone: -15.9 ‰). The different $\Delta^{14}C$ values between the limestone and the sandstone sites might be related to the higher clay and C content (von Lützow et al. 2006) and more processed SOM (smaller C/N ratio and higher $\delta^{13}C$ values; Jenkinson et al. 2008) at the limestone sites. Clay minerals have very active chemical surfaces, which might be responsible for stabilizing organic compounds (Welte 1969). Other factors of SOM stabilization might be different aggregate protection and organo-mineral associations of soils with different bedrock materials (Mikutta et al. 2006; Rasmussen et al. 2005), and geomorphic controls (Doetterl et al. 2012). Additionally, the likely lower amount of exchangeable bases at the sandstone sites may result in less stabilization of SOM (Blume et al. 2016; Rasmussen et al. 2018).

$\Delta^{14}C$ decreases with depth at all sites (limestone: TOP: 2.8 ‰; BOT: -177.0; sandstone: TOP: 18.4 ‰; BOT: -37.9 ‰; Figure 11). The drivers and their contribution controlling increasing radiocarbon ages with depths are still uncertain (Trumbore 2009) because a substantial input of younger C can also be found in deeper soils and vice versa (Balesdent et al. 2018; Rasse et al. 2005). The input of younger C into older soil horizons can be caused by the input of young roots, leaching of mobile organic compounds through the soil profile, bioturbation, and deposition of allochthonous OM (Trumbore 2009). Therefore, a more differentiated look at individual sites and fractions of more homogenous SOM pools is needed (Section 4.2).

The **limestone sites** spread by more than 100 ‰ of $\Delta^{14}C$ in the TOP layer (median: 2.8 ‰). This large span is mainly driven by the low value of -89.90 ‰ at GOT$_L$. Such small $\Delta^{14}C$ value (below 0 ‰) at a surface mineral layer is quite unique (He et al. 2016; Trumbore 2009). Fresh plant residues, which usually have a positive $\Delta^{14}C$ value (Gaudinski et al. 2000) are constantly added to the surface mineral layer, resulting in a similar $\Delta^{14}C$ value. A source of old C is necessary to explain those low $\Delta^{14}C$ value in topsoil sample. One hypothesis would be that fossil C from airborne dust without significant ^{14}C enters the soil system at that site. Those emissions could come from the *Ruhr* coal mining area, which is only about 100 km to the west of GOT$_L$. Therefore, dominating westerly winds could easily transport fossil C-containing dust there. This assumption is supported by the negative $\Delta^{14}C$ value measured in the TOP layer at SOL$_S$. That site lies only a few kilometers to the west from GOT$_L$ (Figure 3). Lemke (2006) also reported negative soil surface $\Delta^{14}C$ values from a Solling site, as well as Angst et al. (2016) from a study site 140 km north of Goettingen. Additionally, charred material, e.g., from fires can lower soil radiocarbon ages. Charcoal tends to resist decomposition and can be very old (Kuzyakov et al. 2009). One approach to test this hypothesis is to apply physical density fractionation. Such fractionation divides soil material by flotation or sedimentation in different solutions according to particle density. In the presence of charcoal, the light

fraction (< 1.6–1.8 g cm^{-3}) would contain the charred material, resulting in a much older radio-carbon than usually expected (Crow et al. 2007). Time did not allow to test for this hypothesis.
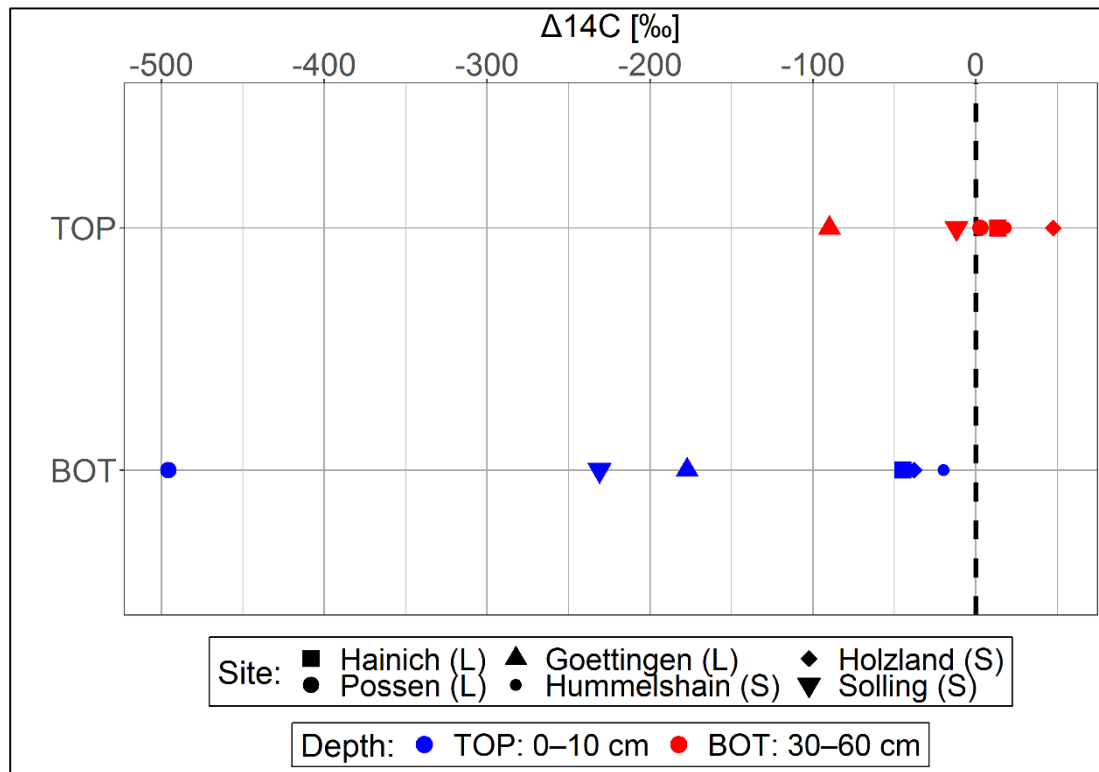

Figure 11: Δ^{14}C [‰] of TOP (0–10 cm) and BOT (30–60 cm) bulk soil samples for limestone (HAI$_L$, POS$_L$, GOT$_L$) and sandstone (HUM$_S$, HOL$_S$, SOL$_S$) sites

In the BOT layer, differences between the three sites HAI$_L$, POS$_L$ and GOT$_L$ were even larger, ranging between -44.8 ‰ (HAI$_L$) and -495.8 ‰ (POS$_L$; Figure 11). The low Δ^{14}C POS$_L$ value might be due to the fact that the sampling depth (~ 60 cm) was the lowest of all sites and/or that charred material was sampled. Additionally, this sample was pretreated with HCl to remove carbonates which would influence the Δ^{14}C value (Steinhof et al. 2017) but probably not to such large extend. The BOT sample at POS$_L$ contains the highest IC content (1.39 wt-%) followed by GOT$_L$ (0.63 wt-%), which also shows a small Δ^{14}C value (-177.3 ‰). Yet, no reliable evidence for this correlation could be found in the literature.

The distribution of the Δ^{14}C values cannot be correlated with the clay or C content of those sites (Appendix A5). HAI$_L$, ranging between POS$_L$ and GOT$_L$ in clay and C content, shows the highest Δ^{14}C value, whereas GOT$_L$ with the highest clay and C content has a Δ^{14}C value between HAI$_L$ and POS$_L$. This indicates that other factors control the Δ^{14}C distribution in those soils. Yet, a correlation based on only three samples is difficult to make anyway. However, the Δ^{14}C values for HAI$_L$, are comparable with values found in Schrumpf et al. (2013).

Differences at the **sandstone sites**, especially in the TOP layer, were much smaller than at the limestone sites, with SOL$_S$ showing the lowest Δ^{14}C value (-11.9 ‰) and HOL$_S$ the highest one (47.5 ‰; Figure 11). This indicates that HOL$_S$ and HUM$_S$ (Δ^{14}C: 18.4 ‰) contain substantial amounts of modern C, whereas SOL$_S$ does not. The differences between the sites increase with depth, ranging from -231.0 ‰ (SOL$_S$) to -11.9 ‰ (HUM$_S$). The relatively small Δ^{14}C values at SOL$_S$ (TOP and BOT), compared to the other two sites, might be related to its high mean annual precipitation (= 1'190 mm). Similar correlations have been reported by van der Voort et al. (in review, 2018). Doetterl et al. (2015) found a positive correlation

between MAP and SOC stabilization, too, yet they propose that this relation is on the long-term only an indirect one via its influence on soil geochemistry. The low Δ^{14}C value at SOL_S can be an additional result of charred material. However, the comparatively high Δ^{14}C value in deeper soil at HUM_S (-11.9 ‰) might result from erosion processes, since it is the only site that was sampled on a distinct slope (10–15 %; Section *2.2)*. There, C is constantly transported away and is less stabilized due to erosion, resulting in younger C mean ages (Doetterl et al. 2012; 2018).

In conclusion, the physical and chemical soil characterizations at the six different sites show substantial differences between the two depth intervals and between the two parent materials. TOP samples received higher C and N input than BOT material (30–60 cm) and are less processed (higher C/N ratios). The lower decomposition in the TOP layers is supported by generally smaller δ^{13}C values in those samples. Δ^{14}C increases with depth, caused by greater contribution of older C to total C. The origin of this protected C cannot be assessed with the analytical methods used here.

The three limestone (HAI_L, POS_L, GOT_L) sites usually show neutral to slightly acidic pH values since they developed from carbonate-containing limestone. In contrast, the sandstone (HUM_S, HOL_S, SOL_S) sites show acidic soil conditions. The latter ones also have lower C and N concentrations compared to the limestone sites. The higher yield of those elements at the limestone sites correlates with higher clay contents; yet the clay content alone does not predict the SOC content. On average, the limestone sites contain more protected C (lower Δ^{14}C), which could not be explained by the soil properties analyzed (e.g. clay content, SOC). The higher contribution of old C to the total C content at the limestone sites is probably caused by other geochemical parameters that have not been analyzed (e.g. iron and aluminum content. The variation between the limestone sites is quite large for all soil characteristics, except for C/N ratios. Sandstone sites seem to be less processed, visible in larger C/N ratios and smaller δ^{13}C values. To derive meaningful conclusions about the difference of the limestone and the sandstone sites it is necessary to separate the heterogeneous SOM into its different and relatively more homogenous fractions. Such approach helps identifying drivers that control the radiocarbon age at different depth and in different soils.

4.2   Sequential chemical extraction

Results of the extraction method (soil residues and extracts) from all limestone (HAI_L, POS_L, GOT_L) and sandstone (HUM_S, HOL_S, SOL_S) sites are presented and discussed, including C and N content, and their C-isotopic composition. A mass balance of the applied method will be presented as well. Samples represent the TOP (0–10 cm) and BOT (30–60 cm) layers, and the four (TSE, BHY, AHY, and CuO) fractionation steps.

Elemental carbon and nitrogen quantification showed that three soil residue samples from the BOT layer (POS_L-TSE, POS_L-BHY and GOT_L-TSE) contained significant amounts of inorganic C (IC > 0.15 wt-%; Table 7). Those are from the two bulk samples that originally contained IC (Table 6). The first extraction step (TSE) does not mobilize any IC, because dichloromethane (DCM) was used as solvent. Potassium hydroxide (KOH) served as solvent at the beginning of the second extraction step (BHY), which also does not dissolve IC. In the same extraction step, HCl lowered the pH-value of the soil solution to between pH 1 and 3 (Section 3.2). This strong mineral acid is known to dissolve IC. This was not true, however, for the POS_L-BHY BOT sample (IC: 0.79 %;). It is likely that the pH value was not correctly controlled for this sample. For the other samples (soil residues: n = 45; extracts: n= 48) total

C equals organic C. N could only be determined for the soil residues of the sequential chemical extraction. The total weight of the extracts was for most of the extracts too low to quantify N in addition to $\delta^{13}C$ (including OC) and $\Delta^{14}C$.

Table 7: Inorganic carbon (IC), soil organic carbon (SOC), and total nitrogen (TN) [wt-%] of TOP (0–10 cm) and BOT (30–60 cm) bulk and soil residue samples for limestone (HAI$_L$, POS$_L$, GOT$_L$) and sandstone (HUM$_S$, HOL$_S$, SOL$_S$) sites

		Limestone						Sandstone					
		HAI$_L$		POS$_L$		GOT$_L$		HUM$_S$		HOL$_S$		SOL$_S$	
		TOP	BOT	TOP	BOT	TOP	BOT	TOP	BOT	TOP	BOT	TOP	BOT
TSE	IC [wt-%]	LLQ	0.05	LLQ	1.46	0.08	0.63	LLQ	LLQ	LLQ	LLQ	0.04	LLQ
	SOC [wt-%]	3.07	1.75	1.80	0.42	6.03	3.24	2.56	0.83	1.59	0.38	4.38	1.57
	TN [wt-%]	0.26	0.16	0.11	0.05	0.52	0.29	0.14	0.05	0.07	0.02	0.27	0.12
BHY	IC [wt-%]	0.03	0.04	LLQ	0.79	0.04	0.05	LLQ	LLQ	LLQ	LLQ	LLQ	LLQ
	SOC [wt-%]	2.23	1.35	1.19	0.35	5.43	2.86	1.40	0.29	0.77	0.21	3.17	1.35
	TN [wt-%]	0.20	0.14	0.07	0.04	0.50	0.24	0.07	0.02	0.04	0.02	0.21	0.09
AHY	IC [wt-%]	0.04	0.04	LLQ	0.05	0.04	0.06	LLQ	LLQ	LLQ	LLQ	LLQ	LLQ
	SOC [wt-%]	2.03	0.97	0.94	0.23	3.97	2.06	1.12	0.26	0.59	0.22	3.17	1.05
	TN [wt-%]	0.18	0.09	0.05	0.03	0.33	0.18	0.04	0.01	0.02	0.01	0.18	0.08
CuO	IC [wt-%]	LLQ	LLQ	LLQ	LLQ	LLQ	LLQ	LLQ	0.04	0.04	0.05	LLQ	LLQ
	SOC [wt-%]	1.29	0.62	0.70	0.14	2.58	1.71	1.41	0.29	0.52	0.27	2.50	0.75
	TN [wt-%]	0.27	0.22	0.04	0.17	0.36	0.39	0.08	0.01	0.02	0.01	0.18	0.15

TSE: Total solvent extraction; BHY: Base hydrolysis; AHY: Acid hydrolysis; CuO: Copper oxidation; IC: Inorganic carbon; SOC: Soil organic matter; TN: Total nitrogen; LLQ: below lower limit of quantification

Like the bulk sample distributions (Table 6) the soil residues of all limestone sites (HAI$_L$, POS$_L$, GOT$_L$) show higher SOC concentrations compared to the sandstone sites (HUM$_S$, HOL$_S$, SOL$_S$). This distribution is probably caused by the same parameters as for the bulk samples: mainly the higher clay content at the limestone sites. SOC decreased with depth at all sites and for all fractions, like the N content of all samples (Table 7), which correlate with the bulk samples.

The SOC concentration of the individual soil residues at the limestone sites decreased with each extraction step (TSE > BHY > AHY > CuO), since each extraction step removes C from the soil residue. At the sandstone sites, HOL$_S$ and SOL$_S$ show the same SOC distribution. HUM$_S$ showed by 0.29 wt-% higher SOC concentration in the CuO fraction compared to the AHY fraction in the TOP layer and by 0.03 wt-% in the BOT layer. The latter one is within the analytical error of this method. The reason for the higher SOC content in the CuO soil resi-

due compared to the AHY one of the HUM_S TOP sample cannot be explained based on the encountered evidence.

N concentration of the individual soil residues followed a similar trend as compared to SOC. However, at the limestone sites N content of the CuO fraction was usually higher than that of the untreated bulk soil sample (Table 6). This leads to the assumption that those samples were contaminated with N during the last extraction step. Yet, if this would be true, then the soil residues from the sandstone sites should behave the same. This only applies for SOL_S in the BOT layer. The higher N and low SOC concentration in most of the CuO fractions results in a smaller C/N ratio (Figure 12), indicating a more processed sample compared to the others. The high N content of the CuO fractions might be related to the presence of mineral N absorbed to clay minerals (Rumpel and Kögel-Knabner 2011). This might explain why the CuO extract from POS_L contained the lowest N content. This site has the lowest clay content of all three limestone sites. Additionally, the low C/N ratio of some of the CuO soil residues likely indicates that microbial-derived C is the main component left after the sequential chemical extraction procedure. If this was true, then the CuO soil residues should also have a high δ^{13}C value.
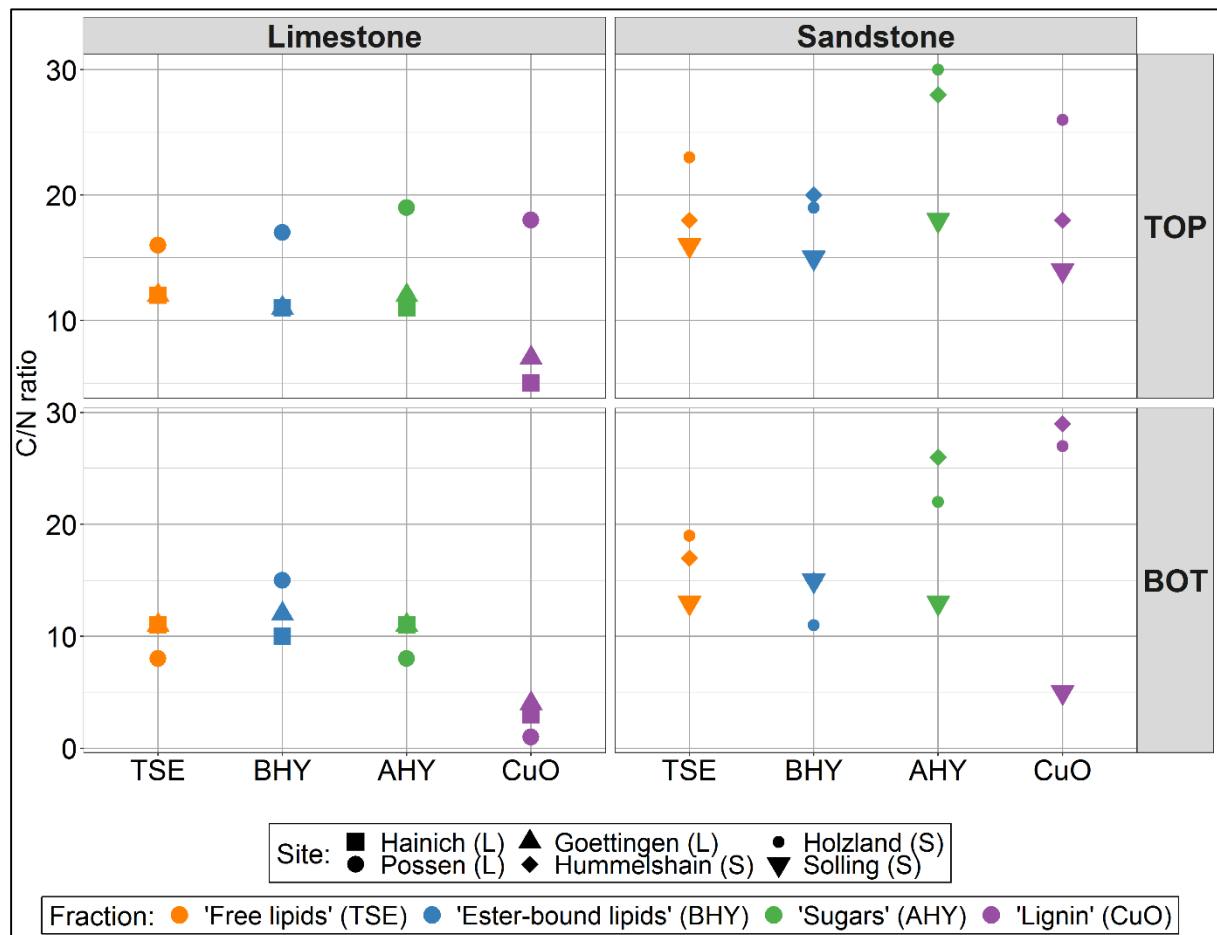
Figure 12: C/N ratio of TOP (0–10 cm) and BOT (30–60 cm) soil residues for limestone (HAI_L, POS_L, GOT_L) and sandstone (HUM_S, HOL_S, SOL_S) sites

Since the chemical composition of the individual soil residue fractions is unknown, it is difficult to interpret them in terms of SOC and N. Chemical extraction methods may also affect soil mineral content and can cause changes in SOM chemistry and structure (Trumbore and Zheng 1996). Additional analyses of the chemical composition of the soil residue fractions

would be needed for verification. Further information on SOM composition and turnover may be obtained with compound-specific C-isotope data.

The dissimilar distribution of SOC and N between the fractions and the two bedrock materials indicates that the sequential chemical extractions method leads to different results for soils with divergent geochemical matrix composition. Trumbore and Zheng (1996) proposed that chemical fractionation is most effective in coarse-textured soils, partly because more of the total C is removed in the hydrolysis procedure. Therefore, it is necessary to calculate the mass balance of the sequential chemical extraction to elucidate differences between the efficiency of the method between the fractions and the different bedrock types. A mass balance helps to test if the obtained data is reliable. This is especially important for empirical operational methods such as the one applied.

A **mass balance** was calculated for the organic C content of the individual fractions for each extracted bulk sample (n = 12). The calculations were based on the absolute weight and OC content of each sample (Appendix A7). The OC content of the untreated bulk sample equaled 100 % of the available C in the extraction procedure (Figure 13). Ideally, the relative portion of OC content in the soil residue and extract from the same chemical treatment (e.g. BHY) should equal the again 100 %. Lower values indicate that OC was lost during the extraction. The large standard deviation (SD) of the individual fractions suggests that the method used always depends on the composition of the sample to be extracted. Yet, different patterns emerge for TOP and BOT, as well as for limestone and sandstone samples.
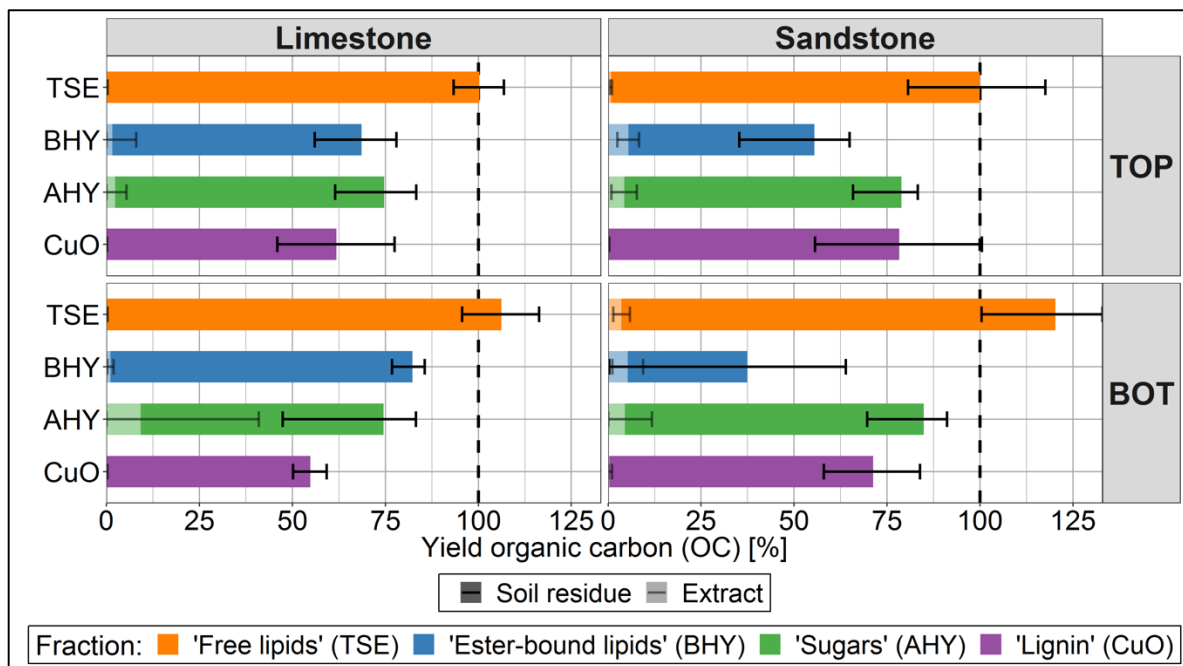
Figure 13: Yield [%] of organic carbon (OC) for TOP (0–10 cm) and BOT (30–60 cm) soil residues and extracts for limestone (HAI$_L$, POS$_L$, GOT$_L$) and sandstone (HUM$_S$, HOL$_S$, POS$_S$) sites

For all sites, the relative OC content in the individual extracts was relatively small (0.1–12 %) compared to the soil residues (Figure 13). Efficiency might be enhanced by repeating the individual extraction steps on the same sample before performing the next extraction step. The obtained yields are difficult to compare with those of other studies. Not only do the individual samples influence the extractable C, but also the method applied (Angst et al. 2017; Otto and Simpson 2007). It seems to be more appropriate to compare and discuss general trends (increasing/decreasing) of the extracted fractions than the absolute amount of the yield.

After the first extraction step (**TSE**) all of the OC of the bulk sample was usually found in the soil residue at all sites (Figure 13). Less than 1 % of the original C was detectable in the extracts in both depths of the three limestone sites. Similar values (ca. 0.4 % of OC) were reported by Angst et al. (2016) for the same fraction in topsoil samples from a central German beech forest. At the sandstone sites, more C was found in the extracts (TOP: 1 ± 0.2 %; BOT: 4 ± 2 %). The extracts at all sites are likely be dominated by free lipids from higher plants (Otto and Simpson 2007). In subsoils, those compound classes are probably derived from roots (Nierop 1998). This leads to the assumption that the sandstone sites receive higher root inputs than the limestone sites. This contradicts the assumption made earlier that the sandstone sites have a shallower root system and less root C input in the BOT layer as compared to the limestone sites (section 4.1). A chemical analysis of the roots from the same sites would help to see if the chemical composition is comparable to that of the extract. On the other hand, the reduced pH value at the sandstone sites might result in reduced microbial activity and in a higher amount of undecomposed free plant-derived lipids (Stevenson 1994). However, the correlation between OC yield and pH-value was not significant for the TSE extracts.

Base hydrolysis (BHY) yields were highest in the sequence, suggesting that the extraction method is better for ester-bound lipids than those for the other compound classes. Again, recovery was larger in those from the sandstone sites (11 ± 8 %) compared to their limestone site counterparts (3 ± 7 %), even though this difference was not statistically significant due to large uncertainties. The abundance of ester-bound lipids increased with decreasing pH-value (Nierop et al. 2003). Based on the calculated yields, the ester-bound lipids seem to be stabilized by acidic pH-values (Figure 14).

$$y = -2.22x + 16.66$$
$$R^2 = 0.53$$
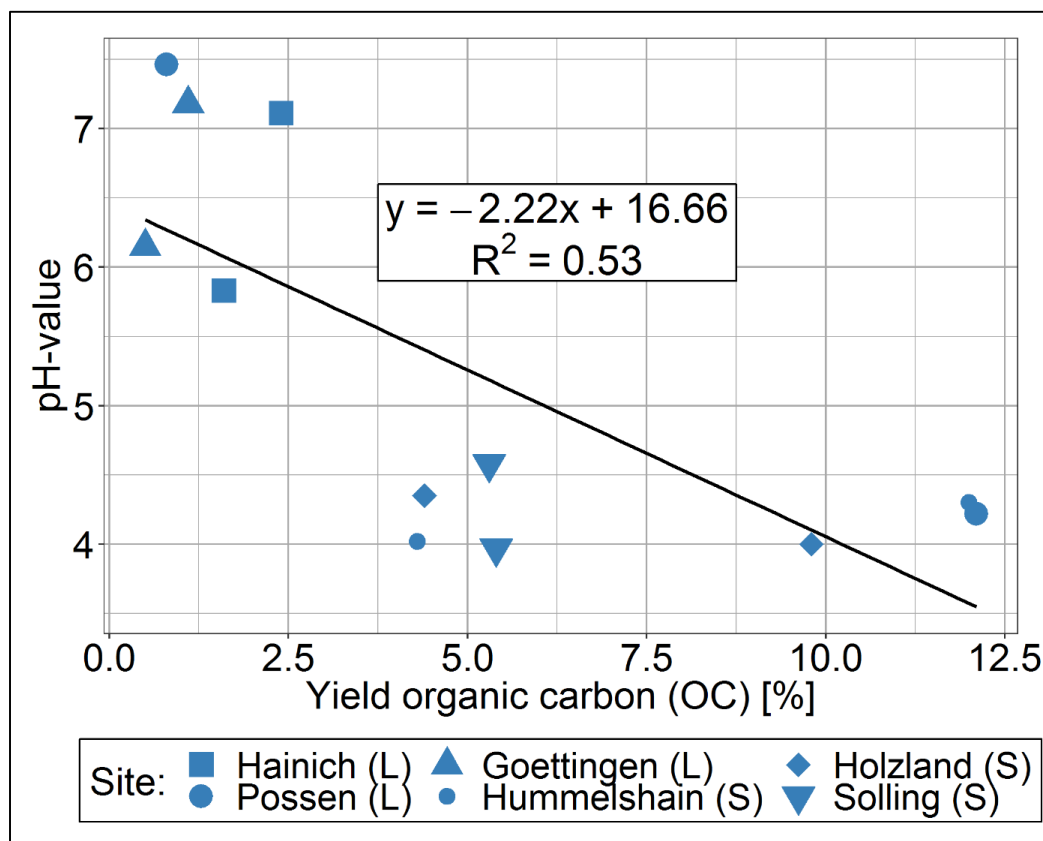
Figure 14: Yield [%] of organic carbon (OC) and pH-value for TOP (0–10 cm) and BOT (30–60 cm) BHY ('Ester-bound lipids') extracts for limestone (HAI_L, POS_L, GOT_L) and sandstone (HUM_S, HOL_S, POS_S) sites

The recovery of OC in the soil residues of the BHY was less efficient compared to the previous TSE extraction step (Figure 13). At the limestone sites, up to 67 ± 11 % of the OC from the previous TSE soil residue were extracted in the TOP layer and 82 ± 5 % in the BOT layer. The differences to the previous fraction in the TOP layer are within the standard deviation (SD). At the sandstone sites, the differences between the BHY fractions (extracts and soil residue) and the TSE soil residue are 44 % and 74 % in the TOP and BOT layer, respectively. Those differences were much higher than the SD (TOP: 37 %; BOT: 58 %) and cannot be explained based on the encountered evidence. Von Lützow et al. (2007) concluded that alkaline extraction procedures simultaneously affect several stabilization mechanisms that are of different relevance in various soils and soil horizons. This might explain the large variance in BHY extract yields among the individual sites.

Acid hydrolysis (AHY) extracted on average about 2 % of the relative C content in the extracts of the previous BHY soil residue (Figure 13). This did not apply for the limestone sites at lower depth, were the yield was 8 ± 27 %. This high SD was caused by POS_L, in which 60 % of the OC from the BHY soil residue was detected in the extract and only about 40 % in the corresponding soil residue. This was the only sample with an extract yield larger than that of the soil residue (Appendix A7). During extraction, it was impossible to dry this extract under N_2 flow; probably caused by the extract's chemical composition. Even after drying for several days, the extract was still jelly-like. A chemical analysis of this sample would help to interpret the much higher yield of this extract. Yet, the high yield of the AHY extract (60 %) from POS_L is in the range of previously reported values (30–90 % of OC; Stevenson 1994). In this study they calculated those values just based on the yield of the AHY soil residue and did not measure the yield in the extracts. Compared to studies that actually measured OC of the AHY extract (5–24 % of OC; Angst et al. 2018; Otto and Simpson 2007), most of the yields of the presented data set were in the same order of magnitude, albeit slightly lower. Again, this shows that extract yields vary a lot depending on sample material and methods (von Lützow et al. 2007). A chemical analysis of those fractions could help to answer those questions and to test if different compounds or compound compositions were extracted for the two different bedrock types.

Yields in AHY extracts increased with depth, therefore microbially-derived products contribute more to OC at depth than in surface soil. This corresponds with observations based on decreasing C/N ratios and increasing $\delta^{13}C$ values for the untreated bulk soils samples. Additionally, the higher yield in the BOT samples at the limestone sites compared to the sandstone sites correlates with higher pH-values and SOC of the bulk samples. This probably also results in higher microbial activity. However, results about the correlation of the yield of the AHY extracts with depth can be found in literature. Angst et al. (2018) showed a decrease of the yield, whereas Paul et al. (1997) found an increase with depth.

The strong solvent of the AHY extraction (12N HCl) might mobilize additional C that was bound in the soil matrix by organomineral interactions. This C is assumed to be very old since it was protected from destabilization (von Lützow et al. 2006). This additional C might be kerogen-type OC which is known to be part of the solid and insoluble organic matter of sedimentary rocks. Such C will be released when destroying the carbonates in the soil, which is of relevance for the limestone sites. Yet, this would not explain why HAI_L had a higher yield (9.2 %) in the BOT layer compared to GOT_L (1.9 %), which contained significant IC amounts as opposed to HAI_L.

The yield of the soil residues of the AHY extraction from the BHY soil residue was larger at the sandstone sites. It decreased with depth at the sandstone sites, while it increased at the

limestone sites (Figure 14). As mentioned before, Paul et al. (1997) reported a general decrease of SOC that is not hydrolysable with HCl (= AHY soil residue) with depth. The sum of the yield of the extract and the soil residues was always smaller than the yield of the previous BHY soil residue. This hampers interpretation of the obtained data for the soil residues. One explanation for the loss could be that the liquid extracts were filtered during the extraction step. The soil material collected on the filter was dried and weighed. Yet, it was not combined with the soil residue, resulting in C loss. On average, 6.7 g of soil material were collected on the filter. Assuming that this material contains 50 % OC (Blume et al. 2016), the missing C in the mass balance could easily be explained (Appendix A7). Yet, this does not explain why the mass balance for the TSE fractions compared to the bulk samples works. During the TSE extraction step, the liquid extracts were filtered as well, and the collected soil material on the filter discarded. This indicates that the high C loss (at least for the limestone sites) during AHY extraction had a different reason which cannot be identified based on the encountered evidence. The difference to the previous extraction step is usually within the error of the AHY.

Copper Oxidation (CuO) resulted in the lowest extraction efficiency of all extracts, less than 1 % was found (Figure 14). The low amount of lignin in the samples suggests that only a small soil fraction correlates with lignin-derived products at the studied sites. This contradicts that lignin is one of the most abundant aromatic plant components (Kögel-Knabner 2000). However, if only a low amount of lignin was extractable, this might be an indicator that lignin is decomposed in the soils. If this was true, the radiocarbon age of those extracts should be relatively young.

Kögel-Knabner (2000) reported that the relative contribution of lignin-derived CuO oxidation products increases with increasing SOC and with depth in forest soils. This cannot be confirmed by the presented data, where the lowest yield was obtained for samples with the highest SOC (TOP limestone sites). However, the distribution of lignin in mineral horizons seems to vary a lot between different sites and the processes involved in the abundance of lignin are not clear (Thevenot et al. 2010).

The CuO soil residues of the sandstone sites contained more C from the previous soil residue (AHY) compared to the limestone sites. Therefore, the C loss between the AHY and the CuO extraction was larger at the limestone sites than at the sandstone sites. An explanation for this could not be found based on the encountered evidence. The sum of the CuO extract and soil residue should equal 100 % – which is not true for any sample. It has to be noted that copper oxide (CuO; ca. 90 g) was added to the soil sample during the extraction procedure. CuO persists during extraction and could not be separated from the soil sample afterwards. To counter the increase of sample weight from CuO addition, 90 g were subtracted from each soil residue of the CuO extraction before calculating the mass balance. This assumption probably increases the error of this extraction step.

Stable isotopic carbon (^{13}C) of the **soil residues** did not differ much between the different fractions. The variation of the extracts between the different fractions was much larger (Table 8). This is probably due to the fact that only a small portion of the OC was extracted from the soil residues (Figure 13). Only some of the CuO soil residues show significant higher ^{13}C values compared to the other fractions for sandstone and limestone sites and for TOP and BOT layer. The higher ^{13}C values of this fraction indicate that the CuO soil residues were more processed compared to the other soil residues, which was corroborated for the C/N ratio in this fraction (Figure 12).

Table 8: $\delta^{13}C$ [‰] of TOP (0–10 cm) and BOT (30–60 cm) soil residues and extracts for limestone (HAI$_L$, POS$_L$, GOT$_L$) and sandstone (HUM$_S$, HOL$_S$, SOL$_S$) sites

		Limestone						Sandstone				
		HAI$_L$		POS$_L$		GOT$_L$		HUM$_S$		HOL$_S$		SOL$_S$	
	TOP	BOT	TOP	BOT	TOP	BOT	TOP	BOT	TOP	BOT	TOP	BOT
TSE (Ex)	-30.87	-30.94	-31.11	-31.48	-30.83	-30.80	-31.17	-31.62	-29.68	-30.48	-31.04	-31.27
TSE (Res)	-26.67	-25.74	-27.31	-25.31	-26.26	-25.71	-27.99	-27.64	-27.56	-26.82	-27.26	-26.82
BHY (Ex)	-29.18	-29.90	-29.54	-29.78	-28.54	-29.14	-29.67	-29.50	-28.65	-28.52	-29.44	-29.66
BHY (Res)	-27.54	-25.72	-26.94	-25.57	-26.06	-23.35	-27.63	-28.51	-27.51	-26.64	-27.20	-26.67
AHY (Ex)	-24.18	-26.27	-23.99	-27.94	-22.46	-25.51	-24.16	-25.25	-24.64	-22.24	-22.95	-23.82
AHY (Res)	-26.90	-26.58	-27.28	-25.23	-26.42	-26.08	-28.37	-28.14	-28.08	-27.08	-27.48	-27.06
CuO (Ex)	-28.57	-26.92	-28.38	-25.43	-25.70	-26.59	-28.85	-28.94	-27.96	-27.75	-28.50	-28.06
CuO (Res)	-26.65	-26.15	-24.43	-23.49	-26.53	-25.91	-28.11	-18.21	-23.31	-20.26	-27.29	-26.84

Ex: Extract; Res: Soil residue

The **extracts** clearly allow differentiating between the fractions from the individual extraction steps and their OC content independent of depth and parent material (Figure 15). For all samples, the $\delta^{13}C$ values increase in the following sequence: TSE > BHY > CuO > AHY. The AHY extracts are 4 to 7 ‰ enriched in ^{13}C compared to the other three extracts (except for the limestone BOT samples). This agrees with the first three extracts of this sequence being derived mainly from plants, which usually have a smaller $\delta^{13}C$ value compared to the AHY extracts which is dominated by sugars (Gleixner et al. 1993). It has also been reported that lignin-containing fractions are usually less depleted in ^{13}C than the fractions with lipids (Ehleringer and Rundel 1989). This is likewise true for this work. Differences between the individual fraction in the TOP layer of limestone and sandstone sites equals or is smaller than 0.2 ‰. There seems to be no substantial difference between limestone and sandstone sites in the TOP layer. The $\delta^{13}C$ signature in topsoils seems to be mainly influenced by vegetation and climatic conditions, resulting in similar $\delta^{13}C$ composition for the same fractions from different sites.

A different picture arose for the BOT layers. $\delta^{13}C$ values of the TSE fractions did not change with depth (TOP and BOT: -30.9 ‰) at the limestone sites, whereas the other fractions show differences (Table 8). The BHY and AHY extracts decreased by 0.6 ‰ and 2.3 ‰, respectively. The depletion of ^{13}C with depth in those two fractions suggests that less processed C contributes to the stable C-isotopic composition. This C could derive from the sedimentary rocks which might consist of ancient algae rich in carbohydrates and amino acids with lower $\delta^{13}C$ values. The CuO extracts were the only fraction that was more enriched in ^{13}C in the BOT layer (median: -26.6 ‰) compared to the TOP layer (median: -28.4 ‰; Figure 15).
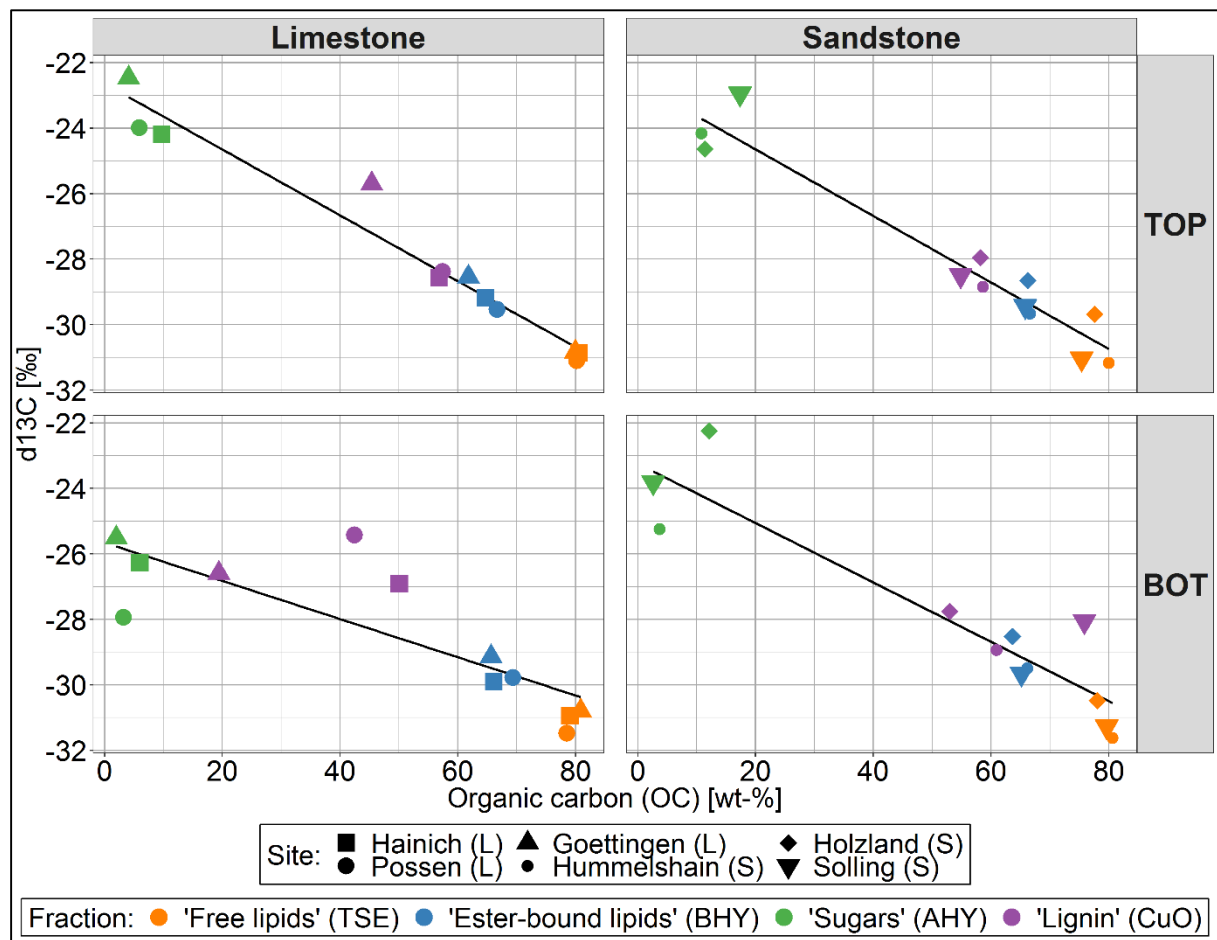
Figure 15: δ^{13}C [‰] and OC [wt-%] of TOP (0–10 cm) and BOT (30–60 cm) extracts for limestone (HAI$_L$, POS$_L$, GOT$_L$) and sandstone (HUM$_S$, HOL$_S$, SOL$_S$) sites

At the sandstone sites, the average δ^{13}C value did not change with depth ($\Delta \leq 0.4$ ‰; Table 8), indicating that all extracts were processed to the same degree in both depth intervals. This is not true for the individual extracts from the AHY fractions. The AHY δ^{13}C value at HOL$_S$ increased by 2.4 ‰ with depth, whereas at HUM$_S$ and SOL$_S$ δ^{13}C values decreased by 1.1 and 0.9 ‰, respectively (Figure 15). This contradictory behavior was probably caused by site-specific soil and environmental conditions and cannot be explained based on the encountered evidence. Differences between the sandstone and limestone sites in the subsoil were negligible for the TSE and BHY fractions ($\Delta \leq 0.4$ ‰). On average, the AHY fractions were by 2.5 ‰ enriched in ^{13}C and by 1.5 ‰ depleted in the CuO fractions at the sandstone sites compared to the limestone sites. Indicating that lignin (CuO) was at least in the BOT layer more processed and sugar-like products (AHY) less processed in soils with sandstone as bedrock material compared to soils that developed from limestone. However, the differences between TOP and BOT were larger at the limestone sites compared to the sandstone sites, indicating that the carbonates and their chemical composition in the subsoils influence the δ^{13}C values, whereas the sandstone material did not influence the distribution of ^{13}C in the fractions much with depth.

Radioactive isotopic composition (^{14}C) of the soil residues and extracts differed between fractions, bedrock materials, and depth (Table 9). Von Lützow et al. (2007) demonstrated in her review that extracts from chemical degradation methods usually have younger radiocarbon ages (higher Δ^{14}C value) compared to the associated soil residue. This is only true for four samples of the presented data set. Two belong to the BHY fraction and were from the TOP and BOT layers of HAI$_L$ and HUM$_S$, respectively. The other two samples were from the TSE and CuO fraction in the

TOP layer from HUM$_S$. Since there is no visible trend, it is difficult to explain this behavior. One hypothesis would be that the lower Δ^{14}C values of the extract were caused by contamination with the corresponding solvent because the solvents contain very old radiocarbon. Yet, if this was the case then all of the extracts should be contaminated with old radiocarbon age; which is not true.

Table 9: Δ^{14}C [‰] of TOP (0–10 cm) and BOT (30–60 cm) soil residues and extracts for limestone (HAI$_L$, POS$_L$, GOT$_L$) and sandstone (HUM$_S$, HOL$_S$, SOL$_S$) sites

	Limestone						Sandstone					
	HAI$_L$		POS$_L$		GOT$_L$		HUM$_S$		HOL$_S$		SOL$_S$	
	TOP	BOT	TOP	BOT	TOP	BOT	TOP	BOT	TOP	BOT	TOP	BOT
TSE (Ex)	-9.8	-41.0	29.7	-587.2	-11.4	-68.3	18.3	4.2	-4.1	-71.8	-31.4	-99.4
TSE (Res)	25.5	-34.0	0.4	-470.1	13.2	-43.3	13.2	-20.1	14.7	-5.9	-14.2	-117.6
BHY (Ex)	58.0	10.9	10.4	-46.7	31.4	-14.0	27.1	-25.4	14.8	-12.4	-72.4	-98.6
BHY (Res)	14.7	-66.4	-8.8	NA	4.4	-150.9	-6.2	-51.5	15.3	-36.3	-13.5	-113.4
AHY (Ex)	-483.7	-765.1	-599.4	-985.3	-567.7	-845.3	-179.6	-744.2	-13.2	-1.2	8.9	-127.0
AHY (Res)	-89.9	-594.3	-21.8	-409.4	-40.7	-51.5	-21.4	-65.2	-19.9	-38.1	-72.8	-145.6
CuO (Ex)	-33.1	-82.8	28.6	-306.4	-11.4	-68.3	14.5	-45.7	11.6	-50.7	-23.6	-142.6
CuO (Res)	15.5	-61.5	-31.0	-412.1	13.2	-43.3	-5.9	-64.2	-16.3	-69.4	-27.4	-120.3

NA: not available; Ex: Extract; Res: Soil residue

The individual **soil residues** from the TOP layers were on average more depleted in ^{14}C at the sandstone sites (median: -13.9 ‰) as compared to the limestone sites (median: 1.7 ‰; Table 9). This contrasts the behavior of the bulk soil samples (Figure 11) and the assumption that the higher clay content at the limestone sites mainly drives lower Δ^{14}C values, which was already questioned previously and by others (Rasmussen et al. 2018). Yet, the higher Δ^{14}C values at the limestone sites are not true for all individual fractions. The TSE soil residues at both sites have a median Δ^{14}C value of 13.2 ‰. The BHY soil residues have a positive Δ^{14}C (4.4 ‰) value at the limestone sites, whereas at the sandstone sites it is negative (-6.2 ‰). The same is true for the CuO soil residues (limestone: 2.9 ‰; sandstone: -16.3 ‰). Both sites show negative median values for the AHY residues. Yet, the limestone sites are almost twice as depleted in ^{14}C (-40.7 ‰) as compared to the sandstone sites (-21.4 ‰).

All soil residues from the BOT layer were more depleted in ^{14}C compared to those from the TOP layer (Figure 16). This indicates an enrichment of stable organic compounds in all fractions with depth and agrees with the bulk soil samples and results from e.g., Paul et al. (1997) and Rethemeyer et al. (2005). The limestone sites show on average slightly lower Δ^{14}C values (median: -66.4 ‰) compared to the sandstone sites (median: -64.7 ‰). This is contrary to the TOP samples. Similar to the δ^{13}C values, the differences between TOP and BOT layers were larger at the limestone sites compared to the sandstone sites. Especially the AHY soil residues became much older with depth at the limestone sites (TOP: -40.7 ‰; BOT: -409.0 ‰). The median Δ^{14}C value at the sandstone sites of the same fraction decreased by 43.8 ‰ (TOP: -21.4 ‰; BOT: -65.2 ‰). Paul et al. (1997) reported similar or even smaller values (Δ^{14}C: -200 to -600 ‰) for AHY soil residues from various grassland sites in North America. Except for the AHY fraction, fractions from POS$_L$ were always much older than the fractions from the other two limestone sites. This might be caused by the highest IC

content at POS_L (note: IC was removed before measuring $\Delta^{14}C$). Carbonate containing soils are usually rich in exchangeable calcium (Blume et al. 2016), which might enhance SOM stabilization (Rasmussen et al. 2018). Yet, this does not explain the AHY fraction from HAI_L is much older compared to the other two sites that contained IC in the untreated bulk sample. The BHY fraction $\Delta^{14}C$ data from POS_L is missing because its C content was wrong. Therefore, the $\Delta^{14}C$ concentration of this sample needs to be re-analyzed. That result was not yet available when submitting this thesis.
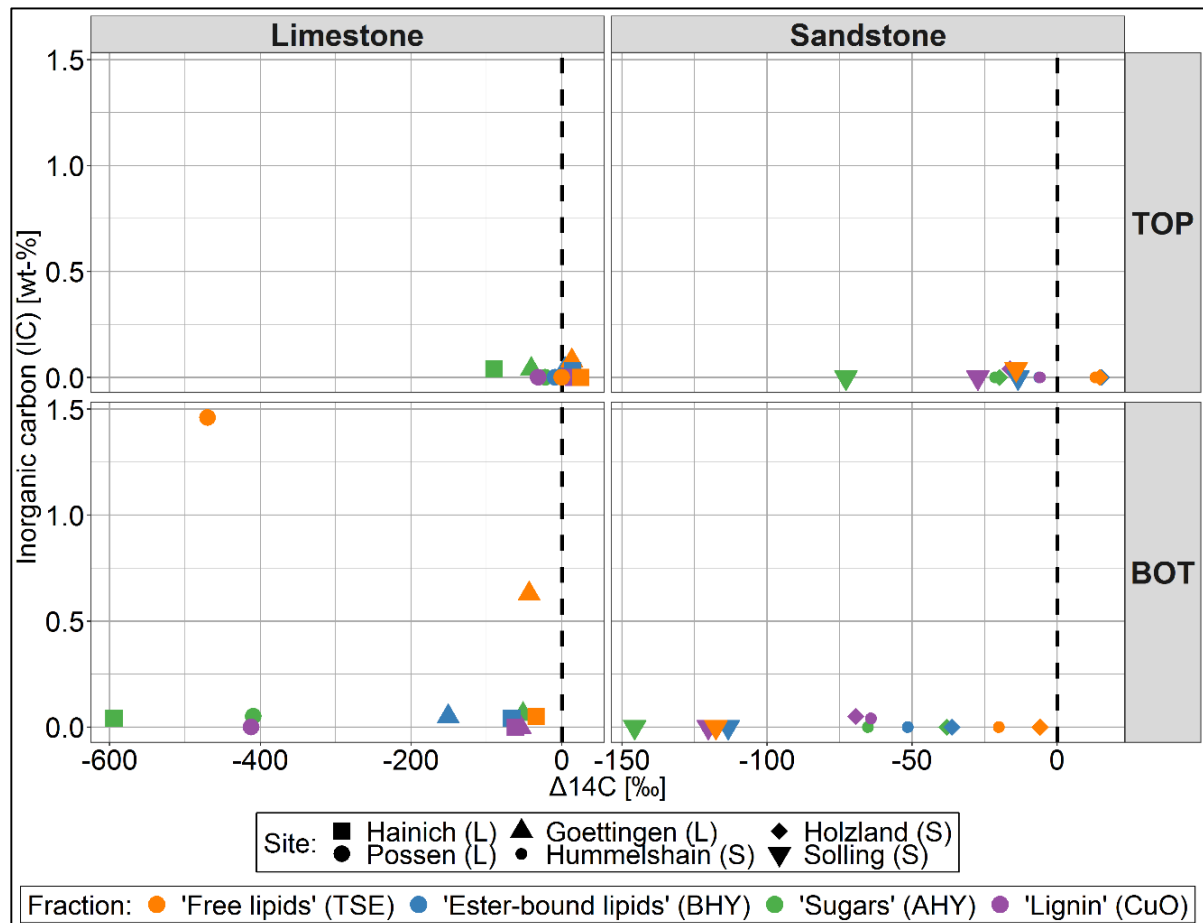
Figure 16: $\Delta^{14}C$ [‰] and IC [wt-%] TOP (0–10 cm) and BOT (30–60 cm) soil residues for limestone (HAI_L, POS_L, GOT_L) and sandstone (HUM_S, HOL_S, SOL_S) sites. Samples below LLQ were set to 0 for IC. Note different scales for x-axis.

A more dynamic picture arises for the **extracts** between different fractions, bedrock materials and depth layers (Figure 17). Again, the AHY extracts yielded the oldest radiocarbon compared to the extracts of the other fractions. The AHY extracts at the limestone sites are on average by more than 600 ‰ depleted in ^{14}C compared to the other three (TSE, BHY, CuO) extracts and at the sandstone sites by about 50 ‰ (Table 9).

The relative high values of $\Delta^{14}C$ of the plant-derived products (TSE, BHY, and CuO extracts) lead to the assumption that those compounds do not or only on a small scale contribute to the existence of very old C in SOM at the study sites and were not stabilized against decomposition. This agrees with other studies, e.g. by Gleixner (2013) concluding that plant-derived compounds do not form an important fraction of mineral soil organic matter. He further postulates (based on other studies) that those compounds are rapidly decomposed. If found in soils, they are not stabilized, only not yet decomposed; probably due to the separation of de-

composers from their substrates. Mikutta et al. (2006) found this correlation also for lignin (CuO extracts).

In the past, plant-derived lignin has been considered comparably resistant against microbial decomposition since only a limited group of fungi (white rot fungi) is able to completely decompose lignin (Kögel-Knabner 2002). The influence of fungi on lignin decomposition can be seen when comparing the sandstone sites with the limestone ones. The first one, likely dominated by fungi due to the relatively low pH-value, showed higher $\Delta^{14}C$ values, leading to the assumption that at those sites lignin was less stabilized due to higher fungal decomposition rates. However, those values did not show a significant contribution of lignin to older radiocarbon ages. Contradictory to that several studies consider microbial biomass to be a major part of the active labile pool as well (von Lützow et al. 2007). Acid hydrolysis (AHY) for example has been proposed to result in the extraction of young, potentially biodegradable compounds (e.g. proteins, nucleic acids, and polysaccharides), leaving an old cC fraction in the corresponding soil residue behind (Paul et al. 1997). This is not true for the data presented here (Figure 17), where the AHY extracts (sugar-like products) shows very old radiocarbon ages at all sites. Similar results have been reported by Gleixner et al. (2002), supporting the hypothesis that the age of different fractions is mainly caused by individual soil sites characteristics (e.g. microbial activity, organo-mineral associations) and not on the chemical recalcitrance of the individual compounds (Marschner et al. 2008). Yet, some studies argue that microorganisms are capable of taking up ancient C from soils and sediments under certain conditions (Kuzyakov et al. 2009; Rethemeyer et al. 2004; Seifert et al. 2011).
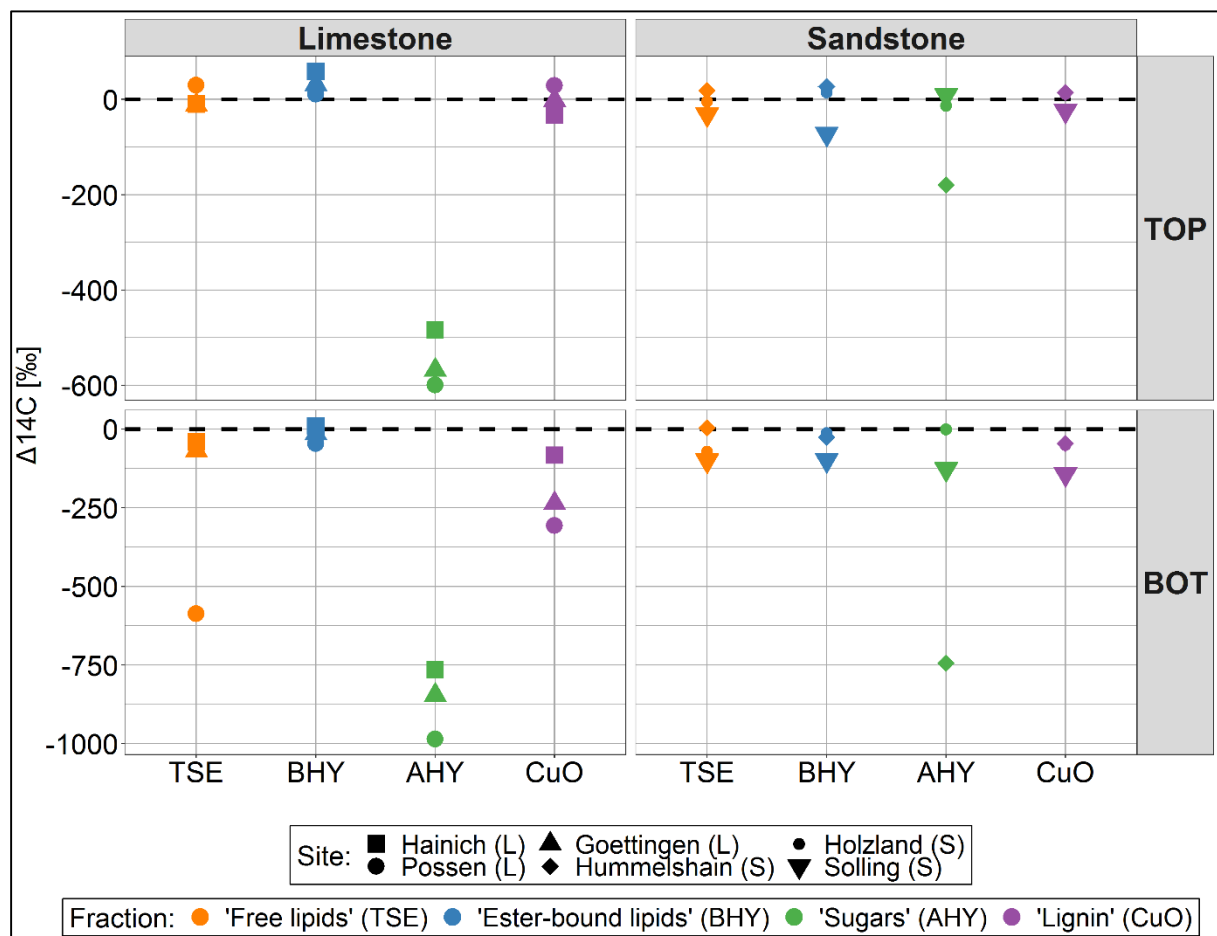
Figure 17: $\Delta^{14}C$ [‰] of TOP (0–10 cm) and BOT (30–60 cm) extracts for limestone (HAI$_L$, POS$_L$, GOT$_L$) and sandstone (HUM$_S$, HOL$_S$, SOL$_S$) sites. Note different scales for y-axis.

Such uptake by microorganisms would explain the depletion of ^{14}C and ^{13}C of those extracts – especially at the limestone sites ($R^2 = 0.88$), yet probably more important and visible at lower depth (Figure 18). However, under natural condition the detected old C in the AHY extracts is probably protected from decomposition in the carbonates and was only dissolved due to the strong solvent (HCl) used during that extraction step. Yet, enhanced weathering due to climate change could lead to dissolution of carbonates, resulting in the release of protected C which would then become available for microorganisms.
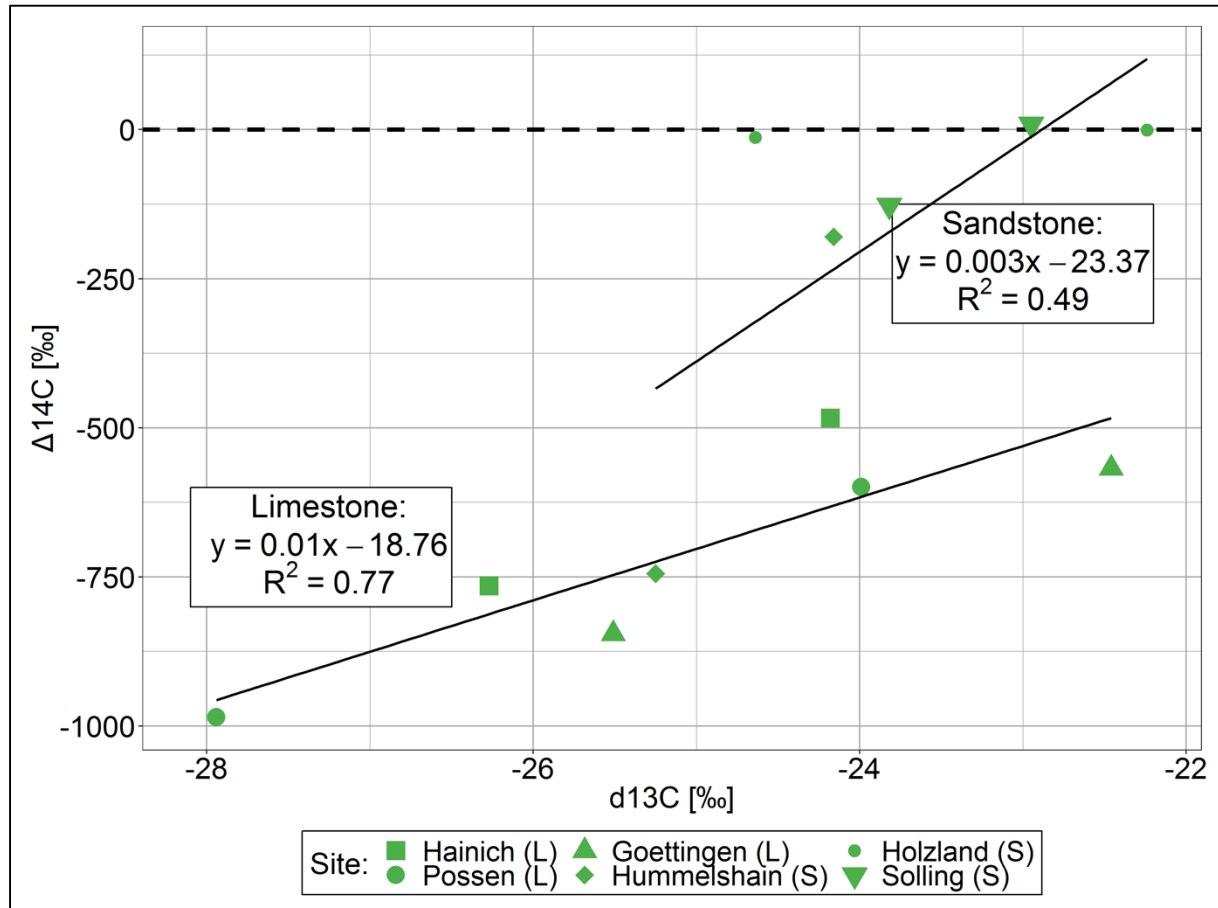
Figure 18: δ^{13}C and Δ^{14}C [‰] of TOP (0–10 cm) and BOT (30–60 cm) AHY ('Sugars') extracts for limestone (HAI$_L$, POS$_L$, GOT$_L$) and sandstone (HUM$_S$, HOL$_S$, SOL$_S$) sites

Similar to the soil residue fractions, the Δ^{14}C value of each extract decreases with depth (Figure 17). This has been observed in several other studies (e.g. Angst et al. 2018; Rethemeyer et al. 2005). The trend is again larger for the limestone sites than for the sandstone sites, indicating that the influence of limestone bedrock material on the Δ^{14}C values of the extracts was larger compared to sandstone sites. The increase in the radiocarbon age of the plant-derived fractions (TSE, BHY, and CuO) can have different reasons. One hypothesis would be that fresh plant input (e.g. litter from aboveground and roots) was decomposed to some degree and then transported via bioturbation and dissolved organic matter into deeper soil layers. This is only possible if the compounds are stabilized against decomposition through protection e.g. their mineral association, aggregates, or spatial isolation (Trumbore 2009).

Another hypothesis would be that the root input (including dead roots and organic materials released from living roots as rhizodeposition), which is probably an important C input in lower soil horizons (Jobbágy and Jackson 2000; Jones et al. 2009), contributes to older radiocar-

bon ages of plant-derived products. Gaudinski et al. (2001) reported an increase of the age of fine roots (< 2 mm) with depth. Sampled live roots from the B horizon had a mean age of 11–18 years compared to a mean age of 3–8 years in the organic horizons. Yet, this alone does not explain the relatively low $\Delta^{14}C$ values for plant-derived products. A combination of both hypotheses is probably more likely. The decomposition of older root products by microorganisms could also contribute to their older radiocarbon age with depth. Again, this would also be only one of several other drivers contributing to older radiocarbon ages and stabilization of SOM. The SOL_S samples were always the ones with the smallest $\Delta^{14}C$ value compared to the other sandstone sites, similar to the bulk soil samples (Figure 11). This might be caused by SOL_S being the only sandstone site influenced by loess deposition and receiving MAP above 1'190 mm.

At the limestone sites the AHY fraction at the BOT layer (median: -845.3‰) was by far the oldest fraction as well. This supports the hypothesis that the $\Delta^{14}C$ values of microbial-derived products was influenced by bedrock material, e.g. different geochemistry and the contribution of ancient C from the sedimentary rocks (Figure 18). The CuO fraction is the second oldest fraction with a median value of -236.4 ‰, followed by the TSE fraction (median: -68.3 ‰) and the BHY fraction (median: -1.55 ‰). The small $\Delta^{14}C$ value of the CuO extracts indicate that with increasing depth (at least at the limestone sites) lignin contributed on a larger scale to old SOM. This contradicts results for the TOP samples and from Mikutta et al. (2006), who could not find an important contribution of lignin to mineral-protected and recalcitrant OM. On the other hand, since the limestone sites are likely dominated by bacteria, the CuO products (lignin) might not be decomposed much, resulting in lower $\Delta^{14}C$ values. POS_L has, similar to the soil residues, the lowest $\Delta^{14}C$ values within each fraction. The site seems to have distinct soil characteristics (e.g. microbial activity, mineralogy) compared to the other sites, resulting in significantly different isotopic signatures. Additional analyses would be needed to corroborate this.

In conclusion, the sequential chemical extraction method is suitable to separate SOM of different soils into distinct chemical pools. This becomes clear when comparing the $\delta^{13}C$ and organic carbon (OC) values of the obtained extracts. Three out of four extraction steps (TSE, BHY, and CuO) result in the isolation of mainly plant-derived products; independent of depth and bedrock material. Yet, to clearly identify the extracted chemical components, more analyses are needed, e.g. GC-MS. The same is true for soil residues where the $\delta^{13}C$ values do not give an idea about the SOM origin. This is probably caused by the methods' low extraction efficiency: only 0.1–12 % of SOC was detectable in the extracts and the OC content of the correlating soil residue did not sum up to 100 % of the original SOC. Yet, the loss of C was usually within the error of the extraction step. The high error relates to operationally-defined and empirical character of the applied method.

Independent of bedrock material, the fractions obtained from the TOP layer (0–10 cm) usually were less depleted in ^{14}C (soil residues and extracts) compared to the BOT layer (30–60 cm); indicating a larger contribution of older C in the subsoils. On average, the AHY fractions (soil residue and extract) always yielded the lowest $\Delta^{14}C$ value. Thus, microbial-derived products either take up ancient C from the soil or they recycle C over a long period of time. In terms of $\delta^{13}C$, the soil residues did not show any significant trend between the two layers, whereas some of the extracts showed changes. Those changes seem to be driven more by the bedrock material, resulting in different microorganism metabolisms and mineral protection of the SOM, and differ for the individual extracts.

Distinct differences also occurred between the two bedrock materials (limestone and sand-stone). The extraction method resulted in different yields for the two bedrock types. Yields of plant-derived products were usually higher at the sandstone sites, possibly correlated with the lower pH-values. The microbially-derived products contained similar amounts of SOC, yet the content was higher in the limestone site BOT layers than in the same layer of the sand-stone sites. The soil residues of the latter were less enriched in ^{13}C compared to the lime-stone sites. The same is true for the extracts in the TOP layer. In the BOT layer, the TSE and BHY extracts showed similar $\delta^{13}C$ values (-31.3 to -29.5 ‰), whereas the CuO extracts were more depleted in ^{13}C (limestone: -26.6 ‰, sandstone: -28.1 ‰) and the AHY extracts more enriched (limestone: -26.3 ‰, sandstone: -23.8 ‰) in the sandstone sites. The increase of differences between the two bedrock materials with depth indicates that the parent material drives those alterations.

The $\Delta^{14}C$ values of the soil residues in the TOP layer show differences between limestone and sandstone sites. The soil residues have higher $\Delta^{14}C$ values (median: 1.7 ‰) at the lime-stone sites compared to the sandstone sites (median: -13.9 ‰). That difference decreased with depth, although the limestone soil age was older (limestone: -66.4 ‰, sand-stone: -64.7 ‰). Differences between the extracts are clearer in comparison. Median extract values had more similar age distribution at the sandstone sites, ranging from -13.2 to 14.8 ‰ at the TOP layer and from -127 to -25.4 ‰ at the BOT layer. The AHY extracts were always the lowest and the BHY on the highest. This is also true for the limestone sites, albeit with higher variation (TOP: -568.0 to 31.4 ‰, BOT: -845.0 to -1.6 ‰). This behavior leads to the assumption that the AHY extracts were mainly influenced by the different parent materials.

5.   Conclusions

This study investigated the influence of parent material and depth effects on radiocarbon ages in different chemical fractions of Central Germany soils. Samples from six sites were taken at two different depth intervals (TOP: 0–10 cm; BOT: 30–60 cm). Three of those soils developed over limestone bedrock material (HAI$_L$, POS$_L$, GOT$_L$), and the other three over sandstone (HUM$_S$, HOL$_S$, SOL$_S$). All sites are characterized by similar vegetation (European beech forest: *Fagus sylvatica L.*) and climate. Soil characteristics (pH, SOC, TN) of the bulk soil samples show distinct differences between the two bedrock materials and between the depth intervals, yet individual sites also differ independent of bedrock material.

TOP samples received higher C and N input from aboveground litter and from roots as compared to BOT samples. This results in higher amounts of processed SOM in the BOT layers (smaller C/N ratios). The three limestone sites show higher SOC and N content in both depths and are more processed with more narrow C/N ratios compared to the sandstone sites. Limestone sites usually showed neutral to slightly acidic pH values. Yet, all those sites were overprinted by loess deposition, which likely suppresses influence of carbonate-containing parent material. In contrast, the sandstone sites showed acidic soil conditions throughout. SOL$_S$ is the only sandstone site influenced by loess deposition, which makes the direct comparison of the two bedrock materials slightly more challenging. Nevertheless, the three limestone sites show higher variance between each other than the sandstone sites.

In the following, the initially formulated research questions will be answered and discussed in detail:

Q1: How do the two different bedrock materials influence Δ^{14}C and δ^{13}C values in the bulk soil samples?

Influence of parent material should be more prominent in the lower soil layers (BOT). Yet, differences already occur in the TOP layers. The sandstone sites are more depleted in ^{13}C (TOP: -27.5 ‰, BOT: -27.4 ‰) in both layers as compared to the limestone sites (TOP: -26.9 ‰, BOT: -25.8 ‰). This agrees with their larger C/N, suggesting lower soil processing. Differences between the TOP and BOT layers are larger at the limestone sites, indicating that the influence of bedrock material on the δ^{13}C value is larger than at the sandstone sites. The same is true for larger differences between the individual sites among the limestone sites.

The limestones sites are more depleted in ^{14}C (TOP: 2.8 ‰, BOT: -177.0 ‰) in both depths as compared to the sandstone sites (TOP: 18.4 ‰, BOT: -37.9 ‰). In the past, higher clay content was usually used to explain lower Δ^{14}C values due to the high sorption capacity of clay minerals. This does not apply for all sites studied here, other minerals (e.g. iron and aluminum) may also influence SOM stabilization. Carbonate-containing soils usually have higher amounts of exchangeable calcium (in the clay fraction), which may explain lower Δ^{14}C values. Additionally, the different pH-values result in modified soil properties (e.g. cation composition) which in turn influence SOC dynamics. All soil properties mentioned influence the soil biota, which make up a large portion of SOM and can therefore control stabilization processes. The limestone sites are likely be more dominated by bacteria, whereas fungi may dominate at the sandstone sites. This is mainly caused by the different pH-values, since bacteria prefer higher pH-values compared to fungi. The influence of different microbial communities on SOC stabilization needs to be investigated deeper, it could not be empirically verified in this study.

As mentioned above, considerable differences emerged between sites with the same bed-rock material. Those differences must be caused by parameters other than parent material. Climatic conditions can influence soil properties on a large scale. Yet, all sites are exposed to similar climate. is the only site with significantly higher MAP (1'190 mm), while the other five sites receive between 700–850 mm/a. SOL_S has the second lowest $\Delta^{14}C$ values of all sites in the TOP and BOT layer. The low $\Delta^{14}C$ value of GOT_L in the TOP layer is probably related to atmospheric input from older C (e.g. fossil fuel-related dust). The low $\Delta^{14}C$ value at POS_L BOT is probably more related to specific soil geochemistry at the site. Sampling depth was deepest (~60 cm) at POS_L and so was the inorganic C content. Yet, the POS_L clay content is the lowest of all three sites, suggesting that clay content seems not to be the controlling soil property of low $\Delta^{14}C$ values. All parameters mentioned and discussed are hypothesis' based on observations. The individual role and distribution of those parameters remain unclear.

In conclusion, various drivers occur in different magnitude and distribution in such complex and heterogeneous system as SOM. No meaningful conclusion can be drawn about the origin and contribution of old C based on single bulk soil samples. It is likely that all of the processes named occur – and even more. Yet, bedrock material seems to influence those drivers.

Q2: How much do the $\Delta^{14}C$ and $\delta^{13}C$ values differ in the individual chemical fractions, soil depths and bedrock materials?

The differences between the fractions (TSE, BHY, AHY, CuO) in terms of $\Delta^{14}C$ and $\delta^{13}C$ are more visible for the extracts than for the soil residues of the sequential chemical extraction. This might be due to the low efficiency of the method. Differences between the **soil residues** increased with depth, indicating an influence of bedrock material on the SOC content in those fractions. The differences were larger at the limestone sites and for $\Delta^{14}C$ values, suggesting that site-specific properties play a significant role. Without chemical analysis on the molecular level of those soil residues it is impossible to identify controlling factors.

The **$\delta^{13}C$** values show that the four different **extracts** contain different organic compounds. Independent of depth and bedrock material, the AHY extracts show the highest $\delta^{13}C$ value (median: -24.2 ‰), whereas the other extracts show much lower values and are more similar between each other (TSE: -31.0 ‰, BHY: -29.5 ‰, CuO: -28.0 ‰). Those values indicate that microbial components mainly dominated the AHY extracts and that plant-derived products dominated the other three extracts. This general pattern remains unchanged for the different depth layers and bedrock materials. Independent of depth and parent material, the TSE and BHY extracts always showed similar isotopic composition, ranging between -32 and -29 ‰. The other two extracts (CuO and AHY) were more dynamic and seemed to be influenced by depth and bedrock material. Differences between the two parent materials was negligible in the TOP layers; both extracts vary by less than 0.2 ‰ (AHY: limestone: -24.0 ‰, sandstone: -24.2 ‰; CuO: limestone: -28.4 ‰, sandstone: -28.5 ‰). Differences became larger with increasing depth (and influence of the bedrock material). The median $\delta^{13}C$ value of the AHY extract decreased by 2.3 ‰ at the limestone sites, whereas it slightly increased by 0.4 ‰ at the sandstone sites. The relatively large ^{13}C depletion of this fraction with depth at the limestone sites indicates that the C source changed. This may be caused by the release of sedimentary C during that extraction step or by microbes metabolizing less enriched C in the deeper layer. The same was true for the CuO fraction, where the median $\delta^{13}C$ value increased in the same magnitude (limestone: $\Delta = 2.0$ ‰, sandstone: $\Delta = 0.4$ ‰). Those patterns indicate that extracts of the limestone bedrock sites were more influenced by the under-

lying parent material than those of the sandstone sites. Further analyses of extracts, soils and parent materials is needed to elucidate the reason for those differences.

The Δ^{14}C values of the different **extracts** also support the hypothesis that they contain distinct organic components that are influenced by depth and bedrock material. Similar to the δ^{13}C values, the AHY fraction showed the largest difference compared to the other extracts independent of depth and bedrock material (AHY: -526.0 ‰, TSE: -21.4 ‰, BHY: 10.4 ‰, CuO: -39.4 ‰). Except for the BHY fraction, all other extracts were on average mainly influenced by C that had been separated from the atmosphere for several hundred years. This contradicts the assumption that the TSE, BHY, and CuO fractions are mainly composed of plant-derived products which should contain mostly younger C. The low Δ^{14}C value of the AHY fraction indicates that the main source of the microbial biomass is ancient C. Such C can have different origins: it can come partly from the sedimentary rocks, it can be protected from decomposition due to physical and or chemical protection, it can be part of continuous recycling processes, or other parameters might play a role that have not been identified yet, based on the encountered soil, bedrock, and environmental characteristics. The applied method might also play a role. However, all fractions show, independent of the bedrock material, a decrease of the Δ^{14}C value with depth.

At the TOP layer the BHY and CuO extracts yielded positive Δ^{14}C values (BHY: 21.0 ‰, CuO: 4.85 ‰), reflecting the influence of fresh plant-derived products. The TSE and AHY extracts showed negative values of -7.0 ‰ and -332.0 ‰, respectively. The largest difference between the two layers occurred for the AHY extracts (Δ = 423.0 ‰), followed by the CuO extracts (Δ = 117.9 ‰), the TSE extracts (Δ = 63.1 ‰), and the BHY extracts (35.0 ‰). The first two are those fractions that showed the largest difference for δ^{13}C, supporting the hypothesis that their C compositions largely depend on parameters controlled by depth (e.g. bedrock material). This might also explain, why their Δ^{14}C values are always lower at the limestone sites than as the sandstone sites, which seem to be less controlled by bedrock material properties. Therefore, the composition of those extracts should be analyzed in more detail.

The variation of the individual extracts is much larger at the limestone sites (especially in the BOT layer) compared to the sandstone sites. Therefore, soil from the same parent material can still have distinctive soil properties resulting in different Δ^{14}C values. This is especially true for the limestone sites, where loess deposition suppresses the signal of the bedrock material. This is also true for the SOL_S site from the sandstone sites. More care needs to be taken when identifying adequate sites to compare the distribution of factors controlling SOC dynamics.

Q3: Do age distribution and differences in Δ^{14}C among chemical fractions change with depth?

The differences between the four extracts increase with depth. This is especially true for the limestone sites. This trend is visible for the soil residues, too, albeit weaker. The larger differences at the limestone sites indicate that the geochemical composition of this bedrock material might have a significant influence on the Δ^{14}C signals (e.g. carbonates). Especially the AHY fractions show high variability, which may be caused by the release of sedimentary C from the soil matrix during that extraction step. Another hypothesis would be that microbes themselves metabolize older C from the soil matrix and/or the rock material. Both hypotheses can be easily distinguished from each other by analyzing the chemical composition. The latter one will consist mainly of low molecular weight biomarkers (Otto and Simpson 2007), whereas the release of sedimentary C due to the extraction will result in higher molecular

weights (Wiedemeier et al. 2016). Yet, it is likely that both processes play an important role at the same time and that a combination of both might explain the low $\Delta^{14}C$ values for the AHY fractions. The CuO fractions also seem to be influenced by the limestone bedrock material. This might be caused by its microbial community, which is either capable of degrading lignin (fungi) or not (bacteria). The role and behavior of lignin has been investigated and discussed in the community for several decades. Until now the question has not been resolved. The presented data set suggest that more detailed analyses of the CuO fractions might help to explain and understand the SOC stabilization, which contradicts some other studies (e.g. Mikutta et al. 2006). Again, this might depend on the bedrock material and cannot be generalized for soils.

When comparing all individual fractions with each other it becomes clear that the AHY fractions seem to play the most crucial role for the SOM dynamics at the studied sites. Recently, more and more studies proposed that the understanding of microbial processes and compositions is crucial to understand and explain SOM stabilization processes. The presented data support those assumptions. The other two fractions (TSE and BHY) might also contribute to the SOC stabilization, yet their relatively high $\Delta^{14}C$ values and low response to depth changes indicates that their role is limited.

The main objective of this work was to better understand SOM stabilization processes on the molecular scale. Obviously, this work could not find definitive answers to questions that have been discussed in the science community for several decades. Yet, it can contribute to understand SOC dynamics and address hypotheses based on the results obtained.

It is likely that the bedrock material contributes to the stabilization of SOM. Such contribution depends on the type of parent material – yet only certain compounds in SOM seem to respond. In this study, limestone material resulted in higher radiocarbon ages in the microbially-derived fraction (AHY). That fraction mostly consists of carbohydrates and amino acids. The low $\Delta^{14}C$ values are probably caused by the dissolution of soil carbonates during extraction, resulting in the release of protected OC. Under natural conditions, this OC would be protected in the carbonates and not available for microorganisms. However, environmental changes (e.g. increasing average temperature) may enhance carbonate weathering. This, in turn, would result in old OC release. Thus, formerly protected OC would become vulnerable to decomposition by microorganisms. If OC gets taken up by microbes it becomes part of the fast soil C pool. If this case, old C does no longer "automatically" imply that it is protected from decomposition, but that it is vulnerable to atmosphere release – enhancing climate change. This additional response should be taken into account when modelling the potential behavior of soils under climate change.

6.   Outlook

Up to the present day, the understanding of SOC dynamics is largely based on processes that occur in surface-near soil (20–30 cm). This focus probably leads to misinterpret certain drivers because many processes occur below 30 cm soil depth and may behave differently at the surface. Especially the influence of bedrock material cannot be investigated close to the surface. A literally a deeper look into the soil profile is paramount to better understand SOC dynamics and to predict how SOC will behave with abrupt environmental change (e.g. temperature increase, land-use change). The role of parent materials on SOC dynamics has gained little attention despite its influencing role on soil (bio)geochemistry in addition to climate. Bedrock geochemistry exerts an influence on composition and behavior of microorganisms. Thus, microbial communities need to be investigated in more detail in order to fully understand the dynamics of stabilization and destabilization of SOC.

Based on the performed literature review and the results of this work, it is clear that more work should focus on the contribution of bedrock material on SOM stabilization and the role of microorganisms therein. More studies should analyze deeper soil material and samples from the underlying bedrocks, as well as composition and degradation of microbially-derived organic components. Ideally, such studies will not only focus on single points in the landscape but investigate transects through e.g. different bedrock materials to better compare different drivers on larger scales.

References

Aditha SK, Kurdekar AD, Chunduri LAA, Patnaik S, Kamisetti V (2016) Aqueous based reflux method for green synthesis of nanostructures: Application in CZTS synthesis. *MethodsX, 3*: pp. 35-40, doi: 10.1016/j.mex.2015.12.003.

Angst G, Cajthaml T, Angst S, Mueller KE, Kögel-Knabner I, Beggel S, Kriegs S, Mueller CW (2017) Performance of base hydrolysis methods in extraction bound lipids from plant material, soils, and sediments. *Organic Geochemistry, 113*: pp. 97-104, doi: 10.1016/j.orggeochem.2017.08.004.

Angst G, John S, Mueller CW, Kögel-Knabner I, Rethemeyer J (2016) Tracing the sources and spatial distribution of organic carbon in subsoils using a multi-biomarker approach. *Scientific Reports, 6*: pp., doi: 10.1038/srep29478.

Angst G, Messinger J, Greiner M, Häusler W, Hertel D, Kirfel K, Kögel-Knabner I, Leuschner C, Rethemeyer J, Mueller CW (2018) Soil organic carbon stocks in topsoil and subsoil controlled by parent material, carbon input in the rizosphere, and microbial-derived compunds. *Soil Biology and Biochemistry, 122*: pp. 19-30, doi: 10.1016/j.soilbio.2018.03.026.

Asch K, Lahner L, Zitzmann A (2003) Die Geologie von Deutschland – ein Flickenteppich. In *Nationalatlas Bundesrepublik Deutschland. Band 2 – Natur und Umwelt I: Relief, Boden und Wasser,* Leibniz-Institut für Länderkunde: Leipzig (Germany), pp. 32-35.

ASTM D1193-91 (1991) Standard Specification for Reagent Water. ASTM International, West Conshohocken, PA 19428-2959, United States.

Baede APM, Ahlonsou E, Ding Y, Schimel D (2001) Observed Climate Variability and Change. In Houghton JT, Ding Y, Griggs DJ, Noguer M, van der Linden PJ, Dai X, Maskell K and Johnson CA (eds.) *Climate Change 2001: The Scientific Basis. Contribution of Working Gropu I to the Third Assessment Report of the Intergovernmental Panel on Climate Change,* Cambridge University Press: Cambridge, United Kingdom and New York, NY, USA, pp. 87-98.

Balesdent J, Basile-Doelsch I, Chadoeuf J, Cornu S, Derrien D, Fekiacova Z, Hatté C (2018) Atmosphere–soil carbon transfer as a function of soil depth. *Nature, 559*(7715): pp. 599-602, doi: 10.1038/s41586-018-0328-3.

Balesdent J, Girardin C, Mariotti A (1993) Site-related ^{13}C of tree leaves and soil organic matter in a temperate forest. *Ecology, 74*(6): pp. 1713-1721, doi: 10.2307/1939930.

Balesdent J, Mariotti A, Guillet B (1987) Natural ^{13}C abundance as a tracer for studies of soil organic matter dynamics. *Soil Biology and Biochemistry, 19*(1): pp. 25-30, doi: 10.1016/0038-0717(87)90120-9.

Blume H-P, Brümmer GW, Fleige H, Horn R, Kandeler E, Kögel-Knabner I, Kretzschmar R, Stahr K, Wilke B-M (2016) *Scheffer/Schachtschabel Soil Science,* Springer: Berlin, Heidelberg, Germany, pp. 618.

Brand WA, Coplen TB (2012) Stable isotope deltas: tiny, yet robust signatures in nature. *Isotopes in Environmental and Health Studies, 48*(3): pp. 393-409, doi: 10.1080/10256016.2012.666977.

Ciais P, Sabine C, Bala G, Bopp L, Brovkin V, Canadell J, Chhabra A, DeFries R, Galloway J, Heimann M, Jones C, Le Quéré C, Myneni R, Piao S, Thornton P (2013) Carbon and other biogeochemical cycles. In Stocker T, Qin D, Plattner G, Tignor M, Allen S, Boschung J, Nauels A, Xia Y, Bex V and Midgley P (eds.) *Climate Change 2013: The Physical Science Basis. Contribution of Working Group I to the Fifth Assessment Report of the Intergovernmental Panel on Climate Change,* Cambridge University Press: Cambridge, United Kingdom and New York, NY, USA, pp. 465-570.

Coplen TB (2011) Guidelines and recommended terms for expresion of stable-isotope-ratio and gas-ratio measurement results. *Rapid Communications in Mass Spectrometry, 25*: pp. 2538-2560, doi: 10.1002/rcm.5129.

Crow SE, Swanston CW, Lajtha K, Brooks R, Keirstead H (2007) Density fractionation of forest soils: methodological questions and interpretation of incubation results and turnover

times in an ecosystem context. *Biogeochemistry, 86*: pp.69-90, doi: 10.1007/ s10533-007-9100-8.

Cubasch U, Wuebbles D, Chen D, Facchini MC, Frame D, Mahowald N, Winther J-G (2013) Introduction. In Stocker T, Qin D, Plattner G, Tignor M, Allen S, Boschung J, Nauels A, Xia Y, Bex V and Midgley P (eds.) *Climate Change 2013: The Physical Science Basis. Contribution of Working Group I to the Fifth Assessment Report of the Intergovernmental Panel on Climate Change,* Cambridge University Press: Cambridge, United Kingdom and New York, NY, USA, pp. 119-158.

Doetterl S, Berhe AA, Arnold C, Bodé S, Fiener P, Finke P, Fuchslueger L, Griepentrog M, Harden JW, Nadeu E, Schnecker J, Six J, Trumbore SE, van Oost K, Vogel C, Boeckx P (2018) Links among warming, carbon and microbial dynamics mediated by soil mineral weathering. *Nature Geoscience, 11*: pp. 589-593, doi: 10.1038/s41561-018-0168-7.

Doetterl S, Six J, van Wesemael B, van Oost K (2012) Carbon cycling in eroding landscapes: geomorphic controls on soil organic C pool composition and C stabilization. *Global Change Biology, 18*: pp. 2218-2232, doi: 10.1111/j.1365-2486.2012.02680.x.

Doetterl S, Stevens A, Six J, Merckx R, Van Oost K, Casanova Pinto M, Casanova-Katny A, Muñoz C, Boudin M, Zagal Venegas E, Boeckx P (2015) Soil carbon storage controlled by interactions between geochemistry and climate. *Nature Geoscience, 8*: pp. 780-783, doi: 10.1038/ngeo2516.

Ehleringer JA, Rundel PW (1989) Stable Isotopes: History, Units, and Instrumentation. In Rundel PW, Ehleringer JR and Nagy KA (eds.) *Stable isotopes in ecological research,* Springer: New York, U.S.A., pp. 1-15.

Elementar Analysensysteme (n.d.) *Bedienungsanleitung vario MAX.* Langenselbold, Germany.

Ellenberg H (1988) *Vegetation Ecology of Central Europe,* Cambridge University Press: Cambridge (U.K.), pp. 731.

Finke P, Opolot E, Balesdent J, Berhe AA, Boeckx P, Cornu S, Harden JW, Hatté C, Williams E, Doetterl S (2019) Can SOC modelling improved by accounting for pedogenesis? *Geoderma, 338*: pp. 513-524, doi: 10.1016/j.geoderma.2018.10.018.

Forsyth WGC (1947) Studies on the more soluble complexes of soil organic matter – A method of fractionation. *Biochemical Journal, 41*(2): pp. 176-181, doi: 10.1042/bj0460141.

Friedlingstein P, Meinshausen M, Arora VK, Jones CD, Anav A, Liddicoat SK, Knutt R (2014) Uncertainties in CMIP5 Climate Projections due to Carbon Cycle Feedbacls. *American Meteorological Society, 27*: pp. 511-526, doi: 10.1175/JCLI-D-12-00579.1.

Fry B (2006) *Stable Isotope Ecology,* Springer: New York, NY, USA, pp. 308.

Gaudinski JB, Trumbore SE, Davidson EA, Cook AC, Markewitz D, Richter DD (2001) The age of fine-root carbon in three forests of the eastern United States measured by radiocarbon. *Oecologia, 129*: pp. 420-429, doi: 10.1007/s004420100746.

Gaudinski JB, Trumbore SE, Davidson EA, Zheng S (2000) Soil carbon cycling in a temperate forest: radiocarbon-based estimates of residence times, sequestration rates and partitioning of fluxes. *Biogeochemistry, 51*(1): pp. 33-69, doi: 10.1023/A:1006301010014.

Glaser B (2005) Compound-specific stable isotope (13C) analysis in soil science. *Journal of Plant Nutrition and Soil Science, 168*: pp. 633-648, doi: 10.1002/jpln.200521794.

Gleixner G (2013) Soil organic matter dynamics: a biological perspective derived from the use of compound-specific isotopes studies. *Trends in Isotope ecology, 28*: pp. 683-695, doi: 10.1007/s11284-012-1022-9.

Gleixner G, Danier H-J, Werner RA, Schmidt H-L (1993) Correlations between the ^{13}C content of primary and secondary plant products in different cell compartments and that in decomposing Basidiomycetes. *Plant Physiology, 102*(4): pp. 1287-1290, doi: 10.1104/pp.102.4.1287.

Gleixner G, Poirier N, Bol R, Balesdent J (2002) Molecular dynamics of organic matter in a cultivated soil. *Organic Geochemistry, 33*(3): pp. 357-366, doi: 10.1016/S0146-6380(01)00166-8.

Goh KM, Reid MR (1975) Molecular weight distribution of soil organic matter as affected by acid pre-treatment and fractionation into humic and fulvic acids. *Journal of Soil Science, 26*(3): pp. 207-222, doi: 10.1111/j.1365-2389.1975.tb01944.x.

Großherr M (2011) *Auswirkungen des Waldumbaus auf bodenchemische Eigenschaften (KAK und Acidität) in Bodenprofilen des Thüringer Forstreviers Leuchtenburg.* Unpublished Wissenschaftliche Hausarbeit, Department of Geography at the Friedrich Schiller University Jena: Jena, pp. 132.

He Y, Trumbore SE, Torn MS, Harden JW, Vaughn LJS, Allison SD, Randerson JT (2016) Radiocarbon constraints imply reduced carbon uptake by soils during the 21st century. *Science, 353*(6306): pp. 1419-1423, doi: 10.1126/science.aad4273.

Hedges JI, Ertel JR (1982) Characterization of Lignin by Gas Capillary Chromatography of Cupric Oxide Oxidation Products. *Analytical Chemistry, 54*(2): pp. 174-178, doi: 10.1021/ac00239a007.

Huss J-M (2017) *Untersuchung der Abhängigkeit des Bodenwasserpotentials von der Entfernung zu einem Baum in einem Buchenmischwald.* Unpublished Bachelor thesis, Department of Geoscience at the University of Jena: Jena, pp. 40.

Ingalls AE, Ellis EE, Santos GM, McDufee KE, Truxal L, Keil RG, Druffel ERM (2010) HPLC purification of higher plant-dervied lignin phenols for compound specific radiocarbon analysis. *Analytical Chemistry, 82*(21): pp. 8931-8938, doi: 10.1021/ac1016584.

Jenkinson DS, Poulton PR, Bryant C (2008) The turnover of organic carbon in subsoils. Part 1. Natural and bomb radiocarbon in soil profiles from the Rothamsted long-term field experiments. *European Journal of Soil Science, 59*: pp. 391-399, doi: 10.1111/j.1365-2389.2008.01025.x.

Jobbágy EG, Jackson RB (2000) The vertical distribution of soil organic carbon and its relation to climate and vegetation. *Ecological Applications, 10*(2): pp. 423-436, doi: 10.1890/1051-0761(2000)010[0423:TVDOSO]2.0.CO;2.

Jones DL, Nguyen C, Finlay RD (2009) Carbon flow in the rhizosphere: carbon trading as the soil-root interface. *Plant and Soil, 321*: pp. 5-33, doi: 10.1007/s11104-009-9925-0.

Kleber M, Nico PS, Plante A, Filley T, Kramer M, Swanston C, Sollins P (2011) Old and stable soil organic matter is not necessarily chemically recalcitrant: implications for modeling concepts and temperature sensitivity. *Global Change Biology, 17*: pp. 1097-1107, doi: 10.1111/j.1365-2486.2010.02278.x.

Knohl A, Schulze E-D, Kolle O, Buchmann N (2003) Large carbon uptake by an unmanaged 250-year-old deciduous forest in Central Germany. *Agricultural and Forest Meteorology, 18*: pp. 151-167, doi: 10.1016/S0168-1923(03)00115-1.

Kögel-Knabner I (2000) Analytical approaches for characterizing soil organic matter. *Organic Geochemistry, 31*(7-8): pp. 609-625, doi: 10.1016/S0146-6380(00)00042-5.

Kögel-Knabner I (2002) The macromolecular organic composition of plant and microbial residues as inputs to soil organic matter. Soil Biology and Biogeochemistry, 34: pp. 139-162, doi: 10.1016/S0038-0717(01)00158-4.

Küsel K, Totsche KU, Trumbore SE, Lehmann R, Steinhäuser C, Hermann M (2016) How deep can surface signals be traced in the critical zone? Merging biodiversity with biogeochemistry research in a central German Muschelkalk landscape. *Frontiers in Earth Science, 4(32)*: pp. 18, doi: 10.3389/ferat.2016.00032.

Kuzyakov Y, Subbotina I, Chen H, Bobomolova I, Xu X (2009) Black carbon decomposition and incorporation into soil microbial biomass estimated by ^{14}C labeling. *Soil Biology and Biochemistry, 41*: pp. 210-219, doi: 10.1016/j.soilbio.2008.10.016.

Le Clercq M, van der Plicht J, Gröning M (1998) New ^{14}C reference materials with activities of 15 and 50 pMC. *Radiocarbon, 40*(1): pp. 295-297, doi: 10.1017/S0033822200018178.

Lehmann J, Kleber K (2015) The contentious nature of soil organic matter. *Nature*, 528: pp. 60-68, doi:10.1038/nature16069.

Lemke M (2006) *Die C-Dynamik von Waldböden bei reduzierten Stoffeinträgen (Dachprojekt Solling),* Forschungszentrum Waldökosysteme Göttingen, pp 100.

Marschner B, Brodowski S, Dreves A, Gleixner G, Gude A, Grootes PM, Hammer U, Heim A, Jandl G, Ji R, Kaiser K, Kalbitz K, Kramer C, Leinweber P, Rethemeyer J, Schäffer A, Schmidt MWI, Schwark L, Wiesenberg GLB (2008) How relevant is recalcitrnace for the stabilization of organic matter in soils? *Journal of Plant Nutrition and Soil Science, 171*: pp. 91-110, doi: 10.1002/jpln.200700049.

Martens DA, Loeffelmann KL (2003) Soil amino acid compsition quantified by acid hydrolysis and anion chromatography – Pulsed Amperometry. *Journal of Agricultural and Food Chemistry, 51*: pp. 6521-6529, doi: 10.1021/jf034422e.

Meesenburg H, Brumme R (2009) General description of study sites. In Brumme R and Khanna PK (eds.) *Functioning and Management of European Beech Ecosystems,* Springer: pp. 7-11.

Meesenburg H, Brumme R, Jacobsen C, Meiwes KJ, Eichhorn J (2009) Soil Properties. In Brumme R and Khanna PK (eds.) *Functioning and Managment of European Beech Ecosystems,* Springer: pp. 265-302.

Meesenburg H, Scheler B, Ahrends B, Klinck U (2011) Environmental monitoring in Northwest Germany – Intensive monitoring site "Goettinger Wald". in *IUFRO Beech Symposium* Dresden Germany: pp. 111-117.

Metzger JC, Wutzler T, Valle ND, Filipzik J, Grauer C, Lehmann R, Roggenbuck M, Schelhorn D, Weckmüller J, Küsel K, Totsche KU, Trumbore SE, Hildebrandt A (2017) Vegetation impacts soil water content patterns by shaping canopy water fluxes and soil properties. *Hydrological Processes, 31*: pp. 3783-3795, doi: 10.1002/hyp.11274.

Mikutta R, Kleber M, Torn MS, Jahn R (2006) Stabilization of soil organic matter: association with minerals or chemical recalcitrance? *Biogeochemistry, 77*: pp. 25-56, doi: 10.1007/s10533-005-0712-6.

Naafs DFW, van Bergen PF (2002) A qualitative study on the chemical composition of ester-bound moieties in an acidic andosolic forest soil. *Organic Geochemistry, 33*: pp. 189-199, doi: 10.1016/S0146-6380(01)00151-6.

Nierop KGJ (1998) Origin of aliphatic compounds in a forest soil. *Organic Geochemistry, 29*(4): pp. 1009-1016, doi: 10.1016/S0146-6380(98)00165-X.

Nierop KGJ, Naafs DFW, Verstraten JM (2003) Occurrence and distribution of ester-bound lipids in Dutch coastal dune soils along a pH gradient. *Organic Geochemistry, 34*: pp. 719-729, doi: 10.1016/S0146-6380(03)00042-1.

Otto A, Simpson MJ (2006) Evaluation of CuO oxidation parameters for determing the source and stage of lignin degradation in soil. *Biogeochemistry, 80*: pp. 121-142, doi: 10.1007/s10533-006-9014-x.

Otto A, Simpson MJ (2007) Analysis of soil organic matter biomarkers by sequential chemical degradation and gas chromatography – mass spectrometry. *Journal of Separation Science, 30*: pp. 272-282, doi: 10.1002/jssc.200600243.

Paul E, Follet RF, Leavitt SW, Halvorson A, Peterson GA, Lyon DJ (1997) Radiocarbon dating for determination of soil organic matter pool sizes and dynamics. *Soil Science Society of America Journal, 61*: pp. 1058-1067, doi: 10.2136/sssaj1997.03615995006100040011x.

Poeplau C, Don A, Six J, Kaiser M, Benbi D, Chenu C, Cotrufo MF, Derrien D, Gioachhini P, Grand S, Gregorich E, Griepentrog M, Gunina A, Haddiy M, Kuzyakov Y, Kühnel A, Macdonald LM, Soong J, Trigalet S, Vermeire M-L, Rovira P, van Sesmael B, Wiesmeier M, Yeasmin S, Yevdokimov I, Nider R (2018) Isolating organic carbon fractions with varying tunrover rates in temperate agricultural soils – A comprehensive method comparison. *Soil Biology and Biocehmistry,* 125: pp. 10-26, doi: 10.1016/j.soilbio.2018.06.025.

Rasmussen C, Heckman K, Wieder WR, Keiluweit M, Lawrence CR, Berhe AA, Blankinship JC, Crow SE, Druhan JL, Hicks Pries CE, Marin-Spiotta E, Plante A, Schädel C, Schimel JP, Sierra CA, Thompson A, Wagai R (2018) Beyond clay: towards an improved set of variables for predicting soil organic matter content. *Biogeochemistry, 137*: pp. 297-306, doi: 10.1007/s10533-018-0424-3.

Rasmussen C, Torn MS, Southard RJ (2005) Mineral assemblage and aggregates control carbon dynamics in a California conifer forest. *Soil Science Society of America Journal, 69*(6): pp. 1711-1721, doi: 10.2136/sssaj2005.0040.

Rasse DP, Dignac H, Rumpel C, Mariotti A, Chenu C (2005) Lignin turnover in an agricultural field: from plant residues to soil-protected fractions. *European Journal of Soil Science, 57*: pp. 530-538, doi: 10.1111/j.1365-2389.2006.00806.x.

Rethemeyer J, Kramer C, Gleixner G, John B, Yamashite T, Flessa H, Andersen N, Nadeau M-J, Grootes PM (2005) Transformation of organic matter in agricultural soils: radiocarbon concentration versus depth. *Geoderma, 128*: pp. 94-105, doi: 10.1016/j.geoderma.2004.12.017.

Rethemeyer J, Kramer C, Gleixner G, Wiesenberg GLB, Schwark L, Andersen N, Nadeau M-J, Grootes PM (2004) Complexity of soil organic matter: AMS ^{14}C analysis of soil lipid fractions and individual compounds. *Radiocarbon, 46*(1): pp. 465-473, doi: 10.1017/S0033822200039771.

Roos M, Porter FC, Aguilar-Benitez M, Montanet L, Walck C, Crawford RL, Kelly RL, Rittenberg A, Trippe TG, Wohl CG, Yost GP, Shimada T, Losty MJ, Copal GP, Hendrick RE, Shrock RE, Frosch R, Roper LD, Armstrong B (1982) Review of particle properties: Particle Data group. *Physical Letters, 111B*: pp. i-xxi, doi: 10.1016/0370-2693(82)91286-2.

Rumpel C, Kögel-Knabner I (2011) Deep soil organic matter – a key but poorly understood component of terrestrial C cycle. *Plant and Soil, 338*: pp. 143-158, doi: 10.1007/s11104-010-0391-5.

Schlesinger WH, Bernhardt ES (2013) *Biogeochemistry – An Analysis of Global Change (3rd edition),* Elsevier: USA, pp. 490.

Schmidt MWI, Torn MS, Abiven S, Dittmar T, Guggenberger G, Janssens IA, Kleber M, Kogel-Knabner I, Lehmann J, Manning DAC, Nannipieri P, Rasse DP, Weiner S, Trumbore SE (2011) Persistence of soil organic matter as an ecosystem property. *Nature, 478*(7367): pp. 49-56, doi: 10.1038/nature10386.

Schrumpf M, Kaiser K, Guggenberger G, Persson T, Kögel-Knabner I, Schulze E-D (2013) Storage and stability of organic carbon in soils as related to depth, occlusion within aggregates, and attachment to minerals. *Biogeosciences, 10*: pp. 1675-1691, doi: 10.5194/bg-10-1675-2013.

Schrumpf M, Kaiser K, Schulze E-D (2014) Soil organic carbon and total nitrogen gains in an old growth decidous forest in Germany. *PLoS ONE, 9*(2): pp. 8, doi: 10.1371/journal.pone.0089364.

Schuur EAG, Carbone MS, Hicks-Pries CE, Hopkins FM, Natali SM (2016a) Radiocarbon in Terrestrial Systems. In Schuur EAG, Druffel ERM and Trumbore SE (eds.) *Radiocarbon and Climate Change – Mechanisms, Applications and Laboratory Techniques,* Springer: Cham, pp. 167-220.

Schuur EAG, Trumbore SE, Druffel ERM, Southon JR, Steinhof A, Taylor RE, Turnbull JC (2016b) Radiocarbon and the global carbon cycle. In Schuur EAG, Druffel ERM and Trumbore SE (eds.) *Radiocarbon and Climate Change - Mechanisms, Applications and Laboratory Techniques,* Springer: Cham, pp. 1-20.

Seifert A-G, Trumbore SE, Xu X, Zhang D, Kothe E, Gleixner G (2011) Variable effects of labile carbon on the carbon use of different microbial groups in black slate degradation. *Geochimica et Cosmochimica Acta, 74*: pp. 2557-2570, doi: 10.1016/j.gca.2011.02.037.

Self R (2005) *Extraction of Organic Analytes from Foods: A Manual of Methods,* The Royal Society of Chemistry: Cambridge, UK, pp. 410.

Sinha MK (1972) Organic matter transformation in soils – Humification of C14-tagged oat roots. *Plant and Soil, 36*(1-3): pp. 283-293, doi: 10.1007/BF01373483.

Steinhof A (2013) Data analysis at the Jena ^{14}C laboratory. *Radiocarbon, 55*(2-3): pp. 282-293, doi: 10.2458/azu_js_rc.55.16350.

Steinhof A (2016) Accelerator Mass Spectrometry of Radiocarbon. In Schuur EAG, Trumbore SE and Druffel ERM (eds.) *Radiocarbon and Climate Change – Mechanisms, Applications and Laboratory Techniques,* Springer: Cham, pp. 253-278.

Steinhof A, Altenburg M, Machts H (2017) Sample preparation at the Jena [14]C Laboratory. *Radiocarbon, 59*(3): pp. 815-830, doi: 10.1017/RDC.2017.50.

Stevenson FJ (1994) Humus chemistry: genesis, composition, reactions. 2nd ed., Wiley: New York, pp. 516.

Stuiver M, Polach HA (1977) Discussion reporting ^{14}C data. *Radiocarbon, 19*(3): pp. 355-363, doi: 10.1017/S0033822200003672.

Suess HE (1955) Radiocarbon concentration in modern wood. *Science, 122(3166*: pp. 415-417, doi: 10.1126/science.122.3166.415-a.

Thevenot M, Dignac M-F, Rumpel C (2010) Fate of lignins in soils: A review. *Soil Biology and Biochemistry, 42*: pp. 1200-1211, doi: 10.1016/j.soilbio.2010.03.017.

Thünen Institute of Forest Ecosystems (2018) *ICP Forests*, Available: http://icp-forests.net/ [Accessed: 23.07.2018].

Thüringen Forst (2007) Soil data – Possen and Holzland. Unpublished data set: Thüringen Forst AöR, FFK Gotha, Germany.

Thüringen Forst (2011) *Revierbuch – Hummelshain*. Unpublished Revierbuch: Forstamt Stadtroda, Germany.

Thüringen Forst (2016) Soil data – Possen and Holzland. Unpublished data set: Thüringen Forst AöR, FFK Gotha, Germany.

TLUG (2011a) *Gebietsniederschlag – Kyffhäuserkreis*, Thüringer Landesanstalt für Umwelt und Geologie, Ref. 51.: Jena.

TLUG (2011b) *Gebietsniederschlag – Saale-Holzland-Kreis*, Thüringer Landesanstalt für Geologie und Umwelt, Ref. 51: Jena.

TLUG (2011c) *Gebietsniederschlag – Unstrut-Hainich-Kreis*, Thüringer Landesanstalt für Umwelt und Geologie, Ref. 51: Jena.

TLUG (2011d) *Lufttemperatur – Kyffhäuserkreis*, Thüringer Landesanstalt für Umwelt und Geologie, Ref. 51.: Jena.

TLUG (2011e) *Lufttemperatur – Saale-Holzland-Kreis*, Thüringer Landesanstalt für Umwelt und Geologie, Ref. 51: Jena.

TLUG (2011f) *Lufttemperatur – Unstrut-Hainich-Kreis*, Thüringer Landesanstalt für Umwelt und Geologie, Ref. 51: Jena.

TLUG (2018a) *Digitale Bodenübersichtskarte – BÜK200*, 1:20'000, Thüringer Landesanstalt für Umwelt und Geologie Ref. 61: Jena.

TLUG (2018b) *Digitale Geologische Karte des Freistaates Thüringen – GK 25*, 1:10'000, Thüringer Landesanstalt für Umwelt und Geologie Ref. 61: Jena.

TLWJF (2009) *Hauptmessstation Possen*. Unpublished, Thüringer Landesanstalt für Wald, Jagd und Fischerei, Referat für Waldzustandsüberwachung: Gotha.

Torn MS, Swanston CW, Castanha C, Trumbore SE (2009) Storage and turnover of organic matter in soil. In Senesi N, Xing B and Huang PM (eds.) *Biophysico-Chemical Processes involving natural nonliving organic matter in environmental systems,* Wiley: Hoboken, USA, pp. 219-272.

Trumbore SE (2009) Radiocarbon and Soil Carbon Dynamics. *Annual Review of Earth and Planetary Sciences, 37*: pp. 47-66, doi: 10.1146/annurev.earth.36.031207.124300.

Trumbore SE, Sierra CA, Hicks-Pries CE (2016) Radiocarbon Nomenclature, Theory, Models, and Interpretation: Measuring Age, Determining Cycling Rates, and Tracing Source Pools. In Schuur EAG, Druffel ERM and Trumbore SE (eds.) *Radiocarbon and Climate Change – Mechanisms, Applications and Laboratory Techniques,* Springer: Cham, pp. 45-82.

Trumbore SE, Vogel JS, Southon JR (1989) AMS ^{14}C measurements of fractionated soil organic matter: an approach to deciphering the soil carbon cycle. *Radiocarbon, 31*(3): pp. 644-654, doi: 10.1017/S0033822200012248.

Trumbore SE, Zheng S (1996) Comparison of fractionation methods for soil organic matter 14C analysis. *Radiocarbon, 38*(2): pp. 219-229, doi: 10.1017/S0033822200017598.

van der Voort TS, Mannu U, Hagedorn F, McIntyre C, Walthert L, Schleppi P, Haghipour N, Eglinton TI (in review, 2018) Dynamics of deep soil carbon – insights from ^{14}C time-series across a climatic gradient. *Biogeosciences Discussion*: pp., doi: 10.5194/bg-2018-361.

von Lützow M, Kögel-Knabner I, Ekschmitt E, Flessa H, Guggenberger G, Matzner E, Marschner B (2007) SOM fractionation methods: Relevance to functional pools and to stabilization mechanisms. *Soil Biology and Biochemistry, 39*: pp. 2183-2207, doi: 10.1016/j.soilbio.2007.03.007.

von Lützow M, Kögel-Knabner I, Ekschmitt E, Matzner E, Guggenberger G, Marschner B, Flessa H (2006) Stabilization of organic matter in temperate soils: mechanisms and their relevance under different soil conditions – a review. *European Journal of Soil Science, 57*: pp. 426-445, doi: 10.1111/j.1365-2389.2006.00809.x.

Welte D (1969) Organic Geochemistry of Carbon. In Wedepohl KH (ed) *Handbook of Geochemistry Vol II/1 Elements H(1) to Al(13),* Springer: Heidelberg, pp. 6L1-6L30*.*

Werner RA, Brand WA (2001) Referencing strategies and techniques in stable isotope ratio analysis. *Rapid Communications in Mass Spectrometry, 15*: pp. 501-519, doi: 10.1002/rcm.258.

Werner RA, Bruch BA, Brand WA (1999) ConFlo III – An Interface for High Precision δ^{13}C and δ^{15}N Analysis with Extended Dynamic Range. *Rapid Communications in Mass Spectrometry, 13*: pp. 1237-1241, doi: 10.1002/(SICI)1097-0231(19990715)13:13<1237::AID-RCM633>3.0.CO;2-C.

Wiedemeier DB, Lang SQ, Gierga M, Abiven S, Bernasconi SM, Früh-Green GL, Hajdas I, Hanke UM, Hilf MD, McIntyre CP, Scheider MPW, Smittenberg RH, Wacker L, Wiesenberg GLB, Schmidt MWI (2016) Characterization, Quantification and Compound-specific Isotopic Analysis of Pyrogenic Carbon Using Benzene Polycarboxylic Acids (BPCA). *JoVE,* 111: pp. 1-9, doi: 10.3791/53922.

Wlotzka F (1972) Nitrogen. Abundancy in common sediments and sedimentary rock types. In Wedepohl KH (ed) *Handbook of Geochemistry Vol II/1 Elements H(1) to Al(13),* Springer: Heidelberg, pp. 7K1-7K7*.*

WRB (2015) *World Reference Base for Soil Resources 2014 – International soil classification system for naming soils and creating legends for soil maps (Update 2015)*. World Soil Resources Reports No. 106. FAO: Rome.

Zhang X, Amelung W (1996) Gas chromatographic determination of muramic acid, glucosamine, mannosamine, and glactosamine in soils. *Soil Biology and Biochemistry, 28*(9): pp. 1201-1206, doi: 10.1016/0038-0717(96)00117-4.

Annex

Digital annex

A1: Results of the test samples of the sequential chemical extraction

Archived soil (sampling year 2017; sampling depth: 40–60 cm) from a grassland at the Hainich National park was used as test sample (TS). Two sub-samples (1 and 2) were extracted in parallel to test the applied sequential chemical extraction method. No data available for the CuO residue since the samples were discarded before measurements were done. Sample was extracted again, $\delta^{13}C$ and $\Delta^{14}C$ of this sample were not available when this thesis was submitted.

Sample	Treatment	Fraction	Duplicate	OC [%]	$\delta^{13}C$ [‰]	$\Delta^{14}C$ [‰]	$\Delta^{14}C$ error [‰]
TS_1	Bulk	Residue	1	1.51	-25.81	-124.3	2.6
TS_2	Bulk	Residue	2	1.49	-25.91	-120.5	1.4
TS_1	Total solvent extraction	Residue	1	1.45	-25.77	-273.5	1.2
TS_2	Total solvent extraction	Residue	2	1.44	-26.06	-279.8	1.2
TS_1	Total solvent extraction	Extract	1	62.93	-29.85	-45.4	2.5
TS_2	Total solvent extraction	Extract	2	62.94	-29.77	-41.0	2.4
TS_1	Base hydrolysis	Residue	1	1.11	-25.78	-120.5	1.3
TS_2	Base hydrolysis	Residue	2	1.10	-25.80	-121.1	1.3
TS_1	Base hydrolysis	Extract	1	52.25	-29.18	-29.4	2.5
TS_2	Base hydrolysis	Extract	2	50.21	-29.19	-22.6	2.8
TS_1	Acid hydrolysis	Residue	1	0.73	-26.22	-140.4	1.3
TS_2	Acid hydrolysis	Residue	2	0.73	-26.23	-128.7	1.3
TS_1	Acid hydrolysis	Extract	1	1.42	-24.00	-90.55	2.3
TS_2	Acid hydrolysis	Extract	2	1.14	-24.45	-85.75	2.4
TS_1	Copper Oxidation	Residue	1	0.44	NA	NA	NA
TS_2	Copper Oxidation	Residue	2	0.43	NA	NA	NA
TS_1	Copper Oxidation	Extract	1	40.21	-26.64	-117.0	2.1
TS_2	Copper Oxidation	Extract	2	53.88	-26.27	-244.6	1.3

OC: Organic carbon; NA: not available

A2: Quality control – C and N determination

Carbon (TC and IC) and nitrogen (TN) duplicate measurements of TOP (0–10 cm) and BOT (30–60 cm) of bulk and soil residues samples from limestone (HAI$_L$, POS$_L$, GOT$_L$) and sandstone (HUM$_S$, HOL$_S$, SOL$_S$) sites. Lower limit of quantification (LLQ) was 0.03 wt-% and 0.01 wt-% for carbon and nitrogen, respectively.

Sample	Site	Depth	Bedrock	Treatment	Duplicate	TC [wt-%]	IC [wt-%]	TN [wt-%]
HAI-A_TSE	Hainich	TOP	Limestone	Total solvent extraction	1	3.07	LLQ	0.26
HAI-A_TSE	Hainich	TOP	Limestone	Total solvent extraction	2	3.06	LLQ	0.26
HAI-A_AHY	Hainich	TOP	Limestone	Acid hydrolysis	1	2.00	0.04	0.17
HAI-A_AHY	Hainich	TOP	Limestone	Acid hydrolysis	2	2.03	0.04	0.18
HAI-B_CuO	Hainich	BOT	Limestone	Copper Oxidation	1	0.62	LLQ	0.22
HAI-B_CuO	Hainich	BOT	Limestone	Copper Oxidation	2	0.61	LLQ	0.22
POS-A_CuO	Possen	TOP	Limestone	Copper Oxidation	1	0.70	LLQ	0.04
POS-A_CuO	Possen	TOP	Limestone	Copper Oxidation	2	0.70	LLQ	0.04
POS_B	Possen	BOT	Limestone	Bulk	1	1.83	1.38	0.04
POS_B	Possen	BOT	Limestone	Bulk	2	1.88	1.39	0.05
GOT-B_BHY	Goettingen	BOT	Limestone	Base hydrolysis	1	2.86	0.05	0.24
GOT-B_BHY	Goettingen	BOT	Limestone	Base hydrolysis	2	2.86	0.05	0.24
HUM-A_TSE	Hummelshain	TOP	Sandstone	Total solvent extraction	1	2.57	LLQ	0.14
HUM-A_TSE	Hummelshain	TOP	Sandstone	Total solvent extraction	2	2.54	LLQ	0.13
HUM-B_BHY	Hummelshain	BOT	Sandstone	Base hydrolysis	1	0.28	LLQ	LLQ
HUM-B_BHY	Hummelshain	BOT	Sandstone	Base hydrolysis	2	0.29	LLQ	0.02
HOL-A_AHY	Holzland	TOP	Sandstone	Acid hydrolysis	1	0.59	LLQ	0.02
HOL-A_AHY	Holzland	TOP	Sandstone	Acid hydrolysis	2	0.58	LLQ	0.02
HOL-A_CuO	Holzland	TOP	Sandstone	Copper Oxidation	1	0.52	0.04	0.02
HOL-A_CuO	Holzland	TOP	Sandstone	Copper Oxidation	2	0.51	0.04	0.02
HOL-B_AHY	Holzland	BOT	Sandstone	Acid hydrolysis	1	0.22	LLQ	0.01
HOL-B_AHY	Holzland	BOT	Sandstone	Acid hydrolysis	2	0.22	LLQ	0.01
SOL-A_TSE	Solling	TOP	Sandstone	Total solvent extraction	1	4.38	0.04	0.27
SOL-A_TSE	Solling	TOP	Sandstone	Total solvent extraction	2	4.38	0.04	0.26

LLQ: below lower limit of quantification

A3: Quality control – δ^{13}C determination

δ^{13}C and organic carbon (OC) duplicate measurements of TOP (0–10 cm) and BOT (30–60 cm) of bulk, soil residue and extract samples from limestone (HAI$_L$, POS$_L$, GOT$_L$) and sandstone (HUM$_S$, HOL$_S$, SOL$_S$) sites.

Sample	Site	Depth	Bedrock	Treatment	Fraction	Duplicate	δ^{13}C [‰]	OC [wt-%]
HAI-A	Hainich	TOP	Limestone	Bulk	Residue	1	-26.86	3.20
HAI-A	Hainich	TOP	Limestone	Bulk	Residue	2	-26.93	3.33
HAI-A_AHY	Hainich	TOP	Limestone	Acid hydrolysis	Extract	1	-24.16	11.80
HAI-A_AHY	Hainich	TOP	Limestone	Acid hydrolysis	Extract	2	-24.19	7.64
HAI-B_BHY	Hainich	BOT	Limestone	Base hydrolysis	Extract	1	-29.91	70.67
HAI-B_BHY	Hainich	BOT	Limestone	Base hydrolysis	Extract	2	-29.88	70.91
POS-A_BHY	Possen	TOP	Limestone	Base hydrolysis	Residue	1	-27.05	1.29
POS-A_BHY	Possen	TOP	Limestone	Base hydrolysis	Residue	2	-26.83	0.98
POS-B	Possen	BOT	Limestone	Bulk	Residue	1	-25.45	0.44
POS-B	Possen	BOT	Limestone	Bulk	Residue	2	-25.87	0.45
POS-B_TSE	Possen	BOT	Limestone	Total solvent extraction	Residue	1	-25.13	0.43
POS-B_TSE	Possen	BOT	Limestone	Total solvent extraction	Residue	2	-25.48	0.39
POS-B_TSE	Possen	BOT	Limestone	Total solvent extraction	Extract	1	-31.57	79.95
POS-B_TSE	Possen	BOT	Limestone	Total solvent extraction	Extract	2	-31.39	77.12
POS-B_BHY	Possen	BOT	Limestone	Base hydrolysis	Residue	1	-25.68	0.35
POS-B_BHY	Possen	BOT	Limestone	Base hydrolysis	Residue	2	-25.46	0.35
POS-B_BHY	Possen	BOT	Limestone	Base hydrolysis	Extract	1	-29.92	69.55
POS-B_BHY	Possen	BOT	Limestone	Base hydrolysis	Extract	2	-29.64	69.15
POS-B_CuO	Possen	BOT	Limestone	Copper Oxidation	Residue	1	-23.44	0.17
POS-B_CuO	Possen	BOT	Limestone	Copper Oxidation	Residue	2	-23.54	0.16
GOT-A	Goettingen	TOP	Limestone	Bulk	Residue	1	-25.98	6.05
GOT-A	Goettingen	TOP	Limestone	Bulk	Residue	2	-25.97	6.12
GOT-A_CuO	Goettingen	TOP	Limestone	Copper Oxidation	Residue	1	-26.52	3.23
GOT-A_CuO	Goettingen	TOP	Limestone	Copper Oxidation	Residue	2	-26.53	2.72
GOT-B	Goettingen	BOT	Limestone	Bulk	Residue	1	-25.68	3.19

GOT-B	Goettingen	BOT	Limestone	Bulk	Residue	2	-25.82	2.80
GOT-B_TSE	Goettingen	BOT	Limestone	Total solvent extraction	Residue	1	-25.48	3.46
GOT-B_TSE	Goettingen	BOT	Limestone	Total solvent extraction	Residue	2	-25.94	2.22
GOT-B_TSE	Goettingen	BOT	Limestone	Total solvent extraction	Extract	1	-30.80	82.84
GOT-B_TSE	Goettingen	BOT	Limestone	Total solvent extraction	Extract	2	-30.79	78.89
GOT-B_BHY	Goettingen	BOT	Limestone	Base hydrolysis	Extract	1	-29.14	65.52
GOT-B_BHY	Goettingen	BOT	Limestone	Base hydrolysis	Extract	2	-29.14	65.71
HUM-A_AHY	Hummelshain	TOP	Sandstone	Acid hydrolysis	Extract	1	-24.09	11.63
HUM-A_AHY	Hummelshain	TOP	Sandstone	Acid hydrolysis	Extract	2	-24.23	10.00
HUM-B	Hummelshain	BOT	Sandstone	Bulk	Residue	1	-26.81	0.68
HUM-B	Hummelshain	BOT	Sandstone	Bulk	Residue	2	-27.47	0.86
HUM-B_AHY	Hummelshain	BOT	Sandstone	Acid hydrolysis	Extract	1	-25.60	3.22
HUM-B_AHY	Hummelshain	BOT	Sandstone	Acid hydrolysis	Extract	2	-25.37	3.23
HUM-B_CuO	Hummelshain	BOT	Sandstone	Copper Oxidation	Extract	1	-28.94	63.77
HUM-B_CuO	Hummelshain	BOT	Sandstone	Copper Oxidation	Extract	2	-28.94	58.08
HOL-A_CuO	Holzland	TOP	Sandstone	Copper Oxidation	Extract	1	-27.92	58.38
HOL-A_CuO	Holzland	TOP	Sandstone	Copper Oxidation	Extract	2	-29.99	58.02
HOL-B_TSE	Holzland	BOT	Sandstone	Total solvent extraction	Residue	1	-26.75	0.39
HOL-B_TSE	Holzland	BOT	Sandstone	Total solvent extraction	Residue	2	-26.89	0.41
HOL-B_BHY	Holzland	BOT	Sandstone	Base hydrolysis	Residue	1	-26.67	0.21
HOL-B_BHY	Holzland	BOT	Sandstone	Base hydrolysis	Residue	2	-26.61	0.21
SOL-A_BHY	Solling	TOP	Sandstone	Base hydrolysis	Residue	1	-27.30	3.32
SOL-A_BHY	Solling	TOP	Sandstone	Base hydrolysis	Residue	2	-27.12	3.06
SOL-A_AHY	Solling	TOP	Sandstone	Acid hydrolysis	Extract	1	-23.42	7.19
SOL-A_AHY	Solling	TOP	Sandstone	Acid hydrolysis	Extract	2	-23.62	6.19
SOL-B_BHY	Solling	BOT	Sandstone	Base hydrolysis	Extract	1	-29.69	69.62
SOL-B_BHY	Solling	BOT	Sandstone	Base hydrolysis	Extract	2	-29.63	69.92
SOL-B_AHY	Solling	BOT	Sandstone	Acid hydrolysis	Residue	1	-27.08	1.04
SOL-B_AHY	Solling	BOT	Sandstone	Acid hydrolysis	Residue	2	-27.04	0.99

A4: Quality control – Δ^{14}C determination

Δ^{14}C and the analytical error duplicate measurements of TOP (0–10 cm) and BOT (30–60 cm) of bulk, soil residue and extract samples from lime-stone (HAI$_L$, POS$_L$, GOT$_L$) and sandstone (HUM$_S$, HOL$_S$, SOL$_S$) sites.

Sample	Site	Depth	Bedrock	Treatment	Δ^{14}C_Res [‰]	Error_Res [‰]	Δ^{14}C_Ex [‰]	Error_Ex [‰]
HAI-A	Hainich	TOP	Limestone	Bulk	13.5	3.2	NA	NA
HAI-A_TSE	Hainich	TOP	Limestone	Total solvent extraction	25.5	1.9	-9.8	1.8
HAI-A_BHY	Hainich	TOP	Limestone	Base hydrolysis	14.7	1.5	58.0	1.6
HAI-A_AHY	Hainich	TOP	Limestone	Acid hydrolysis	-89.9	1.5	-483.7	1.2
HAI-A_CuO	Hainich	TOP	Limestone	Copper Oxidation	15.5	1.6	-33.1	1.7
HAI-B	Hainich	BOT	Limestone	Bulk	-44.8	1.4	NA	NA
HAI-B_TSE	Hainich	BOT	Limestone	Total solvent extraction	-34.0	1.5	-41.0	1.8
HAI-B_BHY	Hainich	BOT	Limestone	Base hydrolysis	-66.4	1.6	10.9	1.6
HAI-B_AHY	Hainich	BOT	Limestone	Acid hydrolysis	-594.3	1.0	-765.1	0.8
HAI-B_CuO	Hainich	BOT	Limestone	Copper Oxidation	-61.5	1.4	-82.8	1.4
POS-A	Possen	TOP	Limestone	Bulk	2.8	3.4	NA	NA
POS-A_TSE	Possen	TOP	Limestone	Total solvent extraction	0.4	3.2	29.7	1.9
POS-A_BHY	Possen	TOP	Limestone	Base hydrolysis	-8.8	1.8	10.4	1.6
POS-A_AHY	Possen	TOP	Limestone	Acid hydrolysis	-21.8	1.9	-599.4	1.0
POS-A_CuO	Possen	TOP	Limestone	Copper Oxidation	-31.0	1.7	28.6	1.9
POS-B	Possen	BOT	Limestone	Bulk	-495.8	2.2	NA	NA
POS-B_TSE	Possen	BOT	Limestone	Total solvent extraction	-470.1	2.1	-587.2	1.1
POS-B_BHY	Possen	BOT	Limestone	Base hydrolysis	NA	NA	-46.7	2.0
POS-B_AHY	Possen	BOT	Limestone	Acid hydrolysis	-409.4	2.8	-985.3	0.2
POS-B_CuO	Possen	BOT	Limestone	Copper Oxidation	-412.1	3.3	-306.4	1.4
GOT-A	Goettingen	TOP	Limestone	Bulk	-89.9	3.1	NA	NA
GOT-A_TSE	Goettingen	TOP	Limestone	Total solvent extraction	13.2	1.8	-11.4	2.0
GOT-A_BHY	Goettingen	TOP	Limestone	Base hydrolysis	4.4	1.9	31.4	1.9
GOT-A_AHY	Goettingen	TOP	Limestone	Acid hydrolysis	-40.7	1.6	-567.7	1.0
GOT-A_CuO	Goettingen	TOP	Limestone	Copper Oxidation	2.9	1.6	-1.9	1.6
GOT-B	Goettingen	BOT	Limestone	Bulk	-177.3	2.8	NA	NA
GOT-B_TSE	Goettingen	BOT	Limestone	Total solvent extraction	-43.3	1.7	-68.3	1.8
GOT-B_BHY	Goettingen	BOT	Limestone	Base hydrolysis	-150.9	1.5	-14.0	1.8

GOT-B_AHY	Goettingen	BOT	Limestone	Acid hydrolysis	-51.5	1.5	-845.3	0.6
GOT-B_CuO	Goettingen	BOT	Limestone	Copper Oxidation	-55.3	1.6	-236.4	1.4
HUM-A	Hummelshain	TOP	Sandstone	Bulk	18.4	3.4	NA	NA
HUM-A_TSE	Hummelshain	TOP	Sandstone	Total solvent extraction	13.2	3.7	18.3	1.8
HUM-A_BHY	Hummelshain	TOP	Sandstone	Base hydrolysis	-6.2	3.4	27.1	1.9
HUM-A_AHY	Hummelshain	TOP	Sandstone	Acid hydrolysis	-21.4	3.4	-179.6	1.8
HUM-A_CuO	Hummelshain	TOP	Sandstone	Copper Oxidation	-5.9	1.7	14.5	1.8
HUM-B	Hummelshain	BOT	Sandstone	Bulk	-19.9	3.2	NA	NA
HUM-B_TSE	Hummelshain	BOT	Sandstone	Total solvent extraction	-20.1	3.3	4.2	1.9
HUM-B_BHY	Hummelshain	BOT	Sandstone	Base hydrolysis	-51.5	3.0	-25.4	1.8
HUM-B_AHY	Hummelshain	BOT	Sandstone	Acid hydrolysis	-65.2	3.2	-744.2	0.8
HUM-B_CuO	Hummelshain	BOT	Sandstone	Copper Oxidation	-64.2	2.8	45.7	1.8
HOL-A	Holzland	TOP	Sandstone	Bulk	47.5	3.6	NA	NA
HOL-A_TSE	Holzland	TOP	Sandstone	Total solvent extraction	14.7	3.7	-4.1	1.8
HOL-A_BHY	Holzland	TOP	Sandstone	Base hydrolysis	15.3	1.8	14.8	1.8
HOL-A_AHY	Holzland	TOP	Sandstone	Acid hydrolysis	-19.9	3.6	-13.2	1.9
HOL-A_CuO	Holzland	TOP	Sandstone	Copper Oxidation	-16.3	4.1	11.6	1.8
HOL-B	Holzland	BOT	Sandstone	Bulk	-37.9	3.5	NA	NA
HOL-B_TSE	Holzland	BOT	Sandstone	Total solvent extraction	-5.9	3.1	-71.8	1.7
HOL-B_BHY	Holzland	BOT	Sandstone	Base hydrolysis	-36.3	3.4	-12.4	1.8
HOL-B_AHY	Holzland	BOT	Sandstone	Acid hydrolysis	-38.1	4.9	-1.2	2.0
HOL-B_CuO	Holzland	BOT	Sandstone	Copper Oxidation	-69.4	3.0	-50.7	1.8
SOL-A	Solling	TOP	Sandstone	Bulk	-11.9	1.5	NA	NA
SOL-A_TSE	Solling	TOP	Sandstone	Total solvent extraction	-14.2	1.6	-31.4	1.6
SOL-A_BHY	Solling	TOP	Sandstone	Base hydrolysis	-13.5	1.5	-72.4	1.5
SOL-A_AHY	Solling	TOP	Sandstone	Acid hydrolysis	-72.8	1.5	8.9	1.8
SOL-A_CuO	Solling	TOP	Sandstone	Copper Oxidation	-27.4	1.4	-23.6	1.6
SOL-B	Solling	BOT	Sandstone	Bulk	-231.0	1.3	NA	NA
SOL-B_TSE	Solling	BOT	Sandstone	Total solvent extraction	-117.6	1.4	-99.4	1.5
SOL-B_BHY	Solling	BOT	Sandstone	Base hydrolysis	-113.4	1.4	-98.6	1.7
SOL-B_AHY	Solling	BOT	Sandstone	Acid hydrolysis	-145.6	1.3	-127.0	1.7
SOL-B_CuO	Solling	BOT	Sandstone	Copper Oxidation	-120.3	1.6	-142.6	1.4

NA: not available

A5: Chemical and physical characterization of bulk soil samples

Total carbon (TC), inorganic carbon (IC), total nitrogen (TN), pH, $\Delta^{14}C$, and $\delta^{13}C$ measurements of TOP (0–10 cm) and BOT (30–60 cm) of bulk soil samples from limestone (HAI$_L$, POS$_L$, GOT$_L$) and sandstone (HUM$_S$, HOL$_S$, SOL$_S$) sites. SOC was calculated by subtracting TC from IC, if IC was larger than 0.15 wt-% (= upper limit of quantification. C/N was calculated by dividing SOC with TN.

Sample	Site	Depth	Bedrock	TC [wt-%]	IC [wt-%]	SOC [wt-%]	TN [wt-%]	C/N	pH	$\Delta^{14}C$ [‰]	$\delta^{13}C$ [‰]
HAI-A	Hainich	TOP	Limestone	3.02	LLQ	3.02	0.26	12	5.83	13.5	-26.90
HAI-B	Hainich	BOT	Limestone	1.65	0.05	1.65	0.26	11	7.11	-44.8	-25.90
POS-A	Possen	TOP	Limestone	2.02	LLQ	2.02	0.12	17	4.22	2.8	-27.42
POS-B	Possen	BOT	Limestone	1.86	1.39	0.47	0.05	9	7.46	-495.8	-25.66
GOT-A	Goettingen	TOP	Limestone	6.02	0.08	6.02	0.53	11	6.15	-89.9	-25.98
GOT-B	Goettingen	BOT	Limestone	3.57	0.63	2.94	0.27	11	7.18	-177.3	-25.75
HUM-A	Hummelshain	TOP	Sandstone	2.54	LLQ	2.54	0.13	20	4.02	18.4	-27.80
HUM-B	Hummelshain	BOT	Sandstone	0.71	LLQ	0.71	0.04	18	4.30	-19.9	-27.70
HOL-A	Holzland	TOP	Sandstone	2.34	LLQ	2.34	0.10	23	4.00	47.5	-27.53
HOL-B	Holzland	BOT	Sandstone	0.64	LLQ	0.64	0.03	21	4.35	-37.9	-27.11
SOL-A	Solling	TOP	Sandstone	4.42	0.04	4.42	0.26	17	3.97	-11.9	-27.19
SOL-B	Solling	BOT	Sandstone	1.61	LLQ	1.61	0.11	15	4.58	-231.0	-27.44

LLQ: below lower limit of quantification

A6: Chemical and physical characterization of soil residue and extract samples

See Table A12 in digital annex.

A7: Mass balance calculation

See Table A12 in digital annex.